Dissertation zur Erlangung des Doktorgrades

der Fakultät für Chemie und Pharmazie

der Ludwig-Maximilians-Universität München

Mg-Containing Nitridosilicates as Host Lattices for Novel Luminescent Materials

Sebastian Florian Schmiechen

aus

München, Deutschland

2015

Erklärung

Diese Dissertation wurde im Sinne der von § 7 der Promotionsordnung vom 28. November 2011 von Herrn Prof. Dr. W. Schnick betreut.

Eidesstattliche Versicherung

Diese Dissertation wurde eigenständig und ohne unerlaubte Hilfe erarbeitet.

München, den 26.02.2015

…….

(Sebastian Florian Schmiechen)

Dissertation eingereicht am	05.03.2015
1. Gutachter	Prof. Dr. W. Schnick
2. Gutachter	Prof. Dr. O. Oeckler
Mündliche Prüfung am	13.04.2015

Für meine Familie

Acknowledgement

Herrn Prof. Dr. Wolfgang Schnick möchte ich besonders danken für die Aufnahme in den Arbeitskreis und die Überlassung dieses interessanten und fordernden Themas. Die große Freiheit bei der Umsetzung neuer Ideen, die unzähligen gestalterischen Möglichkeiten, sowie die hervorragenden Arbeitsbedingungen bildeten die besten Voraussetzungen. Auch für die Gelegenheit Ergebnisse in wissenschaftlichen Fachzeitschriften, bzw. auf (inter)nationalen Tagungen darzustellen sowie der Möglichkeit zur aktiven Beteiligung an Projekten wie der Kooperation mit dem LDCA oder der DFG-Forschergruppe FOR-1600 gebührt großer Dank. Der hohe Grad an Abwechslungsreichtum regte stets zu neuen Ideen an. Ferner waren die vielen Gespräche über alle möglichen Dinge stets sehr informativ und haben mich immer wieder zu neuen Anregungen beflügelt. Besonderen Dank möchte ich dafür aussprechen, dass mir die Möglichkeit gegeben wurde als Next-Generation Teilnehmer bei der Preisverleihung zum deutschen Zukunftspreis 2013 in Berlin aktiv beteiligt gewesen zu sein.

Herrn Prof. Dr. Oliver Oeckler danke ich nicht nur für die Übernahme des Korreferats, sondern ganz besonders für die anhaltende Förderung und immer neue Motivation mich in Richtung der Festkörperchemie zu orientieren. Für seine große Hilfsbereitschaft bei jeglichen Fragestellungen in der Chemie oder auch abseits davon bin ich ebenfalls sehr dankbar.

Herrn Prof. Dr. Hubert Huppertz, Prof. Dr. Konstantin Karaghiosoff, Prof. Dr. Hans-Christian Böttcher und Prof. Dr. Peter Wellmann danke ich für die Bereitschaft, als weitere Prüfer zur Verfügung zu stehen.

Herrn Dr. Peter J. Schmidt vom Philips Lumileds Development Center Aachen möchte ich ganz besonders dafür danken, dass immer wieder intensive Diskussionen gestartet wurden die der eigenen Forschung noch mehr Ansporn verliehen haben und es mir ermöglicht haben einen tiefen Einblick in das Gebiet der Lumineszenz zu erhalten.

Auch möchte ich mich ganz herzlich bei allen weiteren Beteiligten des Kooperationsprojekts bedanken. Hierbei möchte ich besonders Cora Hecht, Volker Weiler, Petra Huppertz, Detlef Wiechert und Niels van der Veen hervorheben, die mir durch zahlreiche Synthesen, Lumineszenzmessungen und spannende Diskussionen den langen Weg durch die Doktorarbeit erleichtert haben. Ich freue mich sehr, dass ich durch diese enge Zusammenarbeit einen tiefen Einblick in moderne Beleuchtungstechnologie gewinnen konnte und vor allem auch, dass durch unsere gemeinsame Forschung nachhaltige Ergebnisse geschaffen werden konnten.

Frau Olga Lorenz, Herrn Thomas Miller und Herrn Wolfgang Wünschheim danke ich für die stete Hilfe bei allerlei organisatorischen, computertechnischen und sicherheitsrelevanten Fragen.

Herrn Dr. Constantin Hoch, Dr. Peter Mayer und Frank Tambornino danke ich für zahlreiche Einkristalluntersuchungen und auch für den intensiven Beistand bei diversen Problemdatensätzen.

Herrn Christian Minke gebührt Dank für zahlreiche REM-Sessions mit unzähligen EDX-Messungen und für die aufgenommenen Bilder.

Frau Dr. Saskia Lupart, Herrn Dr. Sandro Pagano, Dr. Christoph Höller und Dr. Martin Zeuner danke ich für die behutsame Heranführung an die Festkörperchemie und die Welt der Leuchtstoffe während meiner Bachelor- und Masterarbeit. Frau Dr. Saskia Lupart möchte ich darüber hinaus herzlichst für ihren ständigen Beistand und die große Unterstützung bei allerlei Fragestellungen danken.

Ganz besonderer Dank gilt auch meinen Laborkollegen aus D2.107 und später D2.074 für die schöne und lustige Zeit. Die Herren Dr. Philipp Pust, Christian Ziegler, Dr. Stephan Werner, Martin Mangstl, Dr. Markus Seibald und Frau Nicole Braml sorgten immer wieder für spaßige Events an zahlreichen Abenden und auch intensive Diskussionen über alle möglichen Themen waren stets willkommen.

Natürlich gilt auch größter Dank meinen Praktikanten Hajnalka Schneider, Frederik Nietschke, Philipp Strobel, Fabian Keßler, Thomas Reith, Peter Wagatha und Markus

Siegert. Ohne den ständigen Ehrgeiz zur Forschung und die tatkräftige Unterstützung beim Synthetisieren und Auswerten wäre all das kaum möglich gewesen. Auch freut es mich sehr, dass ich euch ein guter Lehrer war und euer Interesse an Leuchtstoffen und der Festkörperchemie stärken konnte und euch nahezu alle wieder im Arbeitskreis als diverse Nachfolger antreffen kann.

Ich möchte mich auch bei allen weiteren Kollegen der Arbeitkreise Schnick, Oeckler, Hoch, Schmedt auf der Günne, Johrendt und Lotsch ganz herzlich für die tolle Zeit bedanken.

Allergrößter Dank gilt aber meinen Eltern, die mir alles ermöglicht haben, dass ich meinen Weg gehen konnte.

Meiner Frau Heidi kann ich gar nicht genug danken, dass sie immer hinter mir steht und mich unterstützt soviel wie es nur geht. Auch ein großer Dank, dass du mich so nimmst wie ich bin und der perfekte Gegenpol zu mir bist. Vielen Dank für bislang drei wundervolle Ehejahre. Meinen Zwillingen Lukas und Thomas gebührt größter Dank, dass sie es immer wieder schaffen Papa von der Arbeit abzulenken und mir zeigen, was wirklich wichtig ist, nämlich Spaß am Leben.

“Nur wenige wissen, wie viel man wissen muss,

um zu wissen, wie wenig man weiß.”

(Werner Heisenberg)

Table of Contents

1 Introduction

The industrial revolution yielded numerous world-shaking inventions, whereby one invention is almost steady in use.[1] The incandescent light bulb was finally commercialized by Thomas Alva Edison.[2] This electric lighting device consists of an evacuated glass bulb and originally a carbonized bamboo filament. In the mean time the carbon filament has been replaced by tungsten wires enabling an extended lifetime up to 1000 h (see Fig. 1-1). Nevertheless, the incandescent light bulb is nowadays a symbol for wasting a lot of energy, as only ~5% of the energy is converted into visible light. The major part of the emission is settled in the infrared region, only heating the environment.[3] Soon, various alternatives for electric lighting were explored. Especially, gas-based discharge lamps appeared more and more in focus.[4] Until then, the noble gas neon was excited by an electric current resulting in bright-red emission. More recently, advanced discharge lamps apply vaporized mercury, which emits after excitation by an electric current, in the short-wave ultraviolet (UV) region. For the generation of visible light, as familiarized from the sunlight, the UV emission has to be down converted by luminophores (phosphors). Edmund Germer and his co-workers Meyer and Spanner succeeded and a patent was granted in 1927 for a low-voltage metal-vapor lamp.[5] These colloquially termed fluorescent lamps have a significant advantage over incandescent light bulbs; the device efficiency is highly increased. Nevertheless, the emission spectrum of nowadays used compact fluorescent lamps (CFLs) does not cover the whole visible spectrum, resulting in a poor color rendition. The color rendering index (CRI), which is 100 for sunlight or close to 100 for the incandescent light bulb, is much lower for CFLs (CRI <80). This result in an unnatural color rendition and more importantly, the use of mercury within the CFLs gave raise to ecological concerns among the consumers. The electric-lighting devices described as yet enable on the one side a good color rendition with a bad efficiency (incandescent light bulb) or on the other side vice versa (CFL). Therefore, numerous

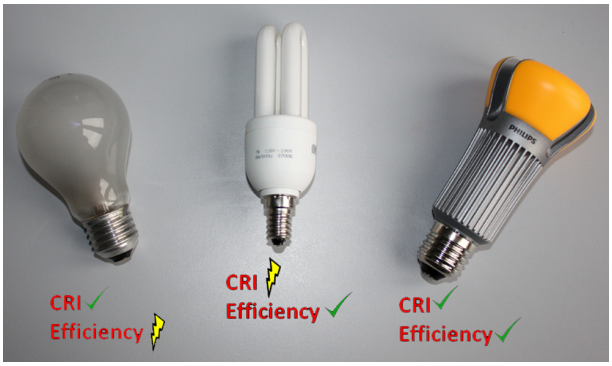

Figure 1-1. Three generations of electric-lighting devices. Incandescent light bulb (left), compact fluorescence lamp (middle), and pc-LED (right).

alternatives were investigated over the last couple of years. Yet, light-emitting diodes (LED) are discussed as the most advanced replacements.As early as in the 1920s the Russian scientist Oleg Vladimirovich Losev observed light emission from silicon carbide crystal rectifier diodes.[6] He published 16 papers between 1924 and 1930 that were the basis for the first patent on a modern LED (infrared-emitting GaAs) by James R. Biard and Gary Pittman from the G.E. labs.[7] Based on these results numerous further semiconductors (e.g., GaAsP, InGaP, GaAlAs) were investigated and enabled access to all colors of the visible spectrum. First commercial LEDs were mainly used as replacements for incandescent and neon indicator lamps or in seven-segment displays as the light output was limited in these times.[8]

The emission of a LED results from electron-hole transitions between different layers (p- and n-doped) of semiconducting materials. The emission color strongly correlates with the band gap of the semiconductor material used and consequently, LEDs are a monochromatic light source. For general illumination white light similar to daylight is required that cannot be created directly with a single LED.[9,10] Based on additive color mixing white light can be generated by the combination of monochromatic red, green and blue emitting LEDs. However, this approach is more expensive and also color rendition is not ideal due to the sharp emission peaks of a LED. Furthermore, tuning the color of the emitted light for various applications is more challenging. Nevertheless, white light can also be created by down conversion of the light from a primary LED by luminophors. This approach was already used by Germer in his mercury-vapor based discharge lamps. In phoshor-converted (pc-)LEDs the UV to blue

light of the primary LED is partially, either by only one single phosphor (1pc-LED) or by a multitude of phosphors (e.g., two phosphors = 2pc-LED) converted to white light. This approach not only shows a much extended tuneability, it is also much more cost effective, as only few *µg* of the phosphor(s) are needed. Furthermore, CRI values close to 100 can be reached. Today, pc-LEDs are unbeaten not only in efficiency but also in environmental acceptability during the whole production and life cycle. A recent McKinsey survey predicts that the global market share of pc-LEDs in general lighting will be about 45% in 2016 and almost 70% in 2020, with a market volume of around 64 billion €.[11] However, it was a challenging route until the first illumination-grade white pc-LEDs were available in consumer markets. Particularly, UV to blue emitting primary LEDs were not obtainable until 1994. As early as the 1950s, GaN was already considered as a UV to blue emitting direct band gap semiconductor.[12,13] In these times, no high quality GaN single crystals were available and also p-doping of GaN was difficult. More advanced crystal growth techniques were invented in the late 1970s,[14] and Isamu Akasaki began to adapt the proposals for GaN single-crystal growth. Finally, in 1986 he and Hiroshi Amano succeeded by obtaining high class GaN single crystals for the first time.[15] Furthermore, first hints on p-doping with either Mg or Zn were reported and an increase in emission intensity after treating the samples with an electron beam was reported.[16] Latter mechanism was further investigated by Shuji Nakamura.[17,18] He concluded that the dopants form complexes with hydrogen and become passive, electron beam treatment dissolves the complexes and the dopants are reactivated. Furthermore, Nakamura demonstrated that already thermal annealing could reactivate the dopants. A further challenge was the growth and p-doping of AlGaN and InGaN, which are necessary to produce heterojunctions. Here, the recombination processes occur more efficiently as described by the groups of Akasaki and Nakamura.[19,20] Finally in 1994, a quantum efficiency of 2.7% with a blue-emitting double heterojunction InGaN/AlGaN LED was reported by Nakamura.[21] All of these results were fundamental steps towards energy-efficient lighting and also pioneering work in solid-state lighting solutions for general illumination.[22] Quite recently, the Nobel committee awarded the 2014 Nobel Prize in physics to Isamu Akasaki, Hiroshi

Amano and Shuji Nakamura for the invention of efficient blue-light emitting diodes which has enabled bright and energy-saving white-light sources.[23]

As soon as UV to blue primary LEDs were available a huge demand for novel phosphor materials arose. Commonly, inorganic crystalline solid materials were investigated as appropriate host lattices. However, only few of these compounds exhibit luminescence and therefore doping with impurities is required.[8] Usually, lanthanides are applied as dopants, whereby 5*d*→4*f* emission is favored for an application in pc-LEDs, as shown for example by Eu^{2+} or Ce^{3+}.[24] In contrast to the 4*f* orbitals of the lanthanides, which are shielded by 6*s* and 5*d* orbitals and therefore, are not influenced by host lattice, the energetic position of 5*d* orbitals is strongly influenced by the surrounding of the dopant.[25,26] These influences are depicted in Fig. 1-2.

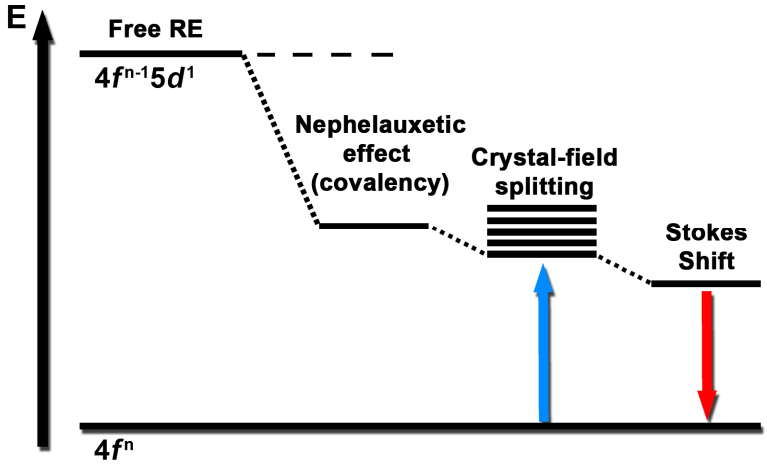

Figure 1-2. General excitation and emission processes in lanthanides, for example Eu^{2+} or Ce^{3+}, depicting the influencing effects like the crystal field around the activator site and the nephelauxetic effect.

First of all, the chemical bond between the activator (i.e., dopant) and the ligands has to be considered. The more covalent the bonding is, the more the 5*d* level is lowered compared to the free lanthanide (nephelauxetic effect). Furthermore, the coordination sphere around the activator leads to degeneration of the 5*d* orbitals (crystal-field splitting). After excitation of an electron from the 4*f* ground state to the lowest 5*d* state, relaxation to the vibronic state with the lowest energy inside the excited state occurs. This process is a non-radiative relaxation. From this point the electron falls back to the 4*f* state under emission of photons. As described, the energy of the

emitted photons is smaller and therefore emission occurs at higher wavelengths (i.e., lower energy) than the excitation wavelength. This energetic difference between the centroid of the excitation and emission band is called Stokes shift. The advantage towards 4*f*→4*f* emission is not only the tuneability of the emission wavelength by the host lattice, but also 5*d*→4*f* emission is a parity allowed process, for Ce^{3+} the transition is also spin allowed. This results in pretty fast decay times of some few *ns* (Ce^{3+}) to *μs* (Eu^{2+}), in contrast typical 4*f*→4*f* emission takes some *ms* (e.g., Eu^{3+}). It enables the use of high-power blue primary LEDs without reaching a saturation of the excited state.[9] Furthermore, 5*d*→4*f* emission shows broad bands in contrast to 4*f*→4*f* line emission. The broad emission bands can once more be used for a more exact tuning of the emitted light of a pc-LED. However, the host lattices not only have to be dopable with lanthanides, which fulfill numerous alkaline-earth containing compounds, there are numerous more specific requirements on suitable host lattices.[27] High chemical and thermal stability are upmost required during manufacturing and the whole product lifetime. Also, high quantum efficiencies (QE) close to 100% are important for a nearly non-dissipative light conversion. Resulting, thermal quenching (TQ) has to be low, even at the operating temperature of a pc-LED. Typically, modern blue-emitting high-power LEDs are operated at currents of ∼350 mA, and due to ohmic losses heating the chip surface causes temperatures of ∼150 °C. A strong electron-phonon coupling is often attributed to high TQ, as the electron in the excited state cannot fall back to ground state potential and the energy is transferred to the host lattice (lattice vibrations). Therefore, a highly condensed rigid and crystallographically ordered network seems to be beneficial for the reduction of phonons and consequently low TQ.

Numerous lanthanide-doped oxide, halide and sulfide phosphors were already known and were intensively investigated.[8] Only few of these compounds were considered for application in pc-LEDs. One prominent Ce^{3+}-doped oxide phosphor is the garnet $Y_{3-x}Gd_xAl_{5-y}Ga_yO_{12}:Ce^{3+}$ (YAG:Ce) which is used as a green to yellow emitting component in modern 1pc-LEDs.[28,29] This material fulfills the above described requirements for pc-LED phosphors, as it exhibits a highly condensed, rigid and ordered network of AlO_x polyhedra (see Fig.1-3 left). Nevertheless, YAG:Ce also shows

some disadvantages, for example at elevated temperatures the QE drops significantly and despite the emission band is broad, there is no noticeable emission in the red part of the visible spectrum. Therefore, common 1pc-LEDs with YAG:Ce show only low CRI values <75 and correlated color temperatures (CCT) around 4000 to 8000 K and cannot be used as illumination-grade white (CCT ~2700-3000 K, CRI >85) pc-LEDs.[30] Thus, there was a huge lack of red-emitting phosphor materials. Commonly used Eu^{3+}- or Mn^{4+}-doped compounds cannot be used in combination with high-power blue LEDs as the relaxation of these dopants is slow and the excited state gets saturated.[9] For a long time Eu^{2+}-doped sulfide and selenide phosphors seemed to be the only ones that could be applied in pc-LEDs. For example, emission of $(Ca_{1-x}Sr_x)Se:Eu^{2+}$ shows a pretty small full width at half maximum (fwhm) of ~1390 cm^{-1} at λ_{em} = 600 nm.[31] Nevertheless, these phosphors suffer from severe thermal quenching at elevated temperatures and a further disadvantage is the low stability of these compounds towards hydrolysis. In presence of moisture toxic H_2S is released, which requires embedding of the phosphor and therefore raises the production costs of a pc-LED. There had not been any alternative until at the end of the 1990s a new material class came into focus; the (oxo)nitridosilicates.[32] This material class can formally be derived from oxosilicates by full or partial substitution of oxygen by nitrogen. In contrast to oxosilicates, nitrogen in nitrodoslicates can significantly extend the structural diversity. Not only can nitrogen connect up to four neighboring tetrahedral centers, for example $AEYbSi_4N_7$ (AE = Sr,Ba),[33-35] but also edge-sharing of SiN_4 tetrahedra, for example in $Ca_5Si_2N_6$,[36] is often observed. Nevertheless, the syntheses of nitridosilicates are more challenging. These have to be carried out under strict exclusion of oxygen and consequently, under inert-gas conditions. Commonly, nitridosilicates are synthesized by pyrolysis of molecular precursors like "$Si(NH)_2$" (SDI), carbon-reduction and nitridation processes (CRN) or more advanced in hot-isostatic pressing (HIP).[37] One prominent host lattice is $AE_2Si_5N_8$ (AE = Sr,Ba).[38] Soon after the optical properties of the respective Eu^{2+}-doped compound had been reported,[39] the solid-state lighting industry realized the potential of this red-emitting phosphor. Nowadays, $(Ba,Sr)_2Si_5N_8:Eu^{2+}$ (λ_{em} = 620 nm, fwhm ~2050-2600 cm^{-1}) is used as highly efficient red component in commercial

illumination-grade white pc-LEDs (see Fig. 1-3 middle).[40-44] Similarly with oxosilicates, the structural diversity of nitridosilicates can be further enhanced by the partial substitution of for example Al^{3+} or Li^{+} for Si^{4+}. Especially, Eu^{2+}-doped nitridoalumosilicates show a high potential for an application as phosphors in pc-LEDs. $(Ca,Sr)SiAlN_3:Eu^{2+}$ (λ_{em} ~610-660 nm, fwhm ~2100-2500 cm^{-1}) is used as an alternative red-emitting component in illumination-grade white pc-LEDs (see Fig. 1-3 right).[45,46]

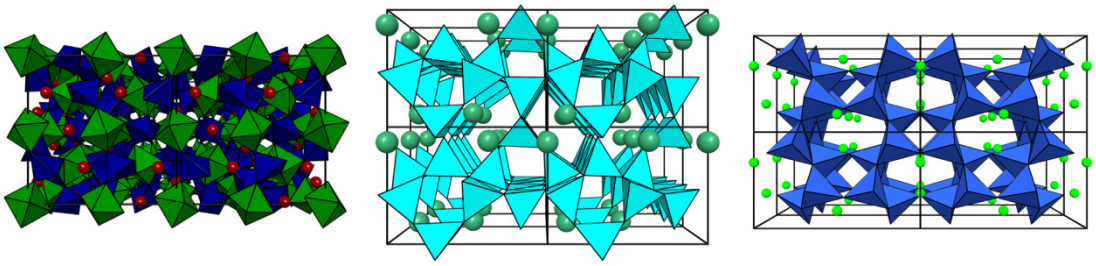

Figure 1-3. Crystal structures of the most prominent phosphors used in pc-LEDs. $Y_3Al_5O_{12}:Ce^{3+}$ (left), $Sr_2Si_5N_8:Eu^{2+}$ (middle), and $CaAlSiN_3:Eu^{2+}$ (right). Spheres: Y^{3+} red, Sr^{2+} dark green, Ca^{2+} green. Polyhedra: AlO_4 tetrahedra dark blue, AlO_6 octahedra green, SiN_4 tetrahedra cyan, $(Al,Si)N_4$ tetrahedra blue.

In contrast, Li-containing nitridosilicates are discussed as Li^{+}-ion conductors, for example $Li_{14}Ln_5Si_{11}N_{19}O_7F_2$ with Ln = Ce,Nd.[47] Nevertheless, there are also reports on Eu^{2+}-doped Li-containing nitridosilicates that show promising luminescence properties. For example, $Sr[Li_2Si_2N_4]:Eu^{2+}$ (λ_{em} = 610 nm, fwhm ~2225 cm^{-1})[48] exhibits pretty similar emission properties to $(Ba,Sr)_2Si_5N_8:Eu^{2+}$. These two examples of Li-containing nitridosilicates illustrate that a greater structural variety can be expected compared to Al-containing nitridosilicates, as Li^{+} can act as a counterion (e.g., $Li_{14}Ln_5Si_{11}N_{19}O_7F_2$ with Ln = Ce,Nd), and can partially replace Si^{4+} in the anionic nitridosilicate substructure (e.g., $Sr[Li_2Si_2N_4]$). Hence, it is quite surprising that there only very few reports on Mg-containing nitridosilicates, though the diagonal relationship between Li^{+} and Mg^{2+} should lead to a similar crystal chemistry in nitridosilicates. Until recently, $MgSiN_2$ was the only Mg-containing nitridosilicate mentioned in the literature.[49,50] Nevertheless, the compound should be more appropriately classified as a double nitride according to its wurtzite-type structure. Quite recently, Yamane et al. reported on $Ba_4Mg[Si_2N_6]$, the first “real” Mg-containing nitridosilicate where Mg^{2+} is fourfold-planar coordinated by

N^{3-} and therefore a counterion for the nitridosilicate substructure.[51] Up to now, there are still reports missing on the partial substitution of Mg^{2+} for Si^{4+}.

Current research in the solid-state lighting industry as well as in academic environment focuses on the enhancement of illumination-grade white pc-LEDs. Commercial devices with $(Ba,Sr)_2Si_5N_8:Eu^{2+}$ or $(Ca,Sr)SiAlN_3:Eu^{2+}$ already show high CRI values up to 95 exhibiting an intriguing color rendition, but at the expense of luminous efficacy (i.e., efficiency of light conversion in reference to the human eye sensitivity). The above mentioned red phosphors show a large portion of emitted light outside the human eye sensitivity in the infrared region thus wasting energy. A better adaption to the visible region of the emission curve of the red component can lead to an increase in efficacy of up to 30%. Therefore, novel narrow-band red-emitting phosphors (λ_{em} ~610-650 nm with an fwhm ~50 nm) are urgently required. Mg-containing nitridosilicates are expected to fulfill these requirements.

Therefore, the focus within this doctoral thesis was based on the syntheses of novel Mg-containing nitridosilicates and the investigation of the optical properties of the respective lanthanide-doped compounds. Reports from the literature have shown that synthesis of nitridosilicates with common solid-state synthesis methods is more and more a challenge. Therefore, advanced and modern synthesis techniques were applied. Both, high-temperature synthesis routes, for example a modified solid-state metathesis route as well as ammonothermal techniques were intensively investigated for the syntheses of Mg-containing nitridosilicates. The here reported Eu^{2+}-doped nitridomagnesosilicates showed outstanding luminescence properties and were further investigated concerning their structure-property relations. The results from this thesis are a breakthrough for the nitridomagnesosilicates and their future application in illumination-grade white pc-LEDs.

References

(1) Stearns, P. N. *The Industrial Revolution in World History*; Westview Press: Boulder, 2012.

(2) Vögtle, F. *Thomas Alva Edison*; Rowohlt: Reinbek near Hamburg, 1982.

(3) Feldmann, C. *Z. Anorg. Allg. Chem.* **2012**, *638*, 2169.

(4) Van Dulken, S.; Phillips, A. *Inventing the 20th Century: 100 Inventions that Shaped the World from the Airplane to the Zipper*; NYU Press: New York, 2002.

(5) Germer, E.; Meyer, F.; Spanner, H. J. Metal vapor lamp. US 2182732 A, December 05th,1939.

(6) Zheludev, N. *Nat. Photon.* **2007**, *1*, 189.

(7) Biard, J. R.; Pittman, G. E. Semiconductor radiant diode. US3293513 A, December 20th, 1966.

(8) Ronda, C. *Luminescence*; Wiley-VCH: Weinheim, 2008.

(9) Krames, M. R.; Mueller, G. O.; Mueller-Mach, R. B.; Bechtel, H.-H.; Schmidt, P. J. Wavelength conversion for producing white light from high power blue LED. PCT Int. Appl.WO 2010131133 A1, November 18th,2010.

(10) Mueller-Mach, R.; Mueller, G. O.; Krames, M. R.; Trottier, T. *IEEE J. Select. Top. Quant. Electron.* **2002**, *8*, 339.

(11) Lighting the way: Perspectives on the global lighting market. www.mckinsey.com/~/media/mckinsey/dotcom/client_service/automotive%20and%20assembly/lighting_the_way_perspectives_on_global_lighting_market_2012.ashx (accessed Nov 04, 2014)

(12) Grimmeiss, H. G.; Koelmans, H. *Z. Naturforsch.* **1959**, *14a*, 264.

(13) Grimmeiss, H. G.; Koelmans, H. *Z. Naturforsch.* **1960**, *15*, 799.

(14) Manasevit, H. M.; Erdman, F. M.; Simpson, W. I. *J. Electrochem. Soc.* **1971**, *118*, 1864.

(15) Amano, H.; Sawaki, N.; Akasaki, I.; Toyoda, Y. *Appl. Phys. Lett.* **1986**, *48*, 353.

(16) Amano, H.; Akasaki, I.; Kozawa, T.; Hiramatsu, K.; Sawaki, N.; Ikeda, K.; Ishii, Y. *J. Lumin.* **1988**, *40-41*, 121.

(17) Nakamura, S.; Iwasa, N.; Senoh, M.; Mukai, T. *Jpn. J. Appl. Phys.* **1992**, *31*, 1258.

(18) Nakamura, S.; Mukai, T.; Senoh, M.; Iwasa, N. *Jpn. J. Appl. Phys.* **1992**, *31*, L139.

(19) Murakami, H.; Asahi, T.; Amano, H.; Hiramatsu, K.; Sawaki, N.; Akasaki, I. *J. Crystal Growth* **1991**, *115*, 648.

(20) Nakamura, S.; Mukai, T. *Jpn. J. Appl. Phys.* **1992**, *31*, L1457.

(21) Nakamura, S.; Mukai, T.; Senoh, M. *Appl. Phys. Lett.* **1994**, *64*, 1687.

(22) Nakamura, S.; Fasol, G. *The blue laser diode*; Springer: Berlin, 1997.

(23) The Nobel Prize in Physics 2014. http://www.nobelprize.org/nobel_prizes/physics/laureates/2014/ (accessed Nov 04th, 2014)

(24) Höppe, H. A. *Angew. Chem. Int. Ed.* **2009**, *48*, 3572.

(25) Blasse, G.; Grabmaier, B. C. *Luminescent Materials*; Springer-Verlag: Berlin, Heidelberg, 1994.

(26) Shionoya, S.; Yen, W. M.; Yamamoto, H. *Phosphor Handbook*; CRC Press: Boca Raton, 2006.

(27) Blasse, G.; Bril, A. *Appl. Phys. Lett.* **1967**, *11*, 53.

(28) Setlur, A. *Electrochem. Soc. Interface* **2009**, *18*, 32.

(29) Moriguchi, T.; Noguchi, Y.; Sakano, K.; Shimizu, Y. Light emitting device having a nitride compound semiconductor and a phosphor containing a garnet fluorescent material. US 5998925 A, July 29th, 1997.

(30) Schlotter, P.; Schmidt, R.; Schneider, J. *Appl. Phys. A* **1997**, *64*, 417.

(31) Zhang, X.; Liang, L.; Zhang, J.; Su, Q. *Mater. Lett.* **2005**, *59*, 749.

(32) Zeuner, M.; Pagano, S.; Schnick, W. *Angew. Chem. Int. Ed.* **2011**, *50*, 7754.

(33) Huppertz, H.; Schnick, W. *Z. Anorg. Allg. Chem.* **1997**, *623*, 212.

(34) Park, W. B.; Son, K. H.; Singh, S. P.; Sohn, K. S. *ACS Comb. Sci.* **2012.**

(35) Huppertz, H.; Schnick, W. *Angew. Chem. Int. Ed. Engl.* **1996**, *35*, 1983.

(36) Ottinger, F.; Nesper, R. *Z. Anorg. Allg. Chem.* **2005**, *631*, 1597.

(37) Chung, S.-L.; Huang, S.-C.; Chou, W.-C.; Tangguh, W. W. *Curr. Opin. Chem. Eng.* **2014**, *3*, 62.

(38) Schlieper, T.; Milius, W.; Schnick, W. *Z. Anorg. Allg. Chem.* **1995**, *621*, 1380.

(39) Höppe, H. A.; Lutz, H.; Morys, P.; Schnick, W.; Seilmeier, A. *J. Phys. Chem. Solids* **2000**, *61*, 2001.

(40) Lee, B.; Lee, S.; Jeong, H. G.; Sohn, K. S. *ACS Comb. Sci.* **2011**, *13*, 154.

(41) Piao, X.; Horikawa, T.; Hanzawa, H.; Machida, K.-i. *Appl. Phys. Lett.* **2006**, *88*, 161908.

(42) ten Kate, O. M.; Zhang, Z.; Dorenbos, P.; Hintzen, H. T.; van der Kolk, E. *J. Solid State Chem.* **2013**, *197*, 209.

(43) Zeuner, M.; Hintze, F.; Schnick, W. *Chem. Mater.* **2008**, *21*, 336.

(44) Zeuner, M.; Schmidt, P. J.; Schnick, W. *Chem. Mater.* **2009**, *21*, 2467.

(45) Uheda, K.; Hirosaki, N.; Yamamoto, H. *Phys. Status Solidi A* **2006**, *203*, 2712.

(46) Uheda, K.; Hirosaki, N.; Yamamoto, Y.; Naito, A.; Nakajima, T.; Yamamoto, H. *Electrochem. Solid-State Lett.* **2006**, *9*, H22.

(47) Lupart, S.; Gregori, G.; Maier, J.; Schnick, W. *J. Am. Chem. Soc.* **2012**, *134*, 10132.

(48) Zeuner, M. *Doctoral Thesis*, Ludwig Maximilian University Munich, 2009.

(49) David, J.; Laurent, Y.; Lang, J. *Bull. Soc. Fr. Mineral. Cristallogr.* **1970**, *93*, 153.

(50) Petukhov, A. G.; Lambrecht, W. R. L.; Segall, B. *Phys. Rev. B: Condens. Matter* **1994**, *49*, 4549.

(51) Yamane, H.; Morito, H. *J. Alloys Compd.* **2013**, *555*, 320.

2 Nitridosilicates containing the Chimera Mg: From Counterion to Incorporation into the Nitridosilicate Substructure

Reports on Mg-containing nitridosilicates are quite rare. Up to now there are only two compounds mentioned in the literature, $MgSiN_2$ and $Ba_4Mg[Si_2N_6]$.[1,2] $MgSiN_2$ crystallizes in a wurtzite-type structure and should therefore be more appropriately classified as a double nitride than a nitridosilicate. In contrast, Mg acts as counterion for the anionic nitridosilicate substructure in $Ba_4Mg[Si_2N_6]$ and is the first Mg-containing nitridosilicate mentioned in the literature. Nevertheless, there are no reports on the partial substitution of Mg^{2+} for Si^{4+} in the nitridosilicate substructure and consequently the nitridosilicate subgroup of nitridomagnesosilicates. Following, numerous compounds of this novel material class are reported. The first representatives of nitridomagnesosilicates are the isotypic compounds $M[Mg_3SiN_4]$ with M = Ca,Sr,Eu. Due to some specific structural features, Eu^{2+}-doped $Sr[Mg_3SiN_4]$ shows outstanding narrow-band red emission. Nevertheless, the compounds exihibts severe thermal quenching already at room temperature that the electronic structure is further investigated. The construction of an energy-level diagram according to Dorenbos and Hintzen et al.[3-5] revealed numerous information on the electronic structure of the host lattice. The isoelectronic compound $Ba[Mg_3SiN_4]:Eu^{2+}$ not only shows a different structure type but also quite different luminescence properties. Especially, anomalous luminescence phenomena were further investigated. All above mentioned compounds are narrow-band red emitting phosphors and can be summarized as “N4-phosphors”. A comment on the luminescene properties of these compounds along with similar nitridoaluminates finishes the first series of Mg-containing nitridosilicates. Afterwards, it is shown that Mg-containing nitridosilicates not only show intriguing luminescence properties but also interesting crystal chemistry. In the strongly to each other related compounds $Ca_2Mg[Li_4Si_2N_6]$ and

$Li_2Ca_2[Mg_2Si_2N_6]$ magnesium acts as a chimera. In $Ca_2Mg[Li_4Si_2N_6]$ Mg is a counterion for the nitridosilicate substructure, whereas in $Li_2Ca_2[Mg_2Si_2N_6]$ it is part of the nitridosilicate substructure. All up to now mentioned features of Mg-containing nitridosilicates, intriguing luminescence properties and an interesting crystal chemistry, are combined in the first representative of "N6-phosphors"; the nitridolithomagnesoalumosilicate $Ba[(Mg_{2-x}Li_x)(Al_{4-x}Si_x)N_6]$ with x = (0-2).

References

(1) David, J.; Laurent, Y.; Lang, J. *Bull. Soc. Fr. Mineral. Cristallogr.* **1970**, *93*, 153.

(2) Yamane, H.; Morito, H. *J. Alloys Compd.* **2013**, *555*, 320.

(3) Dorenbos, P. *ECS J. Solid State Sci. Technol.* **2013**, *2*, R3001.

(4) ten Kate, O. M.; Zhang, Z.; Dorenbos, P.; Hintzen, H. T.; van der Kolk, E. *J. Solid State Chem.* **2013**, *197*, 209.

(5) Zhang, Z.-J.; ten Kate, O. M.; Delsing, A.; Dorenbos, P.; Zhao, J.-T.; Hintzen, H. T. *J. Mater. Chem. C* **2014**, *2*, 7952.

2.1 Toward New Phosphors for Application in Illumination-Grade White pc-LEDs: The Nitridomagnesosilicates $Ca[Mg_3SiN_4]:Ce^{3+}$, $Sr[Mg_3SiN_4]:Eu^{2+}$, and $Eu[Mg_3SiN_4]$

Sebastian Schmiechen, Hajnalka Schneider, Peter Wagatha, Cora Hecht, Peter J. Schmidt, and Wolfgang Schnick

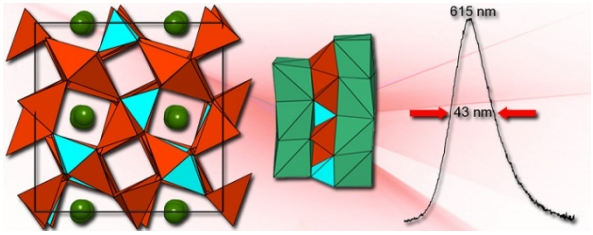

Published in: *Chem. Mater.* **2014**, *26*, 2712; DOI: 10.1021/cm500610v
http://pubs.acs.org/doi/abs/10.1021/cm500610v

Abstract

The isotypic compounds $M[Mg_3SiN_4]$ (M = Ca,Sr,Eu) have been synthesized by solid-state reactions in sealed tantalum ampules or in a radio-frequency furnace. The nitridomagnesosilicates crystallize in space group $I4_1/a$ (no.88). Crystal structures were solved and refined from single-crystal X-ray diffraction data (Z = 16, $Ca[Mg_3SiN_4]:Ce^{3+}$, a = 11.424(2), c = 13.445(3) Å, R_1 = 0.040, wR_2 = 0.106; $Sr[Mg_3SiN_4]:Eu^{2+}$, a = 11.495(2), c = 13.512(3) Å, R_1 = 0.036, wR_2 = 0.102; $Eu[Mg_3SiN_4]$, a = 11.511(4), c = 13.552(4) Å, R_1 = 0.016, wR_2 = 0.039). The nitridomagnesosilicates are isotypic to $Na[Li_3SiO_4]$, containing a condensed tetrahedra network with a high degree of condensation (i.e., atomic ratio (Mg,Si):N) κ = 1. The crystal structures were confirmed by Rietveld refinement, lattice energy (MAPLE) calculations, and further investigated by ^{29}Si-MAS NMR. Ce^{3+}-doped samples of $Ca[Mg_3SiN_4]$ show yellow emission (λ_{max} = 530 and 585 nm, fwhm ~3900 cm^{-1} (~130 nm)), while $Sr[Mg_3SiN_4]:Eu^{2+}$ exhibits red luminescence (λ_{max} = 615 nm) with the most narrow red emission of Eu^{2+}-phosphors reported in the literature so far (fwhm ~1170 cm^{-1} (~43 nm)). According to this

outstanding narrow red emission, originating from parity allowed $4f^6 5d^1 \rightarrow 4f^7$ transition in Eu^{2+}, $Sr[Mg_3SiN_4]:Eu^{2+}$ may point the way to the next generation red phosphor materials for application in illumination-grade white pc-LEDs.

2.1.1 Introduction

Global electricity demand is continuously rising, and an increase of more than 56% is expected by 2040.[1] Especially lighting causes ~17% of electricity consumption in the U.S.[2] Hence, replacement of inefficient incandescent light bulbs, which only convert ~5% of electricity into visible light,[3] is a major goal. Phosphor-converted light-emitting diodes (pc-LEDs) have emerged over the last couple of years as superior candidates for replacement of incumbent light sources. Generally, LED-based light sources have much better energy-conversion capability of up to 50%, lifetimes reaching >25.000 h, and are also environmentally sustainable over the whole life cycle.[4–6] For further improvement of luminous efficacy (efficiency of light generation referring to human eye sensitivity), particularly for illumination-grade white pc-LEDs with high color rendition, novel phosphor materials with optimized luminescence properties are urgently required.[7] Color-rendering index (CRI) and luminous efficacy critically depend on the peak position and on the bandwidth of the red spectral component. Yet, commercially applied red phosphors show a large portion of emitted light outside the human eye sensitivity wasting energy in the infrared region. Therefore, narrow band red-emitting materials are necessary, which can be applied in high-power pc-LEDs, with blue light output of the (In,Ga)N semiconductor LED >100 W/cm^2. This implies short decay times of the activators' excited state to avoid saturation, a small Stokes shift, high chemical stability, and low thermal quenching at temperatures above 100 °C.[8]

Multinary alkaline-earth nitridosilicates and their subgroups (e.g., (oxo)nitridoalumosilicates) have proven their capability to fulfill most of these requirements upon doping with Eu^{2+}. Recently, nitrido(alumo)silicates like $Sr_2Si_5N_8:Eu^{2+}$ or $CaAlSiN_3:Eu^{2+}$ found broad industrial application as highly efficient red-emitting phosphor materials in pc-LEDs.[9–16] Nitridosilicates show an enhanced structural diversity as compared to oxosilicates, because nitrogen can connect up to four

neighboring tetrahedral centers (e.g., $AEYbSi_4N_7$ (AE=Sr,Ba)).[16] Furthermore, the structural variety of nitridosilicates can be further extended by substituting Al or Li for Si resulting in nitridoalumo- or nitridolithosilicates, respectively.[16–18] Unlike Al, Li can act as a counterion for the nitridosilicate substructure (e.g., $LiCa_3Si_2N_5$) as well.[19,20] Despite the diagonal relationship between Mg and Li in the periodic table, there are only few reports on Mg-containing nitridosilicates.[21] Besides some doping experiments on $AE_2Si_5N_8:Eu^{2+}$ and $SrSi_2O_2N_2:Eu^{2+}$ with Mg^{2+},[22,23] $MgSiN_2$ was one of the few "magnesium nitridosilicates" mentioned in the literature so far.[24,25] However, according to its wurtzite type superstructure, it should be more appropriately classified as a double nitride. Recently, Yamane et al. reported on $Ba_4Mg[Si_2N_6]$, a less condensed nitridosilicate containing $[Si_2N_6]^{10-}$ bow-tie units, which results in a low degree of condensation (i.e., atomic ratio Si:N) κ = 1/3. This was the first example of a stoichiometric Mg-containing nitridosilicate where Mg acts as a counterion for the nitridosilicate substructure.[26] To the best of our knowledge, there have been no reports on the substitution of Mg for Si on tetrahedral positions of the silicate network structure of a nitridosilicate accessing the subgroup of nitridomagnesosilicates.

Here, we report on the synthesis and structural characterization of the first representatives of nitridomagnesosilicates, $Ca[Mg_3SiN_4]:Ce^{3+}$, $Sr[Mg_3SiN_4]:Eu^{2+}$, and $Eu[Mg_3SiN_4]$. Especially, $Sr[Mg_3SiN_4]:Eu^{2+}$ shows intriguing narrow band red luminescence due to some special structural features, which could lead to next generation red phosphor materials for application in illumination-grade white pc-LEDs.

2.1.2 Experimental Section

2.1.2.1 Synthesis

Because of the sensitivity against air and moisture of the starting materials, all manipulations were performed in flame-dried Schlenk-type glassware attached to a vacuum line (10^{-3} mbar) or in an argon-filled glovebox (Unilab, MBraun, Garching, O_2 <1 ppm, H_2O <1 ppm). Purification of argon (Messer-Griessheim, 5.0) was carried out by passage through columns filled with silica gel (Merck), molecular sieve

(Fluka, 4 Å), KOH (Merck,≥85%), P_4O_{10} (Roth, ≥99%), and titanium sponge (Johnsen Matthey, 99.5%) at 700 °C.

Single crystals of the title compounds were isolated after reaction in sealed tantalum ampules. The starting materials with a stoichiometric ratio of typically 0.20 mmol of AEF_2 (AE = Ca, 15.62 mg; AE = Sr, 25.12 mg, both from Sigma-Aldrich, 99.99%) or EuF_3 (41.79 mg, Sigma-Aldrich, 99.99%), Mg_3N_2 (20.19 mg, Sigma-Aldrich, 99.5%), and "$Si(NH)_2$" (11.63 mg, synthesized according to the method by Lange et al.)[27] were ground under argon atmosphere in a glovebox. As nitrogen source was added 0.40 mmol of LiN_3 (19.59 mg, synthesized according to the method by Fair et al.),[28] and 2.00 mmol of Li (13.88 mg, Alfa Aesar, 99.9%) was used as fluxing agent. For the Ca and Sr compounds, 2 mol% EuF_3 or CeF_3 (Sigma-Aldrich, 99.99%) as doping agents were added. The mixtures were placed in tantalum ampules, which were subsequently weld shut in an arc furnace under water cooling. The ampules were placed in a silica tube and then heated in a tube furnace under vacuum. The reaction mixtures were heated to 950 °C within 3 h, maintained at this temperature for 24 h, subsequently cooled to 500 °C in 100 h, and finally quenched to room temperature by switching off the furnace.

Bulk samples of $Sr[Mg_3SiN_4]$ were synthesized using a radio frequency (rf-)furnace (type IG 10/200, frequency 200 kHz, max electrical output 12 kW, Hüttinger, Freiburg).[29] The reaction mixture of 2.05 mmol of $Sr(NH_2)_2$ (245.34 mg, synthesized according to the method by Zeuner et al.),[18] 2.05 mmol of Mg_3N_2 (206.95 mg), and 2.05 mmol of "$Si(NH)_2$" (119.17 mg) was placed in a tungsten crucible under argon atmosphere (glovebox) and then transferred into a water-cooled quartz reactor of a rf-furnace under nitrogen atmosphere. The temperature was raised to 1000 °C within 30 min, kept for 6 h, and subsequently quenched to room temperature by switching off the rf-furnace.

2.1.2.2 X-ray Spectroscopy

Concerning the determination of the chemical composition of the title compounds, several crystallites were analyzed by energy dispersive X-ray (EDX) spectroscopy.

Hereto, a JSM-6500F scanning electron microscope (SEM, Jeol) with a Si/Li EDX detector (Oxford Instruments, model 7418) was used.

2.1.2.3 Single-Crystal X-ray Diffraction

Single crystals of the title compounds were isolated from the reaction mixtures under a microscope (glovebox), enclosed in glass capillaries, and sealed under argon. The crystallites were checked with respect to their quality on a Buerger precession camera. X-ray diffraction data of the corresponding single crystals were collected either on a STOE IPDS I diffractometer with graphite monochromator or on a Nonius KappaCCD diffractometer with graded multilayer X-ray optics or on a Bruker D8 Quest diffractometer with microfocus and graphite monochromator. All diffractometers use Mo-K_α radiation (λ = 0.71073 Å). After an absorption correction with XPREP[30] or SADABS,[31] the structures were solved by Direct Methods (SHELXS)[32] and refined by full-matrix least-squares methods (SHELXL);[33,34] see Table 2.1-1 for details. Dopants Eu^{2+} and Ce^{3+} were unheeded for structure determination, because the contribution to scattering density is insignificant.

Further details of the crystal structure investigation may be obtained from Fachinformationszentrum Karlsruhe, 76344 EggensteinLeopoldshafen, Germany (fax, (+49)7247-808-666; e-mail, crysdata@fiz-karlsruhe.de, http://www.fiz-karlsruhe.de/request_for_deposited_data.html) on quoting the depository numbers CSD-427074 ($Ca[Mg_3SiN_4]$), CSD-427076 ($Sr[Mg_3SiN_4]$), and CSD-427075 ($Eu[Mg_3SiN_4]$).

2.1.2.4 Powder X-ray Diffraction

PXRD data were collected on a STOE STADI P diffractometer (Cu-$K_{\alpha1}$ or Mo-$K_{\alpha1}$ radiation, Ge(111) monochromator, position sensitive detector) in Debye−Scherrer geometry. Rietveld refinements were carried out using the TOPAS package.[35] See the Supporting Information for corresponding powder diffractograms.

Table 2.1-1. Crystallographic Data of $M[Mg_3SiN_4]$ (M = Ca,Sr,Eu)

	$Ca[Mg_3SiN_4]$	$Sr[Mg_3SiN_4]$	$Eu[Mg_3SiN_4]$
formula mass/g·mol^{-1}	197.14	244.68	309.02
crystal system		tetragonal	
space group		$I4_1/a$ (no. 88)	
cell parameters/Å	a = 11.424(2) c = 13.445(3)	a = 11.495(2) c = 13.512(3)	a = 11.511(4) c = 13.552(4)
V/Å^3	1754.5(5)	1785.4(5)	1795.5(2)
formula units/cell		16	
X-ray density/g·cm^{-3}	2.985	3.641	4.573
abs. coefficient μ/mm^{-1}	1.982	12.62	14.51
F(000)	1568	1856	2256
diffractometer, radiation	Stoe IPDS I	Nonius Kappa CCD Mo-K_α (λ = 0.71073 Å)	Bruker D8 Quest
temperature/K		293(2)	
absorption correction	numerical[30]	multi-scan[31]	multi-scan[31]
θ range/°	3.94-27.49	3.13-31.51	3.54-27.49
measured reflections	9371	9911	37893
independent reflections	7103	6031	23372
observed reflections	991	864	1032
refined parameters		82	
GoF	1.044	1.088	1.013
R indices ($F_o^2 \geq 2\sigma(F_o^2)$)	R_1 = 0.0403, wR_2 = 0.1063	R_1 = 0.0362, wR_2 = 0.1024	R_1 = 0.0163, wR_2 = 0.0392
R indices (all data)	R_1 = 0.0494, wR_2 = 0.1096	R_1 = 0.0483, wR_2 = 0.1113	R_1 = 0.0185, wR_2 = 0.0403
min / max residual electron density/eÅ^{-3}	-0.85 / 1.07	-0.59 / 1.52	-0.65 / 1.12

2.1.2.5 Luminescence

A HORIBA Fluoromax4 spectrofluorimeter system was used for the investigation of luminescence properties. The system is attached to an Olympus BX51 microscope via fiber optical bundles. The samples were measured inside sealed quartz capillaries. The

excitation wavelength was chosen as 440−460 nm with a spectral width of 10 nm. Excitation spectra were measured between 250 and 600 nm. Emission spectra were collected in the wavelength range between 450 and 800 nm with 2 nm step size. Low temperature emission spectra were recorded between 6 and 300 K.

2.1.2.6 UV/vis Spectroscopy

Reflectance spectra were recorded on an Edinburgh Photonics FLS920-s spectrometer with a Xe900 450 W arclamp (Czerny-Turner monochromator with three gratings, singlephoton-photomultiplier detector). The spectra were measured between 230 and 780 nm with 5 nm step size. The band gap of $Sr[Mg_3SiN_4]$ was derived from UV/vis-reflectance data by drawing a line tangent to the slope of the reflectance curve. The point of intersection of the tangent with the abscissa is the value of the band gap.

2.1.2.7 Solid-State MAS NMR.

^{29}Si-MAS NMR measurement on a non-doped sample of $Sr[Mg_3SiN_4]$ was performed in a ZrO_2 rotor at 11.74 T on a Bruker DSX 500 Advance FT spectrometer with a commercial 2.5 mm triple-resonance MAS probe at ^{29}Si frequency of 99.385 MHz. The chemical shift is reported using the frequency ratios published by IUPAC (δ scale relative to 1% tetramethylsilane (TMS) in $CDCl_3$).[36] The spectrum was acquired at a spinning frequency of 10 kHz with a 90° pulse length of 2.5 µs.

2.1.3 Results and Discussion

2.1.3.1 Synthesis and Chemical Analysis

Syntheses of the title compounds were carried out by two different approaches. Crystals suitable for single-crystal X-ray analysis were obtained by the reaction in sealed tantalum ampules. The heterogeneous reaction products contained red rods of moisture-sensitive $AE[Mg_3SiN_4]$ (deep red for $Eu[Mg_3SiN_4]$), LiF, and some metallic residues, whereas bulk samples of non-doped $Sr[Mg_3SiN_4]$ for UV/vis- and ^{29}Si-MAS NMR spectroscopy were obtained by rf-furnace syntheses in a tungsten crucible under N_2 atmosphere. EDX analyses revealed an atomic ratio M:Mg:Si:N = 1:3:1:4

(M = Ca,Sr,Eu), which agrees well within the standard deviations with the composition obtained from single-crystal structure analysis.

2.1.3.2 Single-Crystal Structure Analysis

The crystal structures of the isotypic compounds $M[Mg_3SiN_4]$ (M = Ca,Sr,Eu) were solved and refined in tetragonal space group $I4_1/a$ (no. 88); crystallographic data are summarized in Table 2.1-1. Atomic coordinates and isotropic displacement parameters are given in Table 2.1-2. Selected bond lengths and anisotropic displacement parameters for all title compounds can be found in the Supporting Information.

The nitridomagnesosilicates $M[Mg_3SiN_4]$ with M = Ca,Sr,Eu are isotypic to the lithosilicate $Na[Li_3SiO_4]$ and exhibit ordering of Mg and Si atoms.[37] This structure type has not been ascribed to any nitridosilicate so far (see Figure 2.1-1).

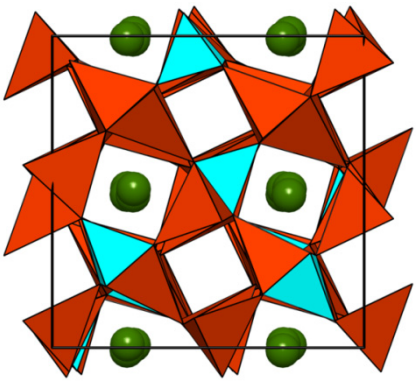

Figure 2.1-1. Crystal structure of $M[Mg_3SiN_4]$ (*M* = Ca,Sr,Eu), projection along [001]. SiN_4 tetrahedra blue, MgN_4 tetrahedra orange and M^{2+} green.

In contrast to $M[Mg_3SiN_4]$, isoelectronic $Sr[Mg_3GeN_4]$ shows disordering of the tetrahedrally coordinated cations (Mg/Ge) and crystallizes in the UCr_4C_4 structure type (*I*4/*m*, no. 87).[38,39]

The crystal structure of $M[Mg_3SiN_4]$ consists of SiN_4 tetrahedra that are connected via two edges and one corner to MgN_4 tetrahedra, forming strands running along [001] (see Figure 2.1-2a). The strands of SiN_4 and MgN_4 tetrahedra are connected to each other by common corners in an up–down sequence forming *vierer* rings[40,41] with one-half of them centered by M^{2+}. This results in a rigid network and a maximum

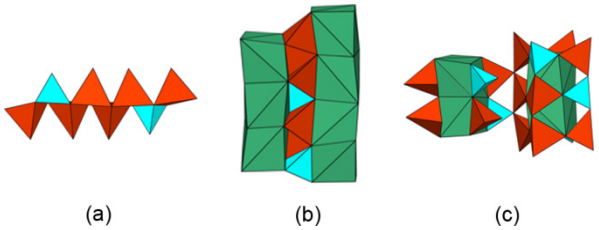

Figure 2.1-2. (a) Strands of SiN_4 and MgN_4 tetrahedra along [001]. (b) Strands of face-sharing enantiomeric MN_8 "cubes", connected by a strand of SiN_4 and MgN_4 tetrahedra. (c) Linked strands of "cubes" by edge sharing with SiN_4 and MgN_4 tetrahedra. SiN_4 tetrahedra blue, MgN_4 tetrahedra orange and MN_8 "cubes" green.

degree of condensation (i.e., atomic ratio (Mg,Si):N) $\kappa = 1$, also found for highly condensed binary nitrides like AlN.The Si–N distances vary from 1.763(4) to 1.773(3) Å (M = Ca), 1.789(5) to 1.824(5) Å (M = Sr), and 1.757(2) to 1.778(2) Å (M = Eu). The values are all in agreement with the sum of the ionic radii (1.79 Å)[42] and typical for nitridosilicates.[16] Mg–N distances are significantly larger, ranging from 1.980(3) to 2.253(3) Å (M = Ca), 1.986(5) to 2.215(5) Å (M = Sr), and 1.996(2) to 2.267(2) Å (M = Eu). Nevertheless, all ranges agree well with the sum of the ionic radii (2.18 Å) according to Baur.[42] Similar Mg–N distances can be found in the only known Mg-containing nitridosilicates $MgSiN_2$[24,25] and $Ba_4Mg[Si_2N_6]$.[26] In the crystal structure of $M[Mg_3SiN_4]$, M occupies only one crystallographic site, which is 7-fold coordinated by N^{3-}. With the inclusion of another N^{3-}, the coordination number is increased to 7 + 1, which results in a distorted cuboidal surrounding. There are two possible configurations for coordination of M^{2+} by N^{3-}, resulting in enantiomeric patterns in the unit cell. The "cubes" are connected via face sharing with ones from the same chirality, forming strands of "cubes" along [001].

There are two enantiomeric strands of "cubes" per unit cell, linked by a SiN_4 and MgN_4 strand. All SiN_4 and MgN_4 tetrahedra have two common edges in *trans* position with the enantiomeric strands of "cubes" (see Figure 2.1-2b). As a consequence, the enantiomeric strands of "cubes" are shifted one-half of the edge length against each other (see Figure 2.1-2c).

Table 2.1-2. Atomic Coordinates and Isotropic Displacement Parameters of $M[Mg_3SiN_4]$ (M = Ca,Sr,Eu); All Atoms are on Wyckoff Position 16*f* [a]

	atom	x	y	z	U_{eq}/Å^3
$Ca[Mg_3SiN_4]$	Ca	0.2641(6)	0.0204(6)	0.1613(6)	0.0105(2)
	Si	0.0380(8)	0.0703(8)	0.3044(7)	0.0103(3)
	Mg1	0.0172(11)	0.0889(12)	0.5604(11)	0.0173(3)
	Mg2	0.0284(12)	0.0944(11)	0.0616(10)	0.0165(3)
	Mg3	0.3645(12)	0.2538(12)	0.0715(10)	0.0180(3)
	N1	0.1692(3)	0.1520(3)	0.2978(3)	0.0174(7)
	N2	0.1734(3)	0.1638(3)	0.5655(3)	0.0174(7)
	N3	0.1776(3)	0.1957(3)	0.0507(3)	0.0172(7)
	N4	0.4588(3)	0.0995(3)	0.0850(3)	0.0182(7)
$Sr[Mg_3SiN_4]$	Sr	0.2591(5)	0.0068(4)	0.1804(4)	0.0152(3)
	Si	0.0331(14)	0.0753(13)	0.3075(10)	0.0131(4)
	Mg1	0.0213(18)	0.0896(17)	0.5607(11)	0.0145(5)
	Mg2	0.0249(17)	0.0944(16)	0.0623(11)	0.0126(4)
	Mg3	0.3569(18)	0.2437(19)	0.0693(11)	0.0178(5)
	N1	0.1648(4)	0.1596(4)	0.3031(3)	0.0193(11)
	N2	0.1717(4)	0.1946(4)	0.0515(3)	0.0182(11)
	N3	0.1735(4)	0.1714(4)	0.5638(3)	0.0169(11)
	N4	0.4527(4)	0.0947(4)	0.0804(3)	0.0218(11)
$Eu[Mg_3SiN_4]$	Eu	0.2612(13)	0.0133(13)	0.1720(13)	0.0094(8)
	Si	0.0362(7)	0.0723(6)	0.3057(5)	0.0031(15)
	Mg1	0.0208(9)	0.0897(8)	0.5600(7)	0.0063(19)
	Mg2	0.0265(9)	0.0958(8)	0.0618(7)	0.0055(19)
	Mg3	0.3619(8)	0.2485(8)	0.0708(7)	0.0060(2)
	N1	0.1640(2)	0.1556(19)	0.3010(16)	0.0046(4)
	N2	0.1735(2)	0.1968(2)	0.0499(16)	0.0058(4)
	N3	0.1747(2)	0.1695(2)	0.5643(17)	0.0061(5)
	N4	0.4574(19)	0.0973(2)	0.0837(15)	0.0060(5)

[a] e.s.d.'s in parentheses

The M–N bond lengths are in a range between 2.569(3) and 3.107(3) Å (M = Ca), 2.647(5) and 2.951(4) Å (M = Sr), and 2.644(2) and 3.014(2) Å (M = Eu). The sum of the ionic radii corresponds well with the observed distances and is in a range characteristic for nitridosilicates.[16,18,20,42–47] The bond lengths for the 7 + 1 coordination are increased to 3.720(4) Å (M = Ca), 3.293(4) Å (M = Sr), and 3.498(2) Å (M = Eu).

2.1.3.3 Lattice-Energy Calculations

The consistency of the structure models was corroborated by lattice-energy calculations (MAPLE, MAdelung Part of Lattice Energy).[42,48–50] This algorithm computes electrostatic interactions in ionic crystals, depending on the charge, distance, and coordination spheres of the constituting atoms. The results of the MAPLE calculations are summarized in Table 2.1-3.

Table 2.1-3. Results of the MAPLE Calculations [kJ/mol] for $M[Mg_3SiN_4]$ with M = Ca,Sr,Eu; Δ = Difference [a]

	Ca	Sr	Eu
M^{2+}	1831	1728	1728
Mg^{2+}	2325 - 2420	2347 - 2430	2357 - 2413
Si^{4+}	9626	9606	9673
N^{3-}	5021 – 5138	4977 - 5091	4974 - 5106
Total	38878	38623	38682
Δ	0.03%	0.5%	0.4%

Total MAPLE
($AESiN_2 + Mg_3N_2$ (*AE* = Ca,Sr); $Eu_2SiN_3 + Mg_3N_2$ - EuN)
M = Ca: 38865 kJ/mol; *M* = Sr: 38447 kJ/mol; *M* = Eu: 38525 kJ/mol

[a] Typical MAPLE values [kJ/mol]: Ca^{2+}: 1700–2200; Sr^{2+}: 1500-2100; Eu^{2+}: 1700-2100; Si^{4+}: 9000-10200; N^{3-}: 4300-6200;[16] Mg^{2+}: 2200-2400.

The partial MAPLE values are in good agreement with reference data reported before,[16] and partial MAPLE values for Mg^{2+} are listed in the Supporting Information. The comparison of the MAPLE sum of all compounds with total MAPLE values of constituting binary and ternary nitrides shows only a minor deviation. With these results, the electrostatic consistency is proven, and the crystal structures of the title compounds are confirmed.

2.1.3.4 Luminescence

Eu^{2+} doping of AE[Mg_3SiN_4] (AE = Ca,Sr) yielded red body colored samples. Under UV to blue irradiation, M[Mg_3SiN_4] (M = Ca,Eu) shows no luminescence; in contrast, Sr[Mg_3SiN_4]:Eu^{2+} exhibits luminescence in the red spectral region. In Figure 2.1-3a are presented excitation and emission spectra of a Sr[Mg_3SiN_4]:Eu^{2+} (2 mol % Eu^{2+}, nominal composition) bulk sample.

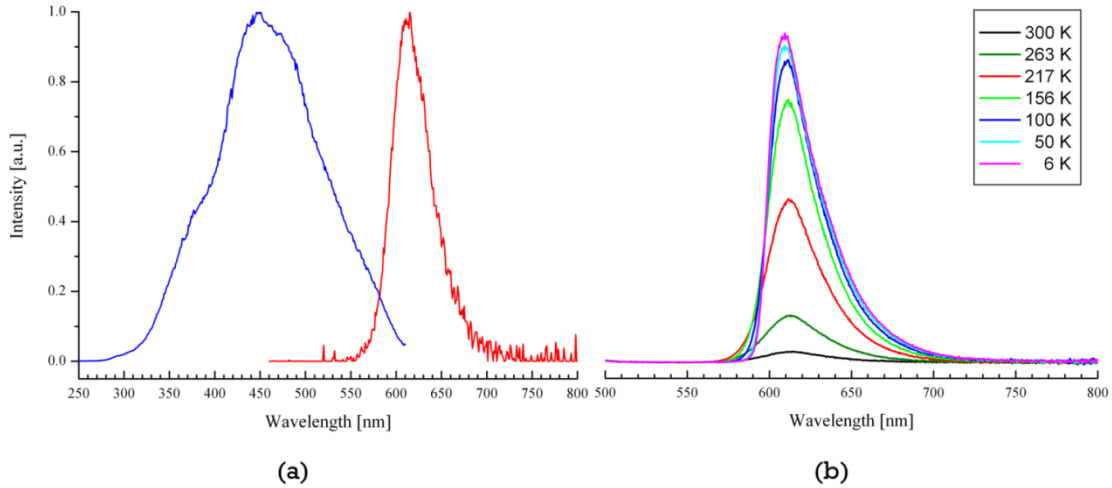

Figure 2.1-3. (a) Excitation (blue) and emission (red) spectra of Sr[Mg_3SiN_4]:Eu^{2+} (2 mol% Eu^{2+}, nominal composition), $\lambda_{exc,\,max}$ = 450 nm, λ_{em} = 615 nm, fwhm ~1170 cm^{-1} (~43 nm); (b) Low-temperature emission spectra of Sr[Mg_3SiN_4]:Eu^{2+} (2 mol% Eu^{2+}, nominal composition) between 6-300 K; both spectra were recorded at λ_{exc} = 440 nm.

The excitation spectrum of Sr[Mg_3SiN_4]:Eu^{2+} shows a broad band with a maximum at 450 nm. Hence, the compound can be excited very well by UV to blue light originating from a (In,Ga)N-LED. The emission spectrum of Sr[Mg_3SiN_4]:Eu^{2+} (λ_{exc} = 440 nm) shows a narrow band peaking at 615 nm with a full width at half-maximum (fwhm) of only ~1170 cm^{-1} (~43 nm). To the best of our knowledge, this is the most narrow emission for Eu^{2+} phosphors in the red spectral region reported so far. Up to now, ($Ca_{1-x}Sr_x$)Se:Eu^{2+} showed the smallest fwhm of ~1390 cm^{-1} (50 nm) in the red spectral region.[51] The emission band in Figure 2.1-3a is assigned to the parity allowed $4f^6 5d^1 \rightarrow 4f^7$ transition in Eu^{2+}. There is only one crystallographic Sr site, and according to the comparable ionic radii of Sr^{2+} (1.23 Å) and Eu^{2+} (1.22 Å),[42] it can be assumed that the luminescence originates from Eu^{2+} in a cuboid surrounding.

The Stokes shift of $Sr[Mg_3SiN_4]:Eu^{2+}$ was determined by the method shown, for example, by Nazarov et al.[52] and van Haecke et al.[53] to a value of ~772 cm^{-1}. $Sr_2Si_5N_8:Eu^{2+}$ shows a similar emission maximum around 620 nm, but with a significantly larger fwhm of ~2050-2600 cm^{-1} (~85-90 nm).[5,15,54–57] Another red phosphor used in illumination-grade white pc-LEDs, $(Ca,Sr)SiAlN_3:Eu^{2+}$ (λ_{em} ~610-660 nm, fwhm ~2100-2500 cm^{-1} (~90 nm)), shows values similar to those of $Sr_2Si_5N_8:Eu^{2+}$.[58,59] For the investigation of the thermal behavior of $Sr[Mg_3SiN_4]:Eu^{2+}$, low-temperature luminescence measurements down to 6 K were carried out. The luminescence spectra are depicted in Figure 2.1-3b. The emission maxima are slightly shifted from 615 nm at room temperature to 610 nm at 6 K. Also, the fwhm is reduced from ~1170 cm^{-1} (~43 nm) to ~900 cm^{-1} (~33 nm). The emission intensity increases significantly by cooling, and relative quantum efficiencies close to 100% are being reached at low temperatures. The very small Stokes shift of $Sr[Mg_3SiN_4]:Eu^{2+}$ of only ~772 cm^{-1} should lead to a good thermal behavior; other loss mechanisms (e.g., photoionization), due to a low band gap (see below), are most likely the reason for reduced luminescence efficacies at higher temperatures.[60,61]

Ce^{3+}-doped samples exhibit yellow luminescence under blue irradiation of the fawn body colored compound. In Figure 2.1-4 is displayed the emission spectrum of a $Ca[Mg_3SiN_4]:Ce^{3+}$ (2 mol% Ce^{3+}, nominal concentration) bulk sample. At 460 nm excitation, a broad-band emission with two maxima at 530 and 585 nm with an overall fwhm of ~3900 cm^{-1} (~130 nm) is observed for $Ca[Mg_3SiN_4]:Ce^{3+}$. The broad emission band is typical for Ce^{3+}-doped materials, due to the spin and parity allowed $5d^1 \rightarrow 4f^1$ transition in Ce^{3+}.

The excitation spectrum displays a maximum peaking at 480 nm, so the compound can be effectively excited by UV to blue light. The activator ions Ce^{3+} and Eu^{2+} are expected to occupy the M site in $M[Mg_3SiN_4]$ with M = Ca,Sr,Eu, hence doping of the Ca compound with Ce^{3+} is more favorable, according to similar ionic radii (Ca^{2+}, 1.05 Å; Ce^{3+}, 1.01 Å), than with Eu^{2+}.[42]

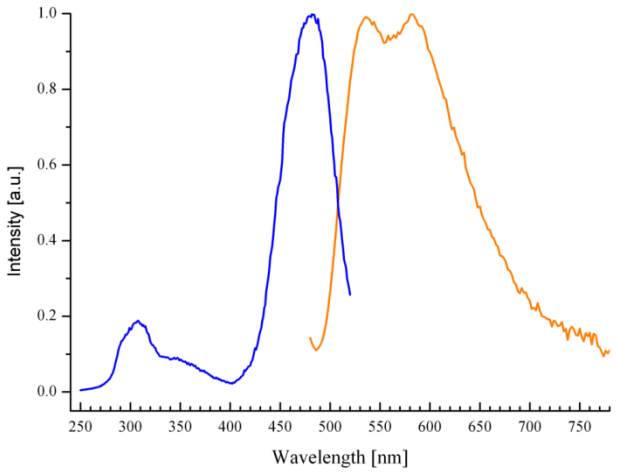

Figure 2.1-4. Excitation (blue) and emission (orange) spectra of $Ca[Mg_3SiN_4]:Ce^{3+}$ (2 mol% Ce^{3+}, nominal composition). Excitation spectrum: $\lambda_{exc,\,max}$ = 480 nm. Emission spectrum: λ_{em} = 530 and 585 nm, fwhm overall ~3900 cm^{-1} (~130 nm) recorded at λ_{exc} = 460 nm.

Charge balancing could be easily achieved by defects in the crystal structure, for example, cation vacancies or a small variation in the atomic ratio Mg^{2+}:Si^{4+}. Other Ce^{3+}-doped materials like $Y_3Al_5O_{12}:Ce^{3+}$ (YAG:Ce) show emission in the same spectral region.[62,63]The emission band of YAG:Ce is centered at ~550–570 nm with a fwhm of ~3700 cm^{-1} (~120 nm). Another yellow-emitting phosphor is $CaAlSiN_3:Ce^{3+}$, with an emission maximum of 580 nm and a fwhm value of ~3900 cm^{-1} (~130 nm), being slightly red-shifted as compared to YAG:Ce.[14,64]

2.1.3.5 UV/vis Spectroscopy

Further investigations on $Sr[Mg_3SiN_4]:Eu^{2+}$ were carried out by UV/vis spectroscopy. Particularly, determination of the band gap was done with UV/vis-reflectance data. A non-doped bulk sample of $Sr[Mg_3SiN_4]$ was investigated (see Figure 2.1-5). The spectrum shows a drop in reflection in the blue region around 430 nm, corresponding to the valence-to-conduction band transition of the host lattice. From the absorption edge in the UV region, a value of ~3.9 eV for the band gap of $Sr[Mg_3SiN_4]$ was derived.

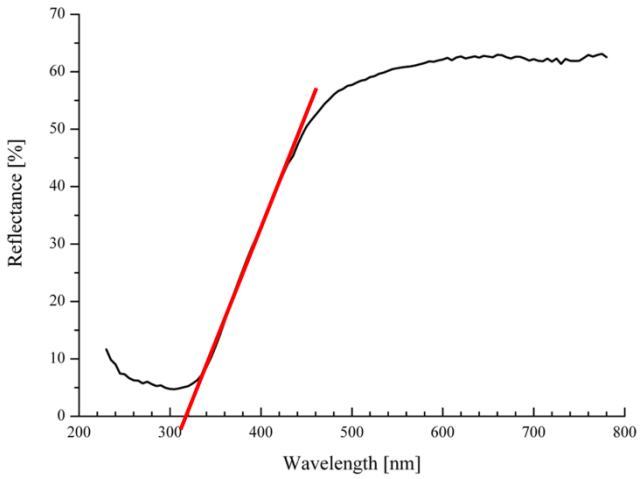

Figure 2.1-5. UV/vis-reflection spectrum of $Sr[Mg_3SiN_4]$. The red line is drawn tangent to the slope of the reflectance curve, at the point of intersection with the abscissa the value of the band gap was estimated.

The intense reflectance in the visible spectral range is in good agreement with the off-white body color of nondoped $Sr[Mg_3SiN_4]$. Several investigations in literature concerning the band gap of $Sr_2Si_5N_8$ were carried out, and a value of 4.9 eV is in accordance with most authors.[10,54-56,65] The results from UV/vis-reflectance data show that the band gap of $Sr[Mg_3SiN_4]$ is ~1.0 eV smaller than the value for $Sr_2Si_5N_8$ and may account for the different high-temperature luminescence efficacies of the respective Eu^{2+}-doped materials.

2.1.3.6 ^{29}Si-MAS NMR

Over the last couple of years, numerous nitridosilicates have been investigated using solid-state MAS NMR, resulting in a δ scale ranging from -28 ppm in reduced nitridosilicates[66] to -68 ppm for oxonitridosilicates.[67] Usually, the chemical shift of ^{29}Si in nitrides is found in the region between -40 and -60 ppm.[18,20,66,67]

For the measurement, a non-doped sample of $Sr[Mg_3SiN_4]$ was used. The ^{29}Si-MAS NMR spectrum (see Figure 2.1-6) shows one narrow peak at -36.69 ppm, which is in accordance with one crystallographic Si site. Furthermore, the ^{29}Si chemical shift is found upfield as compared to other highly condensed nitridosilicates.[18,20]

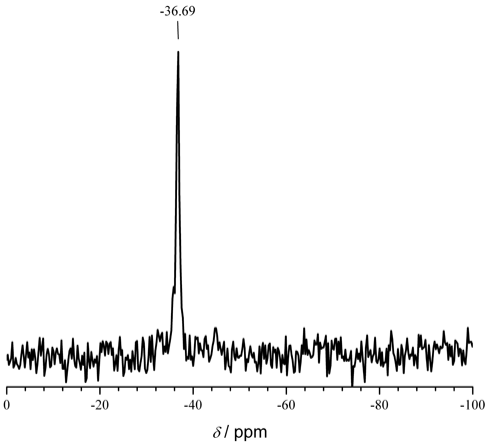

Figure 2.1-6. ^{29}Si-MAS NMR spectrum of Sr[Mg_3SiN_4] (rotation frequency 10 kHz).

Probably, the shift may originate from the linkage of the SiN_4 tetrahedra to less charged MgN_4 tetrahedra. Furthermore, it is the first ^{29}Si-MAS NMR spectrum of a nitridosilicate with formally not to each other linked SiN_4 tetrahedra and extends the range of the ^{29}Si chemical shift found for nitridosilicates in the upfield region.

2.1.4 Conclusion

The luminous efficacy of illumination-grade white pc-LEDs is limited by the performance of the red component, as the corresponding luminescence spectrum shows a large proportion of emission intensity in the deep red to infrared spectral region, where the human eye sensitivity is very low.[8] Hence, it is incidental to reduce the losses in the low-energy visible region for a better adaption to the human eye sensitivity. In this contribution, a new subgroup of nitridosilicates, the nitridomagnesosilicates M[Mg_3SiN_4] with M = Ca,Sr,Eu, have been identified as superior host lattices for Eu^{2+} doping. Especially, Sr[Mg_3SiN_4]:Eu^{2+} has the potential to fulfill the requirements as a next-generation red phosphor material with an fwhm of only ∼1170 cm^{-1} (∼43 nm), which is the most narrow value for Eu^{2+} phosphors in the red spectral region reported so far. This outstanding luminescence properties can be ascribed to some special structural features. The host lattice is built up by a rigid network of $[Mg_3SiN_4]^{2-}$, which is considered as being beneficial for reducing lattice-phonon energies, thus inhibiting relaxation through nonradiative pathways. Furthermore, there is only one crystallographic site for the activator in the ordered

network. Both features reduce inhomogeneous line broadening to a minimum, which are often caused by differing crystal fields around the activator sites. Additionally, high site symmetry, for example, cuboidal coordination as in $M[Mg_3SiN_4]$ (M = Ca,Sr,Eu), is considered as being favorable for a small Stokes shift, and thus a narrower emission band because the structural relaxation of Eu^{2+} in its excited state is hindered.[60,68] $BaSi_2O_2N_2:Eu^{2+}$, a narrow-band green phosphor (λ_{em} = 490 nm, fwhm = 1250 cm^{-1} (~35 nm)), shows a similar cuboidal surrounding.[69,70] For future application in illumination-grade white pc-LEDs, there are still some challenges to overcome. The small band gap of $Sr[Mg_3SiN_4]:Eu^{2+}$ leads to significant thermal quenching of the luminescence. A detailed investigation of the electronic structure is an issue of upcoming work to uncover improvement paths by means of, for example, band gap engineering. Efforts in this direction are justified by the outstanding luminous efficacy of the emission band, which renders $Sr[Mg_3SiN_4]:Eu^{2+}$ attractive for application in high-power illumination-grade white phosphor-converted LEDs.

2.1.5 References

(1) *International Energy Outlook 2013*; U.S. Energy Information Administration, Office of Energy Analysis, U.S. Department of Energy: Washington, DC, 2013.

(2) U.S. Energy Information Administration (EIA) - FAQ; http:// www.eia.gov/tools/faqs/faq.cfm?id=99&t=3 (accessed Nov 14th, 2013).

(3) Born, M.; Jüstel, T. *Chem. Unserer Zeit* **2006**, *40*, 294.

(4) Feldmann, C. *Z. Anorg. Allg. Chem.* **2012**, *638*, 2169.

(5) Mueller-Mach, R.; Mueller, G.; Krames, M. R.; Höppe, H. A.; Stadler, F.; Schnick, W.; Juestel, T.; Schmidt, P. *Phys. Status Solidi A* **2005**, *202*, 1727.

(6) Setlur, A. *Electrochem. Soc. Interface* **2009**, *18*, 32.

(7) Xie, R.-J.; Hirosaki, N.; Takeda, T.; Suehiro, T. *ECS J. Solid State Sci. Technol.* **2013**, *2*, R3031.

(8) Krames, M. R.; Mueller, G. O.; Mueller-Mach, R. B.; Bechtel, H.-H.; Schmidt, P. J. Wavelength conversion for producing white light from high power blue LED. PCT Int. Appl. WO 2010131133 A1, November 18th, 2010.

(9) He, X.-H.; Lian, N.; Sun, J.-H.; Guan, M.-Y. J. *Mater. Sci.* **2009**, *44*, 4763.

(10) ten Kate, O. M.; Zhang, Z.; Dorenbos, P.; Hintzen, H. T.; van der Kolk, E. *J. Solid State Chem.* **2013**, *197*, 209.

(11) Uheda, K.; Hirosaki, N.; Yamamoto, H. *Phys. Status Solidi A* **2006**, *203*, 2712.

(12) Uheda, K.; Hirosaki, N.; Yamamoto, Y.; Naito, A.; Nakajima, T.; Yamamoto, H. *Electrochem. Solid-State Lett.* **2006**, *9*, H22.

(13) Watanabe, H.; Kijima, N. *J. Alloys Compd.* **2009**, *475*, 434.

(14) Xie, R.-J.; Hirosaki, N.; Li, Y.; Takeda, T. *Materials* **2010**, *3*, 3777.

(15) Zeuner, M.; Schmidt, P. J.; Schnick, W. *Chem. Mater.* **2009**, *21*, 2467.

(16) Zeuner, M.; Pagano, S.; Schnick, W. *Angew. Chem. Int. Ed.* **2011**, *50*, 7754.

(17) Pagano, S.; Lupart, S.; Schmiechen, S.; Schnick, W. *Z. Anorg. Allg. Chem.* **2010**, *636*, 1907.

(18) Zeuner, M.; Pagano, S.; Hug, S.; Pust, P.; Schmiechen, S.; Scheu, C.; Schnick, W. *Eur. J. Inorg. Chem.* **2010**, *2010*, 4945.

(19) Tapia-Ruiz, N.; Segalés, M.; Gregory, D. H. *Coord. Chem. Rev.* **2013**, *257*, 1978.

(20) Lupart, S.; Schnick, W. *Z. Anorg. Allg. Chem.* **2012**, *638*, 2015.

(21) Atkins, P.; Overton, T.; Rourke, J.; Weller, M.; Armstrong, F. *Shriver and Atkins' Inorganic Chemistry*, 4th ed.; Oxford University Press: Oxford, 2006; p 259.

(22) Lee, B.; Lee, S.; Jeong, H. G.; Sohn, K. S. *ACS Comb. Sci.* **2011**, *13*, 154.

(23) Lee, S.-H.; Kim, K.-B.; Kim, J.-M.; Jeong, Y.-K.; Kang, J.-G. *Phys. Status Solidi A* **2013**, *210*, 1093.

(24) David, J.; Laurent, Y.; Lang, J. *Bull. Soc. Fr. Mineral. Cristallogr.* **1970**, *93*, 153.

(25) Petukhov, A. G.; Lambrecht, W. R. L.; Segall, B. *Phys. Rev. B: Condens. Matter* **1994**, *49*, 4549.

(26) Yamane, H.; Morito, H. *J. Alloys Compd.* **2013**, *555*, 320.

(27) Lange, H.; Wötting, G.; Winter, G. *Angew. Chem. Int. Ed. Engl.* **1991**, *30*, 1579.

(28) Fair, H. D.; Walker, R. F. *Energetic Materials 1, Physics and Chemistry of Inorganic Azides*, 1st ed.; Plenum Press: New York, London, 1977.

(29) Schnick, W.; Huppertz, H.; Lauterbach, R. *J. Mater. Chem.* **1999**, *9*, 289.

(30) Sheldrick, G. M. *XPREP, v. 2008/2: Data Preparation & Reciprocal Space Exploration*; Bruker-AXS: WA, 2008.

(31) Sheldrick, G. M. *SADABS, v. 2: Multi-Scan Absorption Correction*; Bruker-AXS: WA, 2012.

(32) Sheldrick, G. M. *SHELXS-97: A program for crystal structure solution*; University of Göttingen: Germany, 1997.

(33) Sheldrick, G. M. *Acta Crystallogr., Sect. A* **2008**, *64*, 112.

(34) Sheldrick, G. M. *SHELXL-97: A program for crystal structure refinement*; University of Göttingen: Germany, 1997.

(35) Coelho, A. *TOPAS, v. 4.1: A program for Rietveld refinement*, Coelho Software; 2007.

(36) Harris, R. K.; Becker, E. D.; Cabral de Menezes, S. M.; Goodfellow, R.; Granger, P. *Solid State Nucl. Magn. Reson.* **2002**, *22*, 458.

(37) Nowitzki, B.; Hoppe, R. *Rev. Chim. Miner.* **1986**, *23*, 217.

(38) Park, D. G.; Dong, Y.; DiSalvo, F. J. *Solid State Sci.* **2008**, *10*, 1846.

(39) Behrens, R. K.; Jeitschko, W. *Monatsh. Chem.* **1987**, *118*, 43.

(40) Liebau, F. *Structural Chemistry of Silicates*; Springer: Berlin, NY, 1985.

(41) The term *vierer* ring was coined by Liebau and is derived from the german word “vier”; however, a *vierer* ring is not a four-membered ring, but an eight-membered ring comprising four tetrahedra centers.

(42) Baur, W. H. *Crystallogr. Rev.* **1987**, *1*, 59.

(43) Huppertz, H.; Schnick, W. *Z. Anorg. Allg. Chem.* **1997**, *623*, 212.

(44) Schnick, W.; Huppertz, H. *Chem.-Eur. J.* **1997**, *3*, 679.

(45) Gal, Z. A.; Mallinson, P. M.; Orchard, H. J.; Clarke, S. J. *Inorg. Chem.* **2004**, *43*, 3998.

(46) Ottinger, F.; Nesper, R. *Z. Anorg. Allg. Chem.* **2005**, *631*, 1597.

(47) Yamane, H.; Morito, H. *Inorg. Chem.* **2013**, *52*, 5559.

(48) Hübenthal, R. *MAPLE, v. 4: A program for the calculation of Madelung part of lattice energy*; University of Gießen: Germany, 1993.

(49) Hoppe, R. *Angew. Chem. Int. Ed. Engl.* **1966**, *5*, 95.

(50) Hoppe, R. *Angew. Chem. Int. Ed. Engl.* **1970**, *9*, 25.

(51) Zhang, X.; Liang, L.; Zhang, J.; Su, Q. *Mater. Lett.* **2005**, *59*, 749.

(52) Nazarov, M.; Tsukerblat, B.; Noh, D. Y. *J. Phys. Chem. Solids* **2008**, *69*, 2605.

(53) Van Haecke, J. E.; Smet, P. F.; Poelman, D. *J. Lumin.* **2007**, *126*, 508.

(54) Li, Y. Q.; van Steen, J. E. J.; van Krevel, J. W. H.; Botty, G.; Delsing, A. C. A.; DiSalvo, F. J.; de With, G.; Hintzen, H. T. *J. Alloys Compd.* **2006**, *417*, 273.

(55) Piao, X.; Horikawa, T.; Hanzawa, H.; Machida, K.-i. *Appl. Phys. Lett.* **2006**, *88*, 161908.

(56) Piao, X.; Machida, K.-i.; Horikawa, T.; Yun, B. *J. Lumin.* **2010**, *130*, 8.

(57) Zeuner, M.; Hintze, F.; Schnick, W. *Chem. Mater.* **2008**, *21*, 336.

(58) Li, J. W.; Watanabe, T.; Sakamoto, N.; Wada, H. S.; Setoyama, T.; Yoshimura, M. *Chem. Mater.* **2008**, *20*, 2095.

(59) Li, Y. Q.; Hirosaki, N.; Xie, R.-J.; Takada, T.; Yamamoto, Y.; Mitomo, M.; Shioi, K. *Int. J. Appl. Ceram. Technol.* **2010**, *7*, 787.

(60) Meijerink, A.; Blasse, G. *J. Lumin.* **1989**, *43*, 283.

(61) Dorenbos, P. *J. Phys.: Condens. Matter* **2005**, *17*, 8103.

(62) Moriguchi, T.; Noguchi, Y.; Sakano, K.; Shimizu, Y. Light emitting device having a nitride compound semiconductor and a phosphor containing a garnet fluorescent material. US 5998925 A, July 29th, 1997.

(63) Blasse, G.; Bril, A. *Appl. Phys. Lett.* **1967**, *11*, 53.

(64) Li, Y. Q.; Hirosaki, N.; Xie, R. J.; Takeda, T.; Mitomo, M. *Chem. Mater.* **2008**, *20*, 6704.

(65) Xie, R.-J.; Hirosaki, N.; Kimura, N.; Sakuma, K.; Mitomo, M. *Appl. Phys. Lett.* **2007**, *90*, 191101.

(66) Stadler, F.; Oeckler, O.; Senker, J.; Höppe, H. A.; Kroll, P.; Schnick, W. *Angew. Chem. Int. Ed.* **2005**, *44*, 567.

(67) Stadler, F.; Schnick, W. *Z. Anorg. Allg. Chem.* **2006**, *632*, 949.

(68) Dirksen, G. J.; Blasse, G. *J. Solid State Chem.* **1991**, *92*, 591.

(69) Kechele, J. A.; Oeckler, O.; Stadler, F.; Schnick, W. *Solid State Sci.* **2009**, *11*, 537.

(70) Li, Y. Q.; Delsing, A. C. A.; de With, G.; Hintzen, H. T. *Chem. Mater.* **2005**, *17*, 3242.

2.2 Nitridomagnesosilicate $Sr[Mg_3SiN_4]$: Optical properties of Ce^{3+},Pr^{3+},Sm^{3+}, Eu, Yb Doping and Energy-Level Locations of all Lanthanides in the Host Lattice

Sebastian Schmiechen, Robin Niklaus, Petra Huppertz, Detlef Wiechert, Peter J. Schmidt, and Wolfgang Schnick.

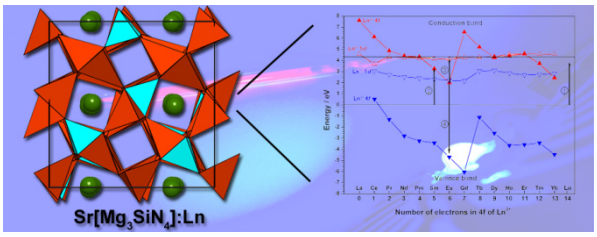

Published in: *To be published*

Abstract

RE-doped $Sr[Mg_3SiN_4]$ (RE = Ce^{3+},Pr^{3+},Sm^{3+},Eu,Yb) was synthesized by means of a modified solid-state metathesis reaction in sealed Ta ampules. The optical properties of the respective compounds were studied. The Ce^{3+}-doped sample shows typical $5d^1 \rightarrow 4f^1$ emission (λ_{em} = 545 and 605 nm, fwhm ~3840 cm^{-1}). Pr^{3+}- and Sm^{3+}-doped samples exhibit typical $4f \rightarrow 4f$ line emission in the green (Pr^{3+}) and red (Sm^{3+}) part of the visible spectrum. UV/vis-reflectance data of $Sr[Mg_3SiN_4]:Pr^{3+}$ also hint at $4f^2 \rightarrow 4f^15d^1$ absorption. The Sm^{3+} CTB was estimated at ~3.2 eV from diffuse-reflectance data. Besides, the $5d \rightarrow 4f$ emission of the RE^{2+}-doped compounds typical for nitridic surroundings, the Eu- and Yb-doped samples also show $4f \rightarrow 4f$ line emissions typical for RE^{3+}-doped compounds. This behavior occurs possibly due to photoionization of RE^{2+} and subsequent absorption and excitation at the *in situ* formed RE^{3+}. With the acquired spectroscopic data a detailed energy-level diagram of the $Sr[Mg_3SiN_4]$ host lattice containing the 4*f* ground state and the lowest excited 5*d* levels of all divalent and trivalent lanthanides was constructed and discussed.

2.2.1 Introduction

Recently, numerous novel multinary nitrides exhibiting narrow-band red emission properties after doping with Eu^{2+} were reported and are being discussed for application as novel red component in phosphor-converted light-emitting diodes (pc-LED).[1-4] Particularly, the nitridomagnesosilicate $Sr[Mg_3SiN_4]:Eu^{2+}$ displays outstanding emission properties. Yet, it shows the most narrow emission in the red part of the visible spectrum for Eu^{2+}-doped phosphors with a full width at half maximum (fwhm) of only ~1170 cm^{-1} (λ_{em} = 615 nm).[1] These superior emission properties are attributed to several specific structural features of the host lattice. The compound crystallizes in the $Na[Li_3SiO_4]$ structure type exhibiting a highly condensed three-dimensional and rigid network of crystallographically ordered SiN_4 and MgN_4 tetrahedra.[1,5] Additionally, there is only one heavy atom site where Sr^{2+} can be substituted by the dopant Eu^{2+}. Furthermore, the heavy atom site is coordinated cuboidally by eight N^{3-}. Especially the latter feature is discussed as a major reason for the outstandingly narrow fwhm of $Sr[Mg_3SiN_4]:Eu^{2+}$ and its substitutional variants, for example $AE[LiAl_3N_4]:Eu^{2+}$ (AE = Ca,Sr).[1-4,6] Nevertheless, for practical applications there are more aspects to be considered. At the operating temperature of a pc-LED (~150 °C) the phosphor material should still show high quantum efficiencies (QE).[7] $Sr[Mg_3SiN_4]:Eu^{2+}$ already exhibits severe thermal quenching at room temperature with a QE ~2%. Therefore, it is reasonable to take a closer look at the electronic structure of the host lattice to find pathways for improvement of the QE. The band gap of the $Sr[Mg_3SiN_4]$ host lattice was estimated to ~3.9 eV from UV/vis-reflectance data giving a first hint on the loss mechanism. It was assumed that the small band gap could lead to photoionization of Eu^{2+} to Eu^{3+} and therefore to reduced efficiency.[1] As will be shown later, it is more important to locate the energetic levels of the 4*f* ground states and lowest 5*d* excited states of the lanthanide dopants within the electronic structure of the host lattice.[8,9] Dorenbos recently summarized his studies on lanthanides in inorganic compounds, establishing the redshift and charge-transfer models. These models allow the construction of energy-level diagrams of specific host lattices doped with lanthanides while requiring only very little spectroscopic data.[10-14] Recently,

Hintzen et al. reported on the construction of such energy-level diagrams for the compounds $M_2Si_5N_8$ (M = Ca,Sr,Ba) and $SrAlSi_4N_7$. With this powerful tool it was possible not only to locate the energy levels of the 4*f* and 5*d* states of all divalent and trivalent lanthanides in the respective host lattices. Furthermore, optical properties of not yet investigated lanthanides in the host lattices $M_2Si_5N_8$ and $SrAlSi_4N_7$ were predicted.[8,9]

Here, we focus on investigating the electronic structure of rare-earth (RE) doped $Sr[Mg_3SiN_4]$:RE (RE = Ce^{3+},Pr^{3+},Sm^{3+},Eu,Yb), enabling the construction of an energy-level diagram containing the energy levels of the 4*f* ground states and lowest 5*d* excited states of all divalent and trivalent lanthanides in the $Sr[Mg_3SiN_4]$ host lattice. Therefore, optical data of $Sr[Mg_3SiN_4]$:RE were evaluated.

2.2.2 Experimental Section

2.2.2.1 Syntheses

The syntheses of $Sr[Mg_3SiN_4]$:RE was carried out in sealed tantalum ampules in a modified solid-state metathesis reaction as already described in previous work.[1] Owing to the sensitivity against air and moisture of the starting materials, all manipulations were performed in flame-dried Schlenk-type glassware attached to a vacuum line (10^{-3} mbar) or in an argon-filled glovebox (Unilab, MBraun, Garching, O_2 <1 ppm, H_2O <1 ppm). Typically, the syntheses started from a stoichiometric mixture of 0.60 mmol SrF_2 (75.36 mg, Sigma-Aldrich, 99.99%), Mg_3N_2 (60.54 mg, Sigma-Aldrich, 99.5%), and "$Si(NH)_2$" (34.86 mg, synthesized according to the method by Lange et al.).[15] For the investigation of the optical properties of $Sr[Mg_3SiN_4]$:RE (RE = Ce,Pr,Sm,Eu,Yb) 3 mol% (nominal composition) of the respective rare-earth fluorides REF_3 (all from Sigma-Aldrich, 99.99%) were added. An excess of 1.26 mmol LiN_3 (61.62 mg, synthesized according to the method by Fair et al.)[16] was used as nitrogen source and for charge compensation of $(Sr^{II}_{1-2x}RE^{III}_xLi^+_x)[Mg_3SiN_4]$. All starting materials were ground in a glove box and then filled into Ta ampules. Subsequently, the ampules were arc-welded under Ar atmosphere and water cooling to prevent any unintended chemical reaction. Subsequently, the sealed ampules were heated in an

evacuated silica tube to 950 °C within 3 h and maintained at this temperature for 24 h. Finally, the reaction mixtures were quenched to room temperature by switching off the furnace and then stored under Ar atmosphere inside a glove box.

2.2.2.2 Powder X-ray Diffraction

The phase composition of the $Sr[Mg_3SiN_4]$:RE samples was investigated by powder X-ray diffraction (PXRD). The corresponding data were collected on a STOE STADI P diffractometer (Cu-$K_{\alpha1}$ radiation, Ge(111) monochromator, Mythen1K detector) in Debye-Scherrer geometry with sealed glass capillaries. Rietveld refinements were carried out using the TOPAS Academic 4.1 package.[17-19] The powder diffractograms are depicted in the Supporting Information.

2.2.2.3 UV/vis Spectroscopy

Optical properties of $Sr[Mg_3SiN_4]$:RE were investigated on a Jasco V-650 UV/vis spectrophotometer with a deuterium and a halogen lamp (Czerny Turner monochromator with 1200 lines/mm concave grating, photomultiplier tube detector). The diffuse reflectance spectra were measured between 200 and 800 nm with 5 nm step size.

2.2.2.4 Luminescence

Luminescence properties of RE-doped $Sr[Mg_3SiN_4]$ were investigated with a VUV spectrometer. The samples were measured inside sealed quartz capillaries. The excitation wavelength was chosen to 254 nm with a spectral width of 10 nm. Emission spectra were collected in the wavelength range between 450 and 800 nm with 2 nm step size.

2.2.3 Results and Discussion

2.2.3.1 Phase Formation of $Sr[Mg_3SiN_4]$:RE (RE = Ce,Pr,Sm,Eu,Yb)

The here described modified solid-state metathesis route proved to be a powerful tool in modern inorganic syntheses.[20] This route enables access to new compounds in

relatively short reaction times and numerous novel nitridosilicates have thus been synthesized recently.[1,6,21] The formation of LiF is the driving force of this reaction type and its presence as a side phase is no hindrance for further investigations. All five RE-doped compounds were synthesized according to Eq. 1.

$$SrF_2 + Mg_3N_2 + \text{“}Si(NH)_2\text{”} + 2\ LiN_3 + REF_3\ (3\ mol\%) \longrightarrow Sr[Mg_3SiN_4]:RE + 2\ LiF \qquad \text{Eq. 1}$$

Synthetic success was verified by Rietveld refinement and the final refinement of $Sr[Mg_3SiN_4]:Ce^{3+}$ is depicted exemplarily in Fig. 2.2-1. Further powder diffractograms are given in the Supporting Information.

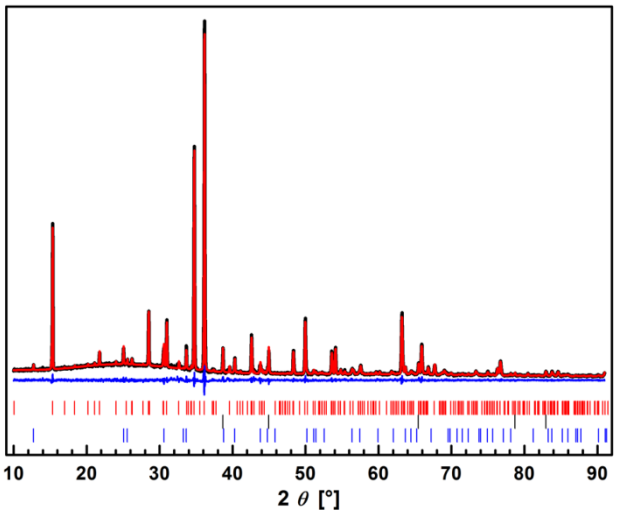

Figure 2.2-1. Rietveld refinement of $Sr[Mg_3SiN_4]:Ce^{3+}$ PXRD data (Cu-$K_{\alpha 1}$) with experimental data (black line), calculated pattern (red line) and difference curve (blue line). Tick marks give the positions of the refined phases: $Sr[Mg_3SiN_4]:Ce^{3+}$ (red, 81 wt%), LiF (black, 14 wt%) and SrClF (blue, 5 wt%).

All syntheses yielded $Sr[Mg_3SiN_4]$:RE with LiF as side phase and a small impurity of SrClF, which was formed due to a contamination of LiN_3 and/or “$Si(NH)_2$” with chlorides. $Sr[Mg_3SiN_4]:Ce^{3+}$ shows a dark yellowish body color and exhibits yellow to orange luminescence under UV to blue irradiation. Pr^{3+}-doped as well as Sm^{3+}-doped $Sr[Mg_3SiN_4]$ are white under daylight and show green (Pr^{3+}) and weak reddish (Sm^{3+}) luminescence under UV excitation. A red body color and emission under UV to blue irradiation is observed for $Sr[Mg_3SiN_4]:Eu^{2+}$. The Yb-doped sample is off-white under daylight and shows weak orange to red luminescence when irradiated with UV light.

2.2.3.2 Optical Properties of $Sr[Mg_3SiN_4]:Ce^{3+}$

Reflectance and emission spectra of Ce^{3+}-doped $Sr[Mg_3SiN_4]$ are shown in Fig. 2.2-2. The UV/vis-reflectance spectrum of $Sr[Mg_3SiN_4]:Ce^{3+}$ shows a drop in reflection around 315 nm that can be assigned to the host-lattice absorption of $Sr[Mg_3SiN_4]$ and defines the band gap of the compound with ~3.9 eV. The absorption band from 430-540 nm is attributed to Ce 4*f*-5*d* absorption as it is missing in the reflectance spectrum of the non-doped host lattice.[1] Furthermore, this absorption band in the visible spectral range is in good accordance with the dark-yellowish daylight color of $Sr[Mg_3SiN_4]:Ce^{3+}$.

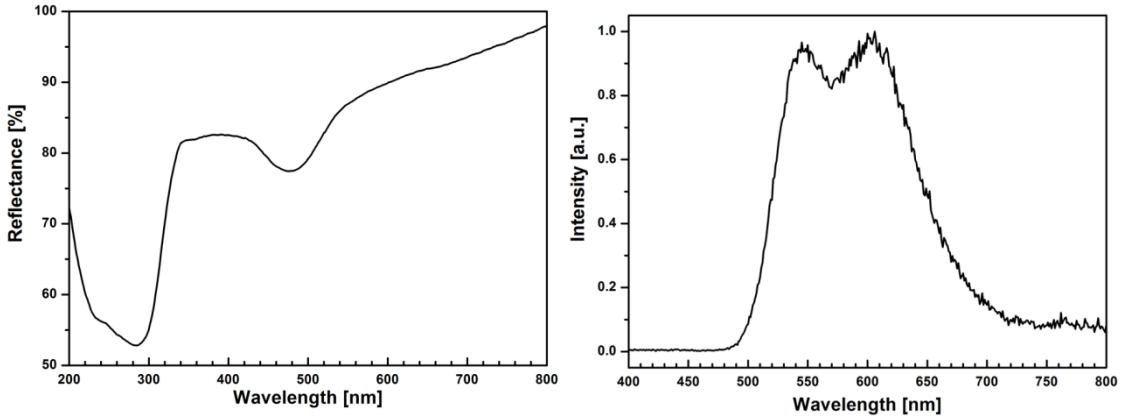

Figure 2.2-2. Left: Diffuse reflectance spectrum of $Sr[Mg_3SiN_4]:Ce^{3+}$. Right: Corresponding emission spectrum. Latter spectrum was measured at an excitation of 254 nm.

Excitation of $Sr[Mg_3SiN_4]:Ce^{3+}$ with light of 254 nm wavelength leads to emission in the yellow to orange region of the visible spectrum. The typical broad emission band has two maxima at 545 and 605 nm. The maxima are separated by ~1820 cm^{-1} and are typical for Ce^{3+} due to its spin-orbit splitting of the ground state ($^2F_{5/2}$ and $^2F_{7/2}$).[22] The asymmetric emission band shows an overall fwhm of ~3840 cm^{-1}.

2.2.3.3 Optical Properties of $Sr[Mg_3SiN_4]:Pr^{3+}$

In contrast to Ce^{3+}, Pr^{3+} with its two 4*f* electrons introduces 4*f*-4*f* transitions. Typical reflectance and emission spectra of $Sr[Mg_3SiN_4]:Pr^{3+}$ are shown in Fig. 2.2-3. The reflectance spectrum of Pr^{3+}-doped $Sr[Mg_3SiN_4]$ shows a drop in reflection at short wavelengths similar to that of Ce^{3+}-doped $Sr[Mg_3SiN_4]$ that is attributed to absorption of the host lattice. A small absorption band is found around 310-350 nm originating

from the $4f^2 \rightarrow 4f^1 5d^1$ transition of Pr^{3+}. In the visible range the typical 4*f*-4*f* absorption lines of Pr^{3+} are identified in the range of 430 to 510 nm. The absorption lines are attributed to the $^3H_4 \rightarrow {}^3P_x$ (x = 0-2) transitions and are centered at 450 (x = 2), 475 (x = 1) and 510 nm (x = 0), respectively.

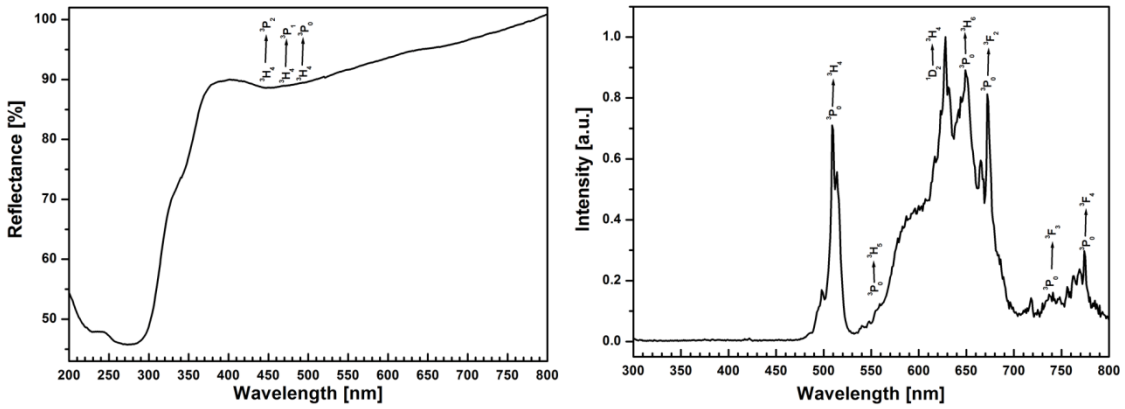

Figure 2.2-3. Left: Diffuse reflectance spectrum of $Sr[Mg_3SiN_4]:Pr^{3+}$. Right: Corresponding emission spectrum (λ_{exc} = 254 nm).

The emission spectrum of Pr^{3+}-doped $Sr[Mg_3SiN_4]$ was measured at an excitation wavelength of 254 nm. The 4*f*-4*f* emission of Pr^{3+} can occur from the $^3P_0$, $^1D_2$ and $^1G_4$ levels, but from latter level no emission was observed in the investigated range of 300 to 800 nm. The emission peaks can be assigned to $^3P_0 \rightarrow {}^3H_4$ (510 nm), $^3P_0 \rightarrow {}^3H_5$ (560 nm), $^1D_2 \rightarrow {}^3H_4$ (630 nm), $^3P_0 \rightarrow {}^3H_6$ (650 nm), $^3P_0 \rightarrow {}^3F_2$ (670 nm), $^3P_0 \rightarrow {}^3F_3$ (720 nm) and $^3P_0 \rightarrow {}^3F_4$ (775 nm), respectively.[22,23]

2.2.3.4 Optical Properties of $Sr[Mg_3SiN_4]:Sm^{3+}$

The ground state configuration of Sm^{3+} is $4f^5$, which will result in a more complicated energy-level structure and various possible transitions between the 4*f* levels compared to the lighter rare-earth elements. In Fig. 2.2-4 reflectance and emission spectra of $Sr[Mg_3SiN_4]:Sm^{3+}$ are shown.

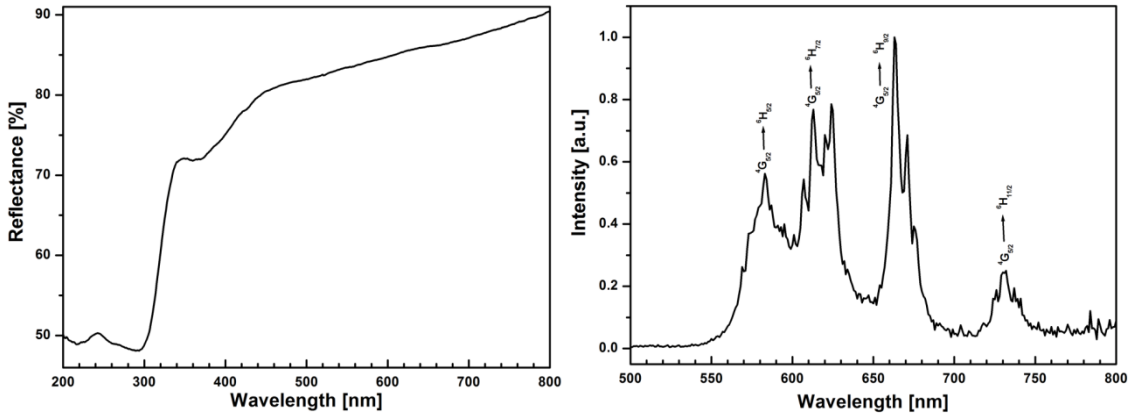

Figure 2.2-4. Left: Diffuse reflectance spectrum. Right: Corresponding emission spectrum (λ_{exc} = 254 nm) of $Sr[Mg_3SiN_4]:Sm^{3+}$.

In Addition to the absorption edge in the UV range around 315 nm, which is again attributed to the host lattice absorption, there is only one broad absorption band ranging from 350 to 420 nm visible in the diffuse-reflectance spectrum of Sm^{3+}-doped $Sr[Mg_3SiN_4]$. This absorption band can be assigned to the Sm^{3+} charge-transfer band (CTB). There are no 4*f*-4*f* absorption lines in the investigated range from 200-800 nm, which is in accordance with the typical Sm^{3+} 4*f*-4*f* absorption lines being centered in the infrared region.[22,23]

Under excitation of 254 nm the emission spectrum of $Sr[Mg_3SiN_4]:Sm^{3+}$ is composed of sharp peaks centered at 580, 610, 665 and 730 nm. These can be attributed to $^4G_{5/2} \rightarrow {}^6H_J$, J = 5/2, 7/2, 9/2 and 11/2, transitions in Sm^{3+}.[22,23] Neither, from reflectance nor from emission spectra there are hints on the presence of Sm^{2+}.

2.2.3.5 Optical Properties of $Sr[Mg_3SiN_4]:Eu^{2+}$

The luminescence properties of Eu^{2+}-doped $Sr[Mg_3SiN_4]$ have been reported previously, exhibiting the most narrow-band red emission for Eu^{2+}-doped phosphors with an fwhm ~1170 cm^{-1} at λ_{em} = 615 nm when excited at 440 nm. However, severe thermal quenching already occurs at room temperature. This behavior was attributed to the small band gap of the host lattice and therefore photoionization of Eu^{2+} by delocalization of the 5*d* electron into the conduction band followed by non-radiative recombination with the Eu^{3+} center.[1] Here, an UV/vis-reflectance and an emission spectrum excited at 254 nm are presented in Fig. 2.2-5.

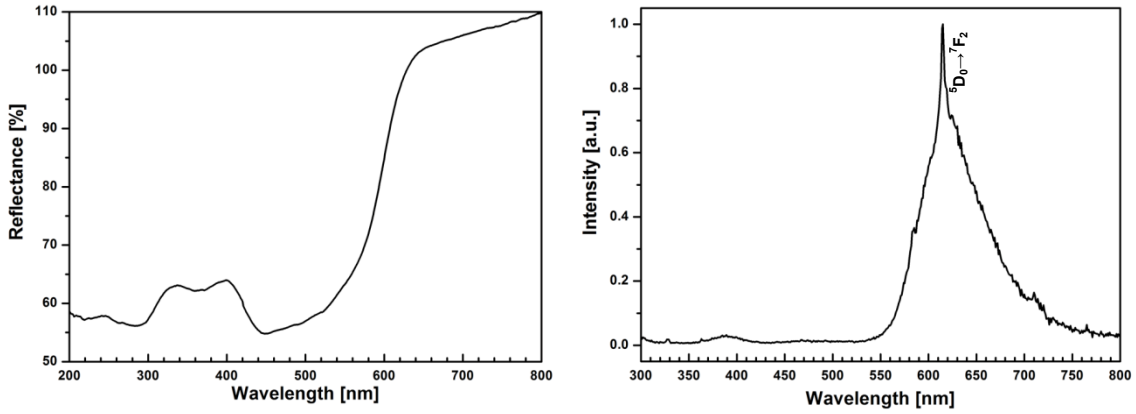

Figure 2.2-5. Left: Diffuse reflectance spectrum. Right: Corresponding emission spectrum (λ_{exc} = 254 nm) of $Sr[Mg_3SiN_4]$:Eu.

A broad absorption band ranging from 410 to 630 nm is identified in the UV/vis-reflectance spectrum of Eu-doped $Sr[Mg_3SiN_4]$. This band can be attributed to the 4*f*-5*d* absorption of Eu^{2+} and is in accordance with the intense red body color of $Sr[Mg_3SiN_4]:Eu^{2+}$. At lower wavelengths another absorption band from 340 to 380 nm is observed and may be assigned to the Eu^{3+} CTB or an energetically higher lying 5*d* state.[23]

The emission spectrum of $Sr[Mg_3SiN_4]:Eu^{2+}$ (λ_{exc} = 254 nm) shows a broad emission band centered at 615 nm with an fwhm of ~1280 cm^{-1} in addition to a sharp peak also centered at 615 nm. The broad emission band is typical for 5*d*-4*f* emission of Eu^{2+}. In contrast, the sharp peak is the typical $^5D_0 \rightarrow {}^7F_2$ emission of Eu^{3+} on a non-centrosymmetric site.[22,23]

2.2.3.6 Optical Properties of $Sr[Mg_3SiN_4]$:Yb

Besides Eu, Yb is also expected to be in oxidation state +2 in $Sr[Mg_3SiN_4]$. This assumption is corroborated by diffuse reflectance and emission spectra (see Fig. 2.2-6). The diffuse reflectance spectrum of $Sr[Mg_3SiN_4]$:Yb shows a broad absorption band covering the entire visible spectrum. In this region the 4*f*-5*d* absorption of Yb^{2+} and also the Yb^{3+} CTB are typically found. Yb^{3+} 4*f*-4*f* absorption lines are centered in the near infrared (NIR) region,[22,23] and could not be detected with the setup used. [22,23]

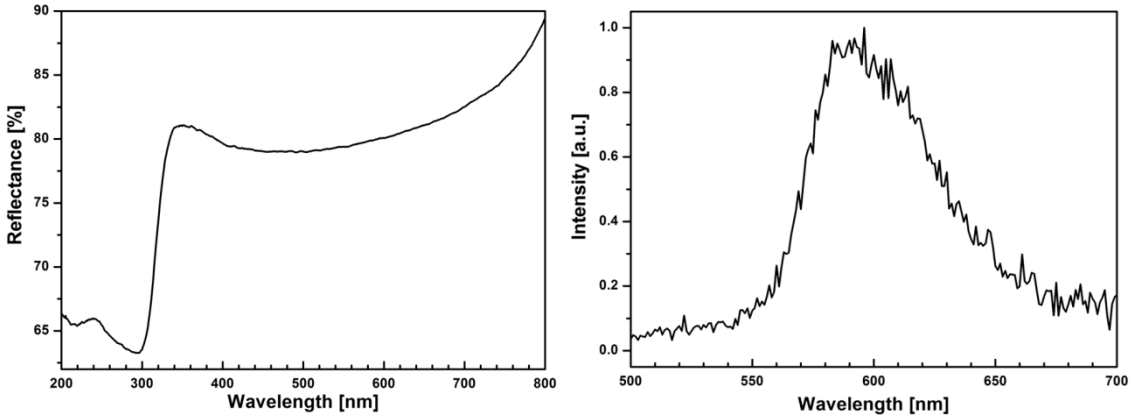

Figure 2.2-6. Left: Diffuse reflectance spectrum, Right: Corresponding emission spectrum (λ_{exc} = 254 nm) of $Sr[Mg_3SiN_4]$:Yb.

Since UV/vis-spectroscopy data does not show conclusive evidence as to whether Yb is in oxidation state +2 or +3, emission spectra of Yb-doped $Sr[Mg_3SiN_4]$ need to be consulted. $Sr[Mg_3SiN_4]$:Yb exhibits emission in the orange part of the visible spectrum. The maximum is centered at 590 nm with an fwhm of ~1230 cm^{-1}. This emission band is typical for the $4f^{13}d^1 \rightarrow 4f^{14}$ transition in Yb^{2+}. The 4*f*-4*f* emission of Yb^{3+} occurs at lower energy (i.e., higher wavelengths). An emission spectrum in the NIR region was therefore measured (see. Fig. 2.2-7). The emission spectrum was not corrected for the emission of the UV lamp used for the excitation of the sample. Therefore sharp emission peaks in the wavelength range of 700 to 910 nm are seen. The NIR emission spectrum of $Sr[Mg_3SiN_4]$:Yb exhibits typical $^2F_{5/2} \rightarrow {}^2F_{7/2}$ line emission of Yb^{3+} at 985 nm as well as 5*d*-4*f* emission of Yb^{2+} centered at 590 nm.[22,23]

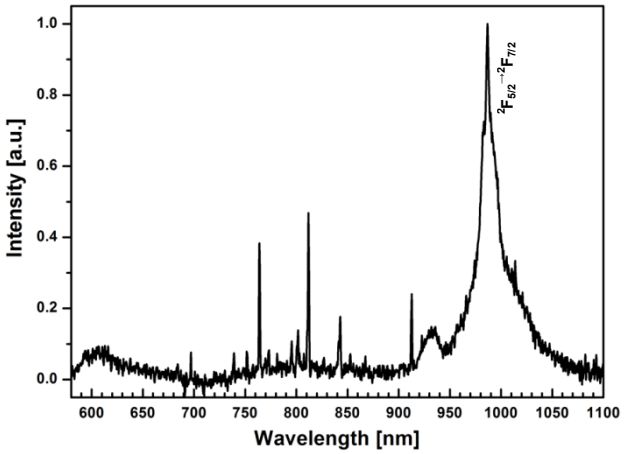

Figure 2.2-7. Uncorrected emission spectrum (λ_{exc} = 254 nm) of $Sr[Mg_3SiN_4]$:Yb. Sharp emission peaks in the range of 700 to 910 nm belong to the excitation lamp.

2.2.3.7 Energy-Level Diagram of Lanthanides in $Sr[Mg_3SiN_4]$

Many investigations concerning the optical properties of various lanthanide-doped compounds were conducted by Dorenbos et al. over the last decades and empirical coherences were found between the different lanthanides. With these results it is possible to construct an energy-level diagram that gives the energetic levels of the 4*f* and 5*d* states of all divalent and trivalent lanthanides with respect to the valence and conduction band in a specific host lattice. It is sufficient to have the spectroscopic data of only few lanthanides, for example Sm^{3+} or Eu^{2+}, to predict the properties of all other lanthanides.[8-14] For the construction of an energy-level diagram of the $Sr[Mg_3SiN_4]$ host lattice it is necessary to first determine the optical band gap of the compound. The band gap was derived from UV/vis-reflectance data of a non-doped sample of $Sr[Mg_3SiN_4]$ to ~3.9 eV (arrow 1 in Fig. 2.2-8).[1] According to Hintzen et al. this value marks the exciton creation energy E^{ex} at ambient temperature and would be located at 0.1 eV higher in energy at 10 K.

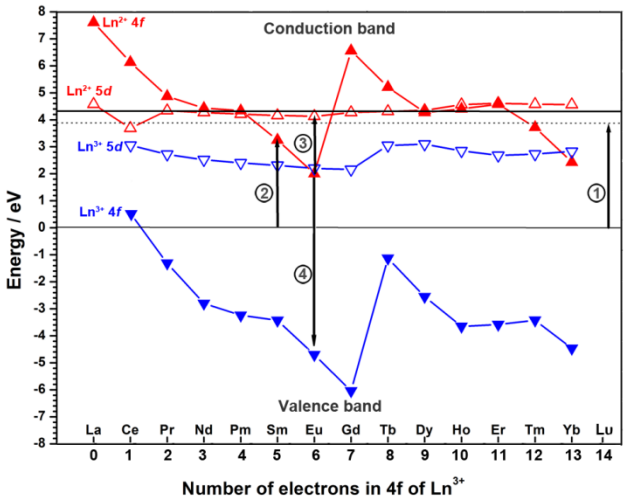

Figure 2.2-8. Energy-level diagram of the $Sr[Mg_3SiN_4]$ host lattice showing the 4*f* ground states and the lowest 5*d* states of all trivalent and divalent lanthanides with respect to the valence and conduction band. The horizontal dashed line marks the optical band gap (E^{ex}) and the horizontal solid line the electronic band gap (E^{ex}(10 K) + 8%).

Dorenbos showed that the electronic band gap can be derived from the optical band gap by the addition of an excess of 8% to the value of E^{ex} at 10 K, therefore the electronic band gap is ~4.3 eV (horizontal solid line above arrow 1 in Fig. 2.2-8).[24] One

important gain from the Dorenbos investigations is the establishment of the charge-transfer model. With this model it is possible to locate the 4*f* ground-state levels of Ln^{2+}. These can be derived for example from the CTB of Sm^{3+} shown in the reflectance spectrum of $Sr[Mg_3SiN_4]:Sm^{3+}$ (Fig. 2.2-4, left, ~3.2 eV,). The ligand-to-metal charge transfer formally is a reduction of Sm^{3+} to Sm^{2+} (arrow 2 in Fig. 2.2-8). According to Dorenbos, the positions of the 4*f* ground states of the other Ln^{2+} differ a value specific for each element and can appropriately be positioned, for example the 4*f* ground state of Eu^{2+} is located at ~2.0 eV. The location of the lowest 5*d* states of the divalent lanthanides can be estimated for example from the excitation spectrum of $Sr[Mg_3SiN_4]:Eu^{2+}$. Herefor, the energy of the first 4*f*-5*d* transition in the Eu^{2+}-doped host lattice is required. This can be estimated from the excitation spectrum at 15 to 20% of the maximum intensity on the low energy site (~2.1 eV). Thus, the location of the lowest Eu^{2+} 5*d* state is at ~4.1 eV with respect to the valence band and ~0.2 eV above the edge of the conduction band (arrow 3 in Fig. 2.2-8). Therefore, the red shift D(Ln2+) which is the energy difference between the free Eu^{2+} ion (4.2 eV) and Eu^{2+} in a specific host lattice, can be calculated to ~2.1 eV. With D(Ln2+) = 2.1 eV, the positions of all other Ln^{2+} 5*d* states can be located (see Fig. 2.2-8). The energy of the 4*f*-5*d* transitions of Ln^{3+} can also be estimated with the redshift model. For this purpose, Dorenbos gives the following empirical relation between Ln^{2+} and Ln^{3+} (Eq. 2).

$$D(Ln3+) = (D(Ln2+)+ 0.233)/0.64 \qquad \text{Eq. 2}$$

The redshift D(Ln3+) for the trivalent lanthanides in $Sr[Mg_3SiN_4]:Ln^{3+}$ is ~3.6 eV. Considering the energy of 4*f*-5*d* transition of the free Ln^{3+} ions, the relative positions of the 4*f* ground states and the lowest 5*d* states of the trivalent lanthanides in $Sr[Mg_3SiN_4]:Ln^{3+}$ are given. The energetic level of the 4*f* ground state of Eu^{3+} can be estimated from 4*f* ground state of Eu^{2+}. Hereto, the Coulomb-repulsion energy is used, which is 6.4 eV in nitridosilicates as shown by many investigations by Dorenbos and Hintzen et al.[8,10,11,13] Therefore, the 4*f* ground state of Eu^{3+} is located at ~-4.4 eV (arrow 4 in Fig. 2.2-8). Under consideration of latter value and the redshift D(Ln3+) all other Ln^{3+} ions can be positioned and the energy-level diagram is completely

constructed.[8-10] However, it is still in a preliminary state. Especially, spectroscopic data (e.g., excitation spectra) of the trivalent lanthanides Ce, Pr and Sm are missing. This data would enable a more exact positioning of the 4*f* ground states of all Ln^{3+} and therefore the lowest 5*d* states of these ions. In general, the construction of such an energy-level diagram is based on numeral estimations, for example the estimated energy of the first 4*f*-5*d* transition in the Eu^{2+}-doped host lattice and therefore the obtained values cannot be seen as absolute values and a standard deviation of ~0.3 eV can be expected. Nevertheless, the constructed energy-level diagram of the $Sr[Mg_3SiN_4]$ host lattice is a powerful tool to discuss thermal quenching or predict the optical properties of not yet investigated lanthanide ions in $Sr[Mg_3SiN_4]$:Ln.

2.2.4 Conclusion

In this contribution the syntheses of $Sr[Mg_3SiN_4]$:RE with RE = Ce^{3+},Pr^{3+},Sm^{3+},Eu,Yb and the investigation of the optical properties of these compounds were reported. An energy-level diagram of the $Sr[Mg_3SiN_4]$ host lattice containing the positions of the 4*f* ground states and the lowest 5*d* states of all divalent and trivalent lanthanides was constructed with the obtained data. This powerful tool allows the discussion and prediction of several properties of $Sr[Mg_3SiN_4]$:Ln. For example, if the 4*f* ground state of any Ln^{2+} is closer to the valence band than to the conduction band, the respective ion is expected to be in oxidation state +2. This assumption fits well within the expected standard deviations for Eu^{2+}, whose optical properties exhibiting outstanding narrow-band red emission in the host lattice were already discussed earlier.[1] In addition, the severe thermal quenching of $Sr[Mg_3SiN_4]$:Eu^{2+} can be explained with the aid of the energy-level diagram. The lowest 5*d* state of Eu^{2+} in $Sr[Mg_3SiN_4]$ is located quite close to the edge of the conduction band and therefore non-radiative transitions due to photoionization and/or thermalionization of the excited electron into the conduction band are observed. Excitation of $Sr[Mg_3SiN_4]$:Eu in the deep UV region (254 nm) leads to typical Eu^{3+} luminescence (see Fig. 2.2-5 right) that can also be observed for VUV photo oxydized $BaMgSiO_4$:Eu.[25] By contrast, the 4*f* ground state of Yb^{2+} in $Sr[Mg_3SiN_4]$ is closer to the conduction band than to the valence band and thus

Yb^{3+} is expected. The emission spectrum of $Sr[Mg_3SiN_4]$:Yb (see Fig. 2.2-7) shows the typical 4*f*-4*f* emission of Yb^{3+} in the NIR region. Nevertheless, Yb^{2+} 5*d*-4*f* emission is also detected in the visible part of the spectrum. On one hand, the ionic radii of Yb^{2+} (1.14 Å) and Sr^{2+} (1.26 Å) differ much less,[26] and on the other hand the 4*f* ground state is located almost equidistant within the expected standard deviations to both the conduction and the valence band. A similar situation was observed for Yb-doped $Sr_2Si_5N_8$ and $SrAlSi_4N_7$.[8,27] The energy-level diagram could also help to analyze non-distinct optical data, for example the UV/vis-reflectance spectrum of $Sr[Mg_3SiN_4]$:Yb (see Fig. 2.2-6 left). The broad absorption band covering the entire spectral range was assumed to consist of the Yb^{2+} 4*f*-5*d* absorption and the Yb^{3+} CTB, but could not be interpreted in more detail. From the energy-level diagram, the Yb^{2+} 4*f*-5*d* absorption should start around 560 nm and the Yb^{3+} CTB is expected to be at lower wavelengths (i.e., higher energy) at 510 nm. Both values could be verified with corresponding excitation spectra with varying monitor wavelengths. Excitation spectra for $Sr[Mg_3SiN_4]:RE^{3+}$ (RE^{3+} = Ce,Pr,Sm) have not yet been obtained. Nevertheless, the lowest 4*f*-5*d* absorption bands can already be predicted from the energy-level diagram. For $Sr[Mg_3SiN_4]:Ce^{3+}$ it is expected at around 490 nm, and for the respective Pr^{3+}-doped compound at around 320 nm. UV/vis-reflectance data of both compounds (Ce^{3+}: Fig. 2.2-2, Pr^{3+}: Fig. 2.2-3, both left) corroborate this assumption. The energy-level diagram can further be used to predict the optical properties of up to now non-investigated Ln ions in $Sr[Mg_3SiN_4]$. Besides Ce^{3+} and Pr^{3+}, 4*f*-5*d* absorption is only expected for Tb^{3+}. Other lanthanides typically showing 4*f*-5*d* absorption are not stable in $Sr[Mg_3SiN_4]$, for example Sm^{2+}.[22,23] Even more, CTBs can be predicted from the energy-level diagram. Usually, Sm^{3+}, Eu^{3+} and Yb^{3+} show charge-transfer bands, which all were observed in the corresponding UV/vis-reflectance spectra. In addition, in nitridosilicates CTBs of Nd, Dy, Ho, Er and Tm (all in oxidation state +3) can be expected.[22,23] However, only a CTB of Tm^{3+} would be expected at 333 nm. The energy for the charge transfer of the other mentioned ions is higher than the band gap of the $Sr[Mg_3SiN_4]$ host lattice. With the aid of the energy-level diagram of $Sr[Mg_3SiN_4]$:Ln it is possible to understand various properties of the respective doped compounds. It is

shown that not only the size of the band gap of a host lattice is important, it is much more important to locate the energetic levels of all dopants inside the host lattice to discuss the structure-property relations of novel doped host lattices for application in pc-LEDs.

2.2.5 References

(1) Schmiechen, S.; Schneider, H.; Wagatha, P.; Hecht, C.; Schmidt, P. J.; Schnick, W. *Chem. Mater.* **2014**, *26*, 2712.

(2) Pust, P.; Hintze, F.; Hecht, C.; Weiler, V.; Locher, A.; Zitnanska, D.; Harm, S.; Wiechert, D.; Schmidt, P. J.; Schnick, W. *Chem. Mater.* **2014**, *26*, 6113.

(3) Pust, P.; Weiler, V.; Hecht, C.; Tücks, A.; Wochnik, A. S.; Henß, A.-K.; Wiechert, D.; Scheu, C.; Schmidt, P. J.; Schnick, W. *Nat. Mater.* **2014**, *13*, 891.

(4) Pust, P.; Wochnik, A. S.; Baumann, E.; Schmidt, P. J.; Wiechert, D.; Scheu, C.; Schnick, W. *Chem. Mater.* **2014**, *26*, 3544.

(5) Nowitzki, B.; Hoppe, R. *Rev. Chim. Miner.* **1986**, *23*, 217.

(6) Schmiechen, S.; Strobel, P.; Hecht, C.; Reith, T.; Siegert, M.; Schmidt, P. J.; Huppertz, P.; Wiechert, D.; Schnick, W. *Chem. Mater.* **2015**, *27*, 1780.

(7) Krames, M. R.; Mueller, G. O.; Mueller-Mach, R. B.; Bechtel, H.-H.; Schmidt, P. J. Wavelength conversion for producing white light from high power blue LED. PCT Int. Appl.WO 2010131133 A1, November 18th, 2010.

(8) ten Kate, O. M.; Zhang, Z.; Dorenbos, P.; Hintzen, H. T.; van der Kolk, E. *J. Solid State Chem.* **2013**, *197*, 209.

(9) Zhang, Z.-J.; ten Kate, O. M.; Delsing, A.; Dorenbos, P.; Zhao, J.-T.; Hintzen, H. T. *J. Mater. Chem. C* **2014**, *2*, 7952.

(10) Dorenbos, P. *ECS J. Solid State Sci. Technol.* **2013**, *2*, R3001.

(11) Dorenbos, P. *J. Phys.: Condens. Matter* **2003**, *15*, 575.

(12) Dorenbos, P. *J. Phys.: Condens. Matter* **2005**, *17*, 8103.

(13) Dorenbos, P. *J. Lumin.* **2000**, *91*, 155.

(14) Dorenbos, P. *J. Alloys Compd.* **2009**, *488*, 568.

(15) Lange, H.; Wötting, G.; Winter, G. *Angew. Chem. Int. Ed. Engl.* **1991**, *30*, 1579.

(16) Fair, H. D.; Walker, R. F. *Energetic Materials 1, Physics and Chemistry of Inorganic Azides*; 1st ed.; Plenum Press: New York, London, 1977.

(17) Coelho, A. TOPAS, v. 4.1: A program for Rietveld refinement, Coelho Software, 2007.

(18) Bergmann, J.; Kleeberg, R.; Haase, A.; Breidenstein, B. *Mater. Sci. Forum* **2000**, *347-349*, 303.

(19) Cheary, R. W.; Coelho, A. A.; Cline, J. P. *J. Res. Natl. Inst. Stand. Technol.* **2004**, *109*, 1.

(20) Meyer, H. J. *Dalton Trans.* **2010**, *39*, 5973.

(21) Schmiechen, S.; Nietschke, F.; Schnick, W. *Eur.J. Inorg. Chem.* **2015**, 1592.

(22) Blasse, G.; Grabmaier, B. C. *Luminescent materials*; Springer-Verlag: Berlin, Heidelberg, 1994.

(23) Shionoya, S.; Yen, W. M.; Yamamoto, H. *Phosphor Handbook*; CRC Press: Boca Raton, 2006.

(24) Dorenbos, P. *J. Lumin.* **2005**, *111*, 89.

(25) Li, Y.; Wang, Y.; Gong, Y.; Xu, X.; Zhang, F. *Acta Mater.* **2011**, *59*, 3174.

(26) Shannon, R. D. *Acta Crystallogr. Sect. A: Found. Crystallogr.* **1976**, *32*, 751.

(27) Zhang, Z.; ten Kate, O. M.; Delsing, A. C. A.; Man, Z.; Xie, R.; Shen, Y.; Stevens, M. J. H.; Notten, P. H. L.; Dorenbos, P.; Zhao, J.; Hintzen, H. T. *J. Mater. Chem. C* **2013**, *1*, 7856.

2.3 Nitridomagnesosilicate $Ba[Mg_3SiN_4]:Eu^{2+}$ and Structure-Property Relations of Similar Narrow-Band Red Nitride Phosphors

Sebastian Schmiechen, Philipp Strobel, Cora Hecht, Thomas Reith, Markus Siegert, Peter J. Schmidt, Petra Huppertz, Detlef Wiechert, and Wolfgang Schnick

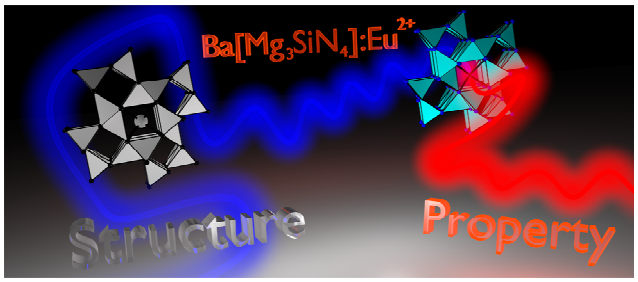

Published in: *Chem. Mater.* **2015**, *27*, 1780; DOI: 10.1021/cm504604d
http://pubs.acs.org/doi/abs/10.1021/cm504604d

Abstract

The nitridomagnesosilicate $Ba[Mg_3SiN_4]$ has been synthesized in an arc-welded Ta ampule. The crystal structure was solved and refined from single-crystal X-ray data and Rietveld refinement on the basis of powder X-ray diffraction data, revealing a distorted triclinic variant of the UCr_4C_4 structure type (space group $P\bar{1}$ (no. 2), Z = 1, a = 3.451(1), b = 6.069(5), c = 6.101(4) Å, α = 85.200(7), β = 73.697(5), γ = 73.566(8)°, R_p = 0.0218, R_{wp} = 0.0290). The crystal structure of $Ba[Mg_3SiN_4]$ consists of a highly condensed network of $(Mg,Si)N_4$ tetrahedra with Ba^{2+} centered inside *vierer* ring channels along [100] in a cuboidal coordination by N^{3-}. From UV/vis-reflectance data, a band gap of ~4.0 eV was estimated. Doping with Eu^{2+} shows promising luminescence properties of λ_{em} = 670 nm with an fwhm ~1970 cm^{-1}. Furthermore, anomalous luminescence phenomena, such as trapped-exciton emission, were identified and considered. $Ba[Mg_3SiN_4]:Eu^{2+}$ is a further narrow-band red-emitting phosphor and is

discussed concerning the structure-property relations of recently reported Eu^{2+}-doped nitrides with narrow-band red emission.

2.3.1 Introduction

Energy-efficient light-emitting diodes (LEDs) are widely seen as a superior replacement for inefficient common light sources such as incandescent light bulbs or compact fluorescent lamps (CFLs).[1-3] Based on semiconductor technology, each single LED can only emit light in one color tone depending on the band gap of the used material. However, for general illumination purposes, white light covering the whole visible spectrum from blue to red is essential. Therefore, the emitted blue light of a (In,Ga)N semiconductor chip is partially converted by phosphors to white light. There are several possibilities to achieve this goal; however, only a multiphosphor approach with at least a green to yellow and an orange to red component can realize illumination-grade phosphor-converted (pc-)LEDs.[4] Widely used phosphors are Ce^{3+}-doped garnets such as $Y_{3-x}Gd_xAl_{5-y}Ga_yO_{12}:Ce^{3+}$ (YAG:Ce) as green to yellow components,[5,6] and Eu^{2+}-doped nitrides such as $(Ba,Sr)_2Si_5N_8:Eu^{2+}$ or $(Ca,Sr)AlSiN_3:Eu^{2+}$ as orange to red components.[7-11] Yet, most red phosphors show a large portion of emitted light outside the human eye sensitivity in the infrared region and therefore are wasting a lot of energy. A further increase of the luminous efficacy (i.e., efficiency of light conversion in reference to the human eye sensitivity) of pc-LEDs can be achieved especially by novel red-emitting phosphors. For many years, the hunt for narrow-band red-emitting phosphors has been a major goal for the solid-state lighting industry. The search for suitable materials is difficult as specific requirements have to be fulfilled. Next-generation LED phosphors have to be chemically and thermally stable and show high quantum efficiencies (QE) at the operating temperature (~150 °C) of the pc-LED.[12] Additionally, there are several special requirements for the host lattice of Eu^{2+}-doped phosphors. For example, a rigid network seems to be favorable for inhibiting relaxation through non-radiative pathways.[13] Furthermore, crystallographic ordering within the network and only one single crystallographic site for the activator seem to be important preconditions for reduction of inhomogeneous line broadening

caused by different crystal fields around the activator. Particularly, it has been shown that coordination around the activator site that combines a strong ligand field with rather long activator-ligand distances is beneficial for a small Stokes shift and consequently a narrow-band emission, as the structural relaxation of the activator is hindered in its excited state.[14–20] Last but not least, the relative energetic distance of the $4f^6 5d^1$ Eu^{2+} excited state to the bottom of the conduction band needs to be large enough to avoid photoionization at elevated temperatures.[13] Quite recently, we reported in detail on novel narrow-band red-emitting Eu^{2+}-doped nitrides that meet some or all of these requirements. The first representatives were the nitridomagnesogallate ($Ba[Mg_2Ga_2N_4]:Eu^{2+}$) and -aluminates ($AE[Mg_2Al_2N_4]:Eu^{2+}$; AE = Ca-Ba), which crystallize in the UCr_4C_4 structure type and fulfill all requirements mentioned above except for a crystallographically ordered network and a large band gap.[15] Further investigations revealed more promising compounds with an ordered network. The nitridomagnesosilicate $Sr[Mg_3SiN_4]:Eu^{2+}$ crystallizes in the $Na[Li_3SiO_4]$ structure type and shows the up to date most narrow-band red emission for Eu^{2+}-doped phosphors with a full width at half-maximum (fwhm) of only ~1170 cm^{-1}. Yet, a small band gap and therefore small quantum efficiency (QE) values hinder application in illumination-grade pc-LEDs.[18] By contrast, $Sr[LiAl_3N_4]:Eu^{2+}$, a nitridolithoaluminate, combines such a small fwhm of ~1180 cm^{-1} with outstanding high QE values up to 500 K due to a more suited electronic structure.[16]

Here we report on the synthesis and characterization of a novel nitridomagnesosilicate, namely $Ba[Mg_3SiN_4]$. Especially, luminescence properties of the Eu^{2+}-doped compound were investigated and structure-property relations are discussed in comparison to our recently reported narrow-band red emitting Eu^{2+}-doped nitrides.

2.3.2 Experimental Section

2.3.2.1 Synthesis

With respect to the air and moisture sensitivity of some starting materials, all manipulations were performed in flame-dried Schlenk-type glassware attached to a vacuum line (10^{-3} mbar) or in argon-filled glove boxes (Unilab, MBraun, Garching, O_2 <1 ppm, H_2O <1 ppm). Argon (Messer-Griessheim, 5.0) was purified by passage through columns filled with silica gel (Merck), molecular sieves (Fluka, 4 Å), KOH (Merck, ≥85%), P_4O_{10} (Roth, ≥99%), and titanium sponge (Johnsen Matthey, 99.5%) at 700 °C. $Ba[Mg_3SiN_4]$ was obtained by a solid-state metathesis reaction of 0.40 mmol of BaF_2 (70.1 mg, Sigma-Aldrich, 99.99%), 0.20 mmol of Mg_3N_2 (20.2 mg, Sigma-Aldrich, 99.5%), and "$Si(NH)_2$" (11.6 mg, synthesized according to the method given by Lange et al.).[21] A portion of 0.40 mmol of LiN_3 (19.6 mg, synthesized according to the method reported by Fair et al.)[22] was added as the nitrogen source. For doping experiments, 0.5-2.5 mol% EuF_3 (nominal composition, Sigma-Aldrich, 99.99%) was added. The mixture was ground under argon atmosphere in a glovebox and placed in a tantalum ampule. A 1.0 mmol amount of Li (6.9 mg, Alfa Aesar, 99.9%) was added as fluxing agent to enhance crystal growth. The Ta ampule was subsequently weld shut in an arc furnace under water cooling to prevent any chemical reaction. The sealed ampule was placed in a silica tube, evacuated, and heated in a tube furnace. The reaction mixture was heated to 1050 °C within 3 h, kept at this temperature for 24 h, cooled to 500 °C in 250 h, and subsequently quenched to room temperature by switching off the furnace.

2.3.2.2 X-ray Spectroscopy

The chemical composition of $Ba[Mg_3SiN_4]$ was determined by energy-dispersive X-ray (EDX) spectroscopy. Several crystallites and bulk samples were investigated with a JSM-6500F scanning electron microscope (SEM, Jeol) containing a Si/Li EDX detector (Oxford Instruments, model 7418). The given results are an average of ten measurements on different particles and were normalized according to the Ba content.

2.3.2.3 Single-Crystal X-ray Diffraction

Crystals of $Ba[Mg_3SiN_4]:Eu^{2+}$ were separated from the reaction mixture with the aid of a microscope integrated into a glovebox, enclosed afterward in glass capillaries, and finally sealed under argon atmosphere. The isolated crystallites were checked on a Buerger precession camera in respect to their quality. X-ray diffraction data were collected on a STOE IPDS I diffractometer (Ag-K_α radiation, λ = 0.56087 Å) with a graphite monochromator. A semiempirical absorption correction was carried out with XPREP,[23] and the structure was solved by Direct Methods (SHELXS)[24] and refined by full-matrix least-squares methods (SHELXL).[25,26] Eu^{2+} was neglected for structure determination; due to the low content the contribution to scattering density is insignificant.

2.3.2.4 Powder X-ray Diffraction

The structural model obtained from single-crystal data was verified and optimized from powder X-ray data with the TOPAS Academic 4.1 package.[27] Therefore, a product mixture containing non-doped $Ba[Mg_3SiN_4]$ was measured in a sealed capillary on a STOE STADI P diffractometer (Cu-$K_{\alpha1}$ radiation, Ge(111) monochromator, Mythen1K detector) in Debye–Scherrer geometry. Refinement was carried out using the Rietveld method, employing the fundamental parameters approach (direct convolution of source emission profiles, axial instrument contributions, crystallite size, and microstrain effects). Capillary absorption correction (inner diameter 0.18 mm) was carried out using the calculated absorption coefficient.[28,29]

Further details of the crystal structure investigation may be obtained from Fachinformationszentrum Karlsruhe, 76344 Eggenstein-Leopoldshafen, Germany (fax, (+49)7247-808-666; e-mail, crysdata@fizkarlsruhe.de, http://www.fiz-karlsruhe.de/request_for_deposited_data.html) upon quoting the depository number CSD-428510.

2.3.2.5 UV/vis Spectroscopy

Optical properties of $Ba[Mg_3SiN_4]$ were investigated on a Jasco V-650 UV/vis spectrophotometer with a deuterium and a halogen lamp (Czerny-Turner

monochromator with 1200 lines/mm concave grating, photomultiplier tube detector). The spectra were measured between 200 and 800 nm with 5 nm step size. The band gap of $Ba[Mg_3SiN_4]$ was derived from acquired data by drawing a line tangent to the slope of the reflectance curve. The point of intersection of the tangent with the abscissa is the value of the band gap.

2.3.2.6 Luminescence

Investigations of luminescence properties of Eu^{2+}-doped $Ba[Mg_3SiN_4]$ were carried out with a luminescence microscope consisting of a HORIBA Fluoromax4 spectrofluorimeter system attached to an Olympus BX51 microscope via fiber optical bundles. The samples were measured inside a glass capillary. The excitation wavelength was chosen to 450 nm with a spectral width of 10 nm. The emission spectra were collected in the wavelength range between 450 and 800 nm with 2 nm step size.

2.3.3 Results and Discussion

2.3.3.1 Synthesis and Chemical Analysis

For the synthesis of $Ba[Mg_3SiN_4]$, different routes were elaborated and only the one described above yielded less impurities such as $LiBaF_3$, LiF, and BaClF. $Ba[Mg_3SiN_4]$ was obtained as a white microcrystalline powder, but no single crystals suitable for further characterization could be obtained. Doping with Eu^{2+} resulted in a reddish colored sample with intense red luminescence under blue irradiation. From the Eu^{2+}-doped sample, some crystallites could be isolated and used for single-crystal X-ray diffraction. Elemental analysis with the aid of EDX spectroscopy gave an atomic ratio Ba:Mg:Si:N of 1:3.2:0.9:4.4 for $Ba[Mg_3SiN_4]$ single crystals and bulk samples. No further elements, besides a small amount of oxygen, were detected, which can be attributed to the high sensitivity against moisture of the product.

Table 2.3-1. Crystallographic Data of $Ba[Mg_3SiN_4]$ (Standard Deviations in Parentheses)

formula	$Ba[Mg_3SiN_4]$
formula mass / g·mol^{-1}	294.39
crystal system, space group	triclinic, $P\bar{1}$ (no. 2)
lattice parameters / Å,°	a = 3.4508(1)
	b = 6.0686(5)
	c = 6.1005(4)
	α = 85.200(7)
	β = 73.697(5)
	γ = 73.566(8)
cell volume / Å^3	117.606(14)
formula units per cell Z	1
X-ray density / g · cm^{-1}	4.157
linear absorption coefficient / cm^{-1}	70.993
radiation	Cu-$K_{\alpha1}$ (λ = 1.540596 Å)
monochromator	Ge(111)
diffractometer	Stoe Stadi P
detector	Mythen1K
2θ -range /°	10–100
temperature / K	297(2)
data points	6067
number of reflections	251
number of parameters	95
constraints	0
program used	TOPAS Academic
structure refinement	Rietveld-method
profile function	fundamental parameters model
background function	shifted Chebychev (18 parameters)
R_{wp}	0.0290
R_p	0.0218
R_{Bragg}	0.0083
χ^2	1.329

2.3.3.2 Crystal-Structure Determination

A first structural model was obtained by single-crystal structure elucidation. However, the investigated crystallites were of insufficient quality for a good and complete structure determination. The crystal structure of $Ba[Mg_3SiN_4]$ was solved and refined in the triclinic space group $P\bar{1}$ (no. 2), and the crystallographic data are summarized in Supporting Information. To substantiate the obtained structural model of $Ba[Mg_3SiN_4]$, it was further investigated by Rietveld refinement with the aid of the TOPAS Academic 4.1 package.[27-29] The refinement was carried out by the fundamental parameters approach. Site parameters of all network-forming atoms were refined without any constraints or restraints. Occupancy of tetrahedrally coordinated cations was also refined freely, giving a ~75:25 occupation for Mg^{2+} and Si^{4+} on both sites. Isotropic displacement parameters were refined for all ions without any constraints. For the final refinement, $LiBaF_3$ (25%) and BaClF (7%) were included as side phases (see Figure 2.3-1).The final crystallographic data are summarized in Table 2.3-1, and in Table 2.3-2 atomic parameters and isotropic displacement parameters are given. Selected bond lengths are listed in Supporting Information.

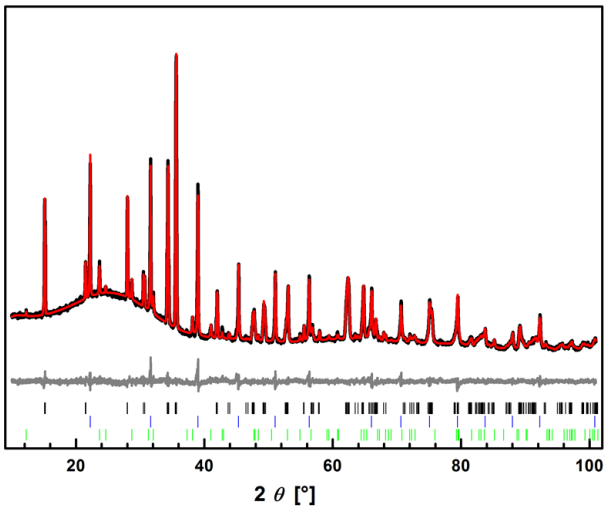

Figure 2.3-1. Rietveld refinement of the final structural model of $Ba[Mg_3SiN_4]$ (Cu-$K_{\alpha 1}$ radiation). Experimental data (black line), calculated pattern (red line) and difference curve (gray line). Tickmarks: black, $Ba[Mg_3SiN_4]$ (68%); blue, $LiBaF_3$, (25%); green, BaClF (7%).

Table 2.3-2. Atomic Coordinates, Isotropic Displacement Parameters / Å^2 and Occupancy of Ba[Mg_3SiN_4] (Standard Deviations in Parentheses)

atom (Wyck.)	*x*	*y*	*z*	U_{iso}	*sof*
Ba (1*a*)	0	0	0	0.028(4)	1
Mg1 (2*i*)	0.177(3)	0.191(13)	0.456(11)	0.022(2)	0.75
Si1 (2*i*)	0.177(3)	0.191(13)	0.456(11)	0.022(2)	0.25
Mg2 (2*i*)	0.628(4)	0.550(12)	0.184(12)	0.024(2)	0.75
Si2 (2*i*)	0.628(4)	0.550(12)	0.184(12)	0.024(2)	0.25
N1 (2*i*)	0.248(9)	0.381(2)	0.175(3)	0.030(5)	1
N2 (2*i*)	0.618(9)	0.155(3)	0.630(2)	0.037(5)	1

2.3.3.3 Crystal-Structure Description

Ba[Mg_3SiN_4] crystallizes in a distorted triclinic variant of the UCr_4C_4 structure type (see Fig. 2.3-2).[30] Recently published isoelectronic phases M[Mg_3SiN_4] wih M = Ca,Sr,Eu crystallize in the Na[Li_3SiO_4] structure type which represents an ordered variant of the UCr_4C_4 structure type.[18] The three-dimensional network of Ba[Mg_3SiN_4] is built up by strands of edge- and corner-sharing (Mg,Si)N_4 tetrahedra and can therefore be classified as nitridomagnesosilicate.[18] Each tetrahedra strand is connected by common corners to three other strands (see Fig. 2.3-3a). This results in *vierer* ring channels along [100],[31,32] whereby in every second channel Ba^{2+} is centered by N^{3-} in cuboid-like manner (see Fig. 2.3-3b). The highly condensed three-dimensional network of Ba[Mg_3SiN_4] consists exclusively of ammonium-type $N^{[4]}$, resulting in a high degree of condensation (i.e., atomic ratio (Mg,Si):N) of $\kappa = 1$. The tetrahedrally coordinated positions are occupied by crystallographically disordered Mg^{2+} and Si^{4+}. The distances (Mg^{2+},Si^{4+})-N vary from 1.89(3) to 2.14(2) Å with an averaged bond length of 2.03 Å. This value agrees with the averaged sum of the ionic radii of 1.97 Å.[33] Typical Si-N and Mg-N bond length in nitridosilicates range from 1.72 to 1.78 Å (Si-N) and 1.98-2.25 Å (Mg-N),[11,18,34,35] giving an averaged bond length of 1.85-2.01 Å, which also fits well. The Ba-N distances are in a range of 2.88(2)-3.04(3) Å and correspond to the sum of the ionic radii (3.04 Å).[33] Structurally related nitridoaluminates and -gallates with Ba^{2+} in an 8-fold coordination by N^{3-} show similar bond lengths.[15]

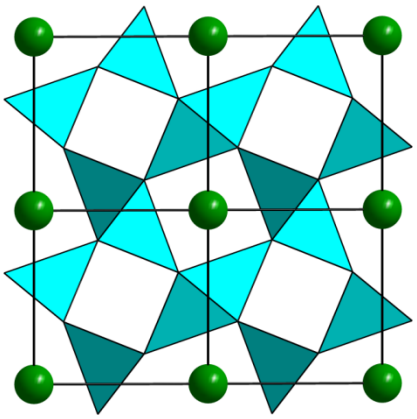

Figure 2.3-2. Crystal structure of $Ba[Mg_3SiN_4]$ with a 2x2x2 super cell, displayed along [100]. Ba^{2+}, green; $(Mg,Si)N_4$ tetrahedra, blue.

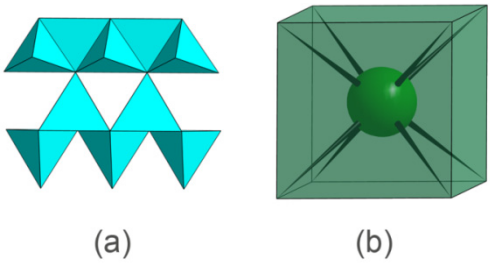

Figure 2.3-3. (a) Edge- and corner-sharing tetrahedra strands of $(Mg,Si)N_4$, connected to each other by common corners. (b) Cuboid-like coordination of Ba^{2+} by N^{3-}. $(Mg,Si)N_4$ tetrahedra, blue; Ba^{2+} green.

2.3.3.4 UV/vis spectroscopy

Non-doped and Eu^{2+}-doped samples of $Ba[Mg_3SiN_4]$ were further investigated by UV/vis spectroscopy. Especially, the band gap was determined with UV/vis-reflectance spectroscopy data. The spectra are depicted in Figure 2.3-4. The reflectance spectrum of non-doped $Ba[Mg_3SiN_4]$ shows a broad absorption band around 310 nm with an estimated band gap of ~4.0 eV. No other absorption band is visible which is in good accordance with the white body color of the non-doped compound. In contrast, the Eu^{2+}-doped sample shows, besides the absorption in the UV region, a large absorption band in the blue to red region of the visible spectrum.

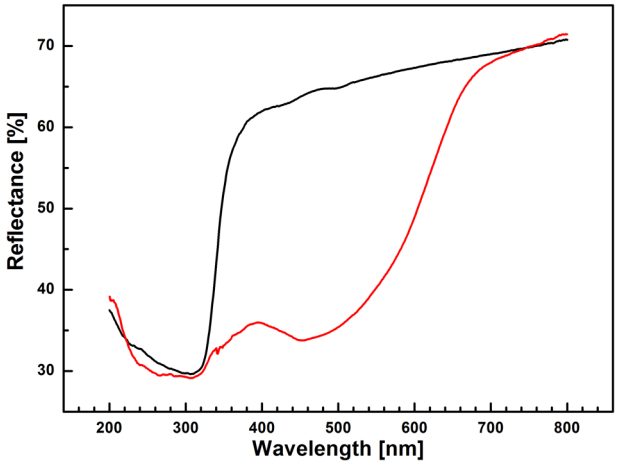

Figure 2.3-4. UV/vis-reflection spectra of nondoped (black curve) and Eu^{2+}-doped (red curve, 2.5 mol% Eu^{2+}, nominal composition) $Ba[Mg_3SiN_4]$.

This band can be ascribed to the $4f^7$ to $4f^{7-N}5d^N$ absorptions in Eu^{2+}. The strong absorption around 450 nm corresponds well with the reddish body color of $Ba[Mg_3SiN_4]:Eu^{2+}$. The band gap of $Ba[Mg_3SiN_4]$ was found to be ~4.0 eV and is in the same magnitude of isoelectronic $Sr[Mg_3SiN_4]$.[18] $Ba_2Si_5N_8:Eu^{2+}$, a commercially available phosphor for pc-LEDs, shows by contrast a band gap of ~4.9 eV.[7,19,36-38]

2.3.3.5 Luminescence

Doping with Eu^{2+} yielded red body colored samples of $Ba[Mg_3SiN_4]:Eu^{2+}$, which show luminescence in the red spectral region under blue irradiation. Figure 2.3-5 displays excitation and emission spectra of $Ba[Mg_3SiN_4]:Eu^{2+}$ crystallites sealed in glass capillaries with varying Eu^{2+}-dopant concentrations. $Ba[Mg_3SiN_4]:Eu^{2+}$ can be efficiently excited with blue light, as the corresponding excitation spectrum (blue line in Fig. 2.3-5 left) shows a broad band with a maximum at 465 nm. Excitation at 450 nm results in an emission band (black curve in Fig. 2.3-5 left; 0.5 mol% Eu^{2+}, nominal composition) in the red spectral region centered at 670 nm with an fwhm of ~1970 cm^{-1}. Increasing the dopant concentration to 2.5 mol% (red curve in Fig. 2.3-5 left) red shifts the emission maximum slightly to 680 nm with approximately a constant fwhm of ~1980 cm^{-1}.

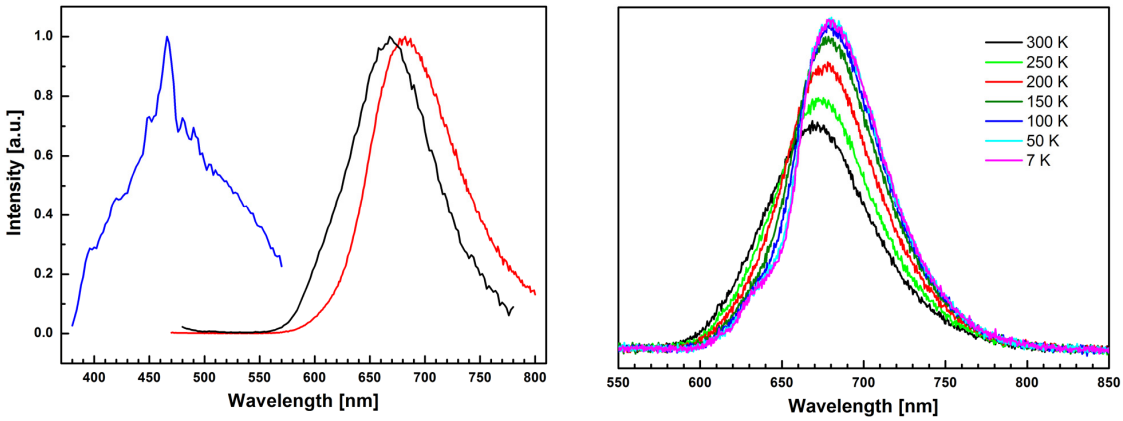

Figure 2.3-5. Left: Excitation (blue) and emission spectra of $Ba[Mg_3SiN_4]:Eu^{2+}$ (black: 0.5 mol%, red: 2.5 mol% Eu^{2+}, nominal composition). Right: Low-temperature emission spectra of the Eu^{2+}-doped barium nitridomagnesosilicate between 7 and 300 K. Emission spectra were recorded at 450 nm excitation.

Furthermore, the QE of the $Ba[Mg_3SiN_4]$ sample doped with 0.5 mol% Eu^{2+} (nominal composition) was measured to 32%, and possible loss mechanisms will be discussed later. Recently reported $Ba[Mg_2T_2N_4]:Eu^{2+}$ (T = Al or Ga) shows, like $Ba[Mg_3SiN_4]:Eu^{2+}$ disordering of the tetrahedrally-coordinated cations (Mg^{2+},Al^{3+},Ga^{3+},Si^{4+}) and therefore quite similar luminescence properties in the red spectral region. $Ba[Mg_2Ga_2N_4]:Eu^{2+}$ exhibits an fwhm of ~2168 cm^{-1} at λ_{em} = 649 nm, whereas the emission spectrum of $Ba[Mg_2Al_2N_4]:Eu^{2+}$ displays a maximum at 666 nm and an fwhm of ~2331 cm^{-1}.[15] Especially, the latter compound was further investigated and anomalous luminescence phenomena from 7 to 600 K were reported. The large Stokes shift (~3475 cm^{-1}) and the broad fwhm of $Ba[Mg_3SiN_4]:Eu^{2+}$ also point toward anomalous trapped-exciton emission (ETE). Therefore, temperature-dependent emission measurements were carried out (see Fig. 2.3-5 right). At low temperatures, the emission maximum is redshifted by ~220 cm^{-1} and the fwhm is reduced to ~1290 cm^{-1}. Both observations corroborate the assumption of ETE luminescence besides typical Eu^{2+} emission for $Ba[Mg_3SiN_4]:Eu^{2+}$. In contrast to $Ba[Mg_2Al_2N_4]:Eu^{2+}$, thermal quenching (TQ) data from 7 to 600 K (see Fig. 2.3-6) of $Ba[Mg_3SiN_4]:Eu^{2+}$ cannot be fitted with a single activation energy. TQ data of the latter compound point toward more complex processes as, for example, already described by Dorenbos for the isotypic compounds $MF_2:Eu^{2+}$ (M = Ca,Sr,Ba)[39] or recently discussed for $Sr_4Al_{14}O_{25}:Eu^{2+}$ and $EuAl_2O_4$.[40,41]

The activation energy for ETE was estimated to ~0.15 eV. The second involved process is the typical Eu^{2+} $4f^6 5d^1 \rightarrow 4f^7$ emission with an activation energy of ~0.4 eV. The latter emission process can be noticed at low temperature as a small side band centered at ~630 nm. At higher temperatures the transition from Eu^{2+} trapped exciton to Eu^{2+} $4f^6 5d^1$ emission occurs more frequently and the room temperature emission spectrum of $Ba[Mg_3SiN_4]:Eu^{2+}$ consists of both involved processes. In contrast to $Ba[Mg_2Al_2N_4]$, the band gap of $Ba[Mg_3SiN_4]$ is increased to ~4.0 eV. As a consequence, the lowest lying excited 5*d* state of Eu^{2+} should have a larger separation from the bottom of the host lattice conduction band and therefore typical Eu^{2+} emission can be observed. Isoelectronic $Sr[Mg_3SiN_4]:Eu^{2+}$ not only shows a crystallographically ordered network of MgN_4 and SiN_4 tetrahedra, but also emission from the Eu^{2+} $4f^6 5d^1$ state is exclusively observed down to low temperatures (λ_{em} = 610 nm, fwhm ~900 cm^{-1}).[18] The band gaps of $AE[Mg_3SiN_4]$ (AE = Sr,Ba) are nearly identical, but emission quenching with temperature is much lower for the respective Eu^{2+}-doped Ba compound.

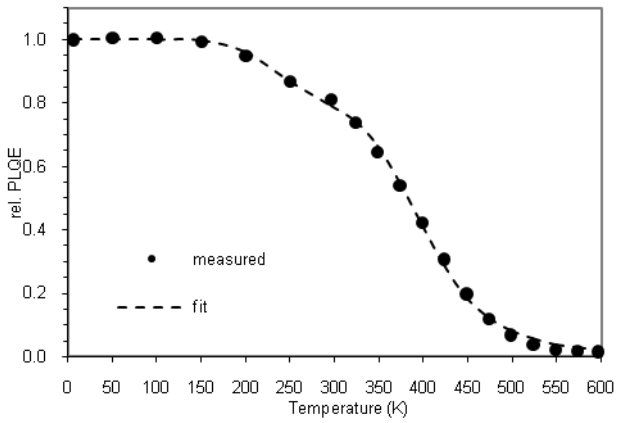

Figure 2.3-6. Relative integrated emission intensity (PLQE) of $Ba[Mg_3SiN_4]$:Eu2+ (2.5 mol%, nominal composition). Dashed line: fit with two activation energies, ~0.15 (ETE) and ~0.4 eV (Eu^{2+} *d-f* emission), respectively.

This indicates a larger distance between the lowest excited 5*d* state of Eu^{2+} to the bottom of the conduction band for the Ba title compound (see configurational coordinate diagram in Supporting Information). Hence, the different high temperature luminescence efficacies of the respective Eu^{2+}-doped compounds can be explained. Furthermore, it is assumed that the increased bond lengths Eu-N in the doped Ba

compound, compared to the Sr one, stabilize the trapped-exciton state at low temperatures.[39]

2.3.4 Conclusion

Recently, we reported on a number of novel Eu^{2+}-doped nitrides with intriguing narrow-band red-luminescence properties. $Ba[Mg_3SiN_4]:Eu^{2+}$ with its above-described luminescence properties can also be ascribed to this group. Nevertheless, there were a lot of challenges to meet *ex ante*. Besides some general requirements on novel host lattices, that were already mentioned in Introduction, such as a highly condensed rigid network, we assumed that only one single crystallographic site for the activator ion in a highly symmetric surrounding will be a major goal to achieve. $BaSi_2O_2N_2:Eu^{2+}$ (λ_{em} = 490 nm, fwhm = 1250 cm^{-1}) was an example that fulfilled the requirement of only one single site for the activator in a highly symmetric cuboidal coordination of Eu^{2+} by O^{2-}. Due to the weaker nephelauxetic effect of O^{2-} vs. N^{3-} the emission was settled in the blue to green region of the visible spectrum.[20] A screening of reported crystallographic structures brought the compounds $Sr[Mg_2Ga_2N_4]$ and $Sr[Mg_3GeN_4]$, synthesized by the DiSalvo group, into our focus.[42] Both compounds crystallize in the UCr_4C_4 structure type, which has a high substitutional variability. It has a highly condensed network with only one heavy atom site in a cuboidal surrounding.[30] Hintze succeeded in synthesis of isotypic $Ba[Mg_2Ga_2N_4]$, which after doping with Eu^{2+} yielded the expected narrow-band red emission.[15,43] Pust et al. were successful with the substitution of Ga by Al, resulting in the nitridoaluminates $AE[Mg_2Al_2N_4]:Eu^{2+}$ (AE = Ca-Ba) with luminescence properties similar to that of the nitridogallate. All compounds show narrow-band emission with fwhm values ranging from 1800 to 2400 cm^{-1}, which is outside the desired range for application in next-generation pc-LEDs.[15] We ascribe these large fwhm values above all to the disordering of the tetrahedrally coordinated cations Mg^{2+}, Al^{3+}, and Ga^{3+}. Hoppe et al. synthesized in the 1980s very interesting oxides, crystallizing in ordered variants of the UCr_4C_4 structure type. Especially, the structural motif of $Na[Li_3SiO_4]$ and some triclinic distorted variants of this structure type, such as $Cs[Na_3PbO_4]$, seemed to be very promising structural

candidates.[44,45] The assumption that an ordered network will finally lead to a sufficiently narrow-band red-emitting phosphor could be verified with the synthesis of the Eu^{2+}-doped nitridomagnesosilicate $Sr[Mg_3SiN_4]$. The compound shows outstanding emission in the red spectral region (λ = 615 nm) with the smallest fwhm of red emitting Eu^{2+}-doped phosphors of only ~1170 cm^{-1}. A further investigation of the electronic structure revealed a small band gap, and therefore distinct thermal quenching due to photoionization occurs already at room temperature.[18] As an implication, compounds of the same structure family made up of lighter elements (e.g., Li^+ for Mg^{2+} and Al^{3+} for Si^{4+}) with a higher average cation charge density have been investigated to increase the covalent bonding character in a wider band gap host lattice. The successful synthesis of a suitable compound, the nitridolithoaluminate $Sr[LiAl_3N_4]:Eu^{2+}$, resulted in a red emitter with an increased band gap of ~4.7 eV and a superb thermal behavior with still more than 95% relative QE at 200 °C. However, in contrast to $Sr[Mg_3SiN_4]:Eu^{2+}$, $Sr[LiAl_3N_4]:Eu^{2+}$ shows two crystallographic sites for the activator ion. This could be a reason for the broader fwhm of ~1180 cm^{-1} of the latter compound. Nevertheless, a next-generation prototype pc-LED with $Sr[LiAl_3N_4]:Eu^{2+}$ as red component already shows an increased luminous efficacy of 14%.[16] For the future, there are still some challenges that have to be considered. A structure prediction for novel advanced phosphors is still missing. Recently reported new host lattices show unexpected crystal chemistry. While disordering on tetrahedrally coordinated sites in the nitridomagnesoaluminates and -gallates, $AE[Mg_2T_2N_4]$ (AE = Sr, Ba,T = Al, Ga) seem to be reasonable with respect to the similar ionic radii of Mg^{2+}, Al^{3+}, and Ga^{3+},[33] whereas for the here reported $Ba[Mg_3SiN_4]$, a reason for the disordering is not obvious. Nevertheless, it was shown how important it is to understand structure-property relations for the synthesis and optimization of tailor-made materials.

2.3.5 References

(1) Born, M.; Jüstel, T. *Chem. Unserer Zeit* **2006**, *40*, 294.

(2) Feldmann, C. *Z. Anorg. Allg. Chem.* **2012**, *638*, 2169.

(3) Mueller-Mach, R.; Mueller, G.; Krames, M. R.; Höppe, H. A.; Stadler, F.; Schnick, W.; Juestel, T.; Schmidt, P. *Phys. Status Solidi A* **2005**, *202*, 1727.

(4) Xie, R.-J.; Hirosaki, N.; Takeda, T.; Suehiro, T. *ECS J. Solid State Sci. Technol.* **2013**, *2*, R3031.

(5) Setlur, A. *Electrochem. Soc. Interface* **2009**, *18*, 32.

(6) Moriguchi, T.; Noguchi, Y.; Sakano, K.; Shimizu, Y. Light emitting device having a nitride compound semiconductor and a phosphor containing a garnet fluorescent material. US 5998925 A, July 29th, 1997.

(7) ten Kate, O. M.; Zhang, Z.; Dorenbos, P.; Hintzen, H. T.; van der Kolk, E. *J. Solid State Chem.* **2013**, *197*, 209.

(8) Uheda, K.; Hirosaki, N.; Yamamoto, H. *Phys. Status Solidi A* **2006**, *203*, 2712.

(9) Uheda, K.; Hirosaki, N.; Yamamoto, Y.; Naito, A.; Nakajima, T.; Yamamoto, H. *Electrochem. Solid-State Lett.* **2006**, *9*, H22.

(10) Zeuner, M.; Hintze, F.; Schnick, W. *Chem. Mater.* **2008**, *21*, 336.

(11) Zeuner, M.; Pagano, S.; Schnick, W. *Angew. Chem. Int. Ed.* **2011**, *50*, 7754.

(12) Krames, M. R.; Mueller, G. O.; Mueller-Mach, R. B.; Bechtel, H.-H.; Schmidt, P. J. Wavelength conversion for producing white light from high power blue LED. PCT Int. Appl.WO 2010131133 A1, November 18th, 2010.

(13) Brgoch, J.; DenBaars, S. P.; Seshadri, R. *J. Phys. Chem. C* **2013**, *117*, 17955.

(14) Dirksen, G. J.; Blasse, G. *J. Solid State Chem.* **1991**, *92*, 591.

(15) Pust, P.; Hintze, F.; Hecht, C.; Weiler, V.; Locher, A.; Zitnanska, D.; Harm, S.; Wiechert, D.; Schmidt, P. J.; Schnick, W. *Chem. Mater.* **2014**, *26*, 6113.

(16) Pust, P.; Weiler, V.; Hecht, C.; Tücks, A.; Wochnik, A. S.; Henß, A.-K.; Wiechert, D.; Scheu, C.; Schmidt, P. J.; Schnick, W. *Nat. Mater.* **2014**, *13*, 891.

(17) Pust, P.; Wochnik, A. S.; Baumann, E.; Schmidt, P. J.; Wiechert, D.; Scheu, C.; Schnick, W. *Chem. Mater.* **2014**, *26*, 3544.

(18) Schmiechen, S.; Schneider, H.; Wagatha, P.; Hecht, C.; Schmidt, P. J.; Schnick, W. *Chem. Mater.* **2014**, *26*, 2712.

(19) Xie, R.-J.; Hirosaki, N.; Kimura, N.; Sakuma, K.; Mitomo, M. *Appl. Phys. Lett.* **2007**, *90*, 191101.

(20) Kechele, J. A.; Oeckler, O.; Stadler, F.; Schnick, W. *Solid State Sci.* **2009**, *11*, 537.

(21) Lange, H.; Wötting, G.; Winter, G. *Angew. Chem. Int. Ed. Engl.* **1991**, *30*, 1579.

(22) Fair, H. D.; Walker, R. F. *Energetic Materials 1, Physics and Chemistry of Inorganic Azides*; 1st ed.; Plenum Press: New York, 1977.

(23) Sheldrick, G. M. XPREP, v. 2008/2: Data Preparation & Reciprocal Space Exploration, Bruker-AXS, 2008.

(24) Sheldrick, G. M. SHELXS-97: A program for crystal structure solution, University of Göttingen, 1997.

(25) Sheldrick, G. M. *Acta Crystallogr. Sect. A: Found. Crystallogr.* **2008**, *64*, 112.

(26) Sheldrick, G. M. SHELXL-97: A program for crystal structure refinement, University of Göttingen, 1997.

(27) Coelho, A. TOPAS, v. 4.1: A program for Rietveld refinement, Coelho Software, 2007.

(28) Bergmann, J.; Kleeberg, R.; Haase, A.; Breidenstein, B. *Mater. Sci. Forum* **2000**, *347-349*, 303.

(29) Cheary, R. W.; Coelho, A. A.; Cline, J. P. *J. Res. Natl. Inst. Stand. Technol.* **2004**, *109*, 1.

(30) Behrens, R. K.; Jeitschko, W. *Monatsh. Chem.* **1987**, *118*, 43.

(31) The term *vierer* ring was coined by Liebau and is derived from the german word "vier"; however, for example a *vierer* ring is not a four-membered ring, but an eight-membered ring comprising four tetrahedra centres.

(32) Liebau, F. *Structural Chemistry of Silicates*; Springer: Berlin, 1985.

(33) Baur, W. H. *Crystallogr. Rev.* **1987**, *1*, 59.

(34) Petukhov, A. G.; Lambrecht, W. R. L.; Segall, B. *Phys. Rev. B: Condens. Matter* **1994**, *49*, 4549.

(35) Yamane, H.; Morito, H. *J. Alloys Compd.* **2013**, *555*, 320.

(36) Li, Y. Q.; van Steen, J. E. J.; van Krevel, J. W. H.; Botty, G.; Delsing, A. C. A.; DiSalvo, F. J.; de With, G.; Hintzen, H. T. *J. Alloys Compd.* **2006**, *417*, 273.

(37) Piao, X.; Horikawa, T.; Hanzawa, H.; Machida, K.-i. *Appl. Phys. Lett.* **2006**, *88*, 161908.

(38) Piao, X.; Machida, K.-i.; Horikawa, T.; Yun, B. *J. Lumin.* **2010**, *130*, 8.

(39) Dorenbos, P. *J. Phys.: Condens. Matter* **2003**, *15*, 2645.

(40) Dutczak, D.; Ronda, C.; Jüstel, T.; Meijerink, A. *J. Phys. Chem. A* **2014**, *118*, 1617.

(41) Liu, F.; Meltzer, R. S.; Li, X.; Budai, J. D.; Chen, Y.-S.; Pan, Z. *Sci. Rep.* **2014**, *4*, 1.

(42) Park, D. G.; Dong, Y.; DiSalvo, F. J. *Solid State Sci.* **2008**, *10*, 1846.

(43) Hintze, F. *Master Thesis*, Ludwig Maximilian University Munich, 2009.

(44) Nowitzki, B.; Hoppe, R. *Rev. Chim. Miner.* **1986**, *23*, 217.

(45) Stoll, H.; Hoppe, R. *Rev. Chim. Miner.* **1987**, 96.

2.4 Narrow-Red Emitters for Brighter White Light

Philipp Pust, Sebastian Schmiechen and Wolfgang Schnick

Published in: *Mater. Today* **2014**, Comment, 29.08.2014
http://www.materialstoday.com/optical-materials/comment/narrow-red-emitters-for-brighter-white-light/#disqus_thread

2.4.1 Comment

More than two decades ago the lighting industry was one of the most stable, slow but steadily growing business sectors in the entire world. Well-established lighting systems like incandescent light bulbs based on glowing tungsten wires were superseded by the more energy efficient fluorescent lamps. These were mounted on standardized sockets, allowing easy exchanges of different products. However, both those systems have advantages and disadvantages. On the one hand, the color rendering index (CRI) of a classical light bulb reaches a maximum of 100, correlating with daylight, while on the other hand only about 5-10% of the consumed electrical energy is converted to light. Commercial fluorescent lamps show an increased efficiency, but with typical CRI values as low as 70-80, the emitted light is significantly lacking in color rendition. Furthermore, the use of toxic Hg is unavoidable in this type of device.

Nowadays, lighting business has changed dramatically. Environmental policy has driven a strong movement towards sustainability and “greener” products. Classical inefficient incandescent light bulbs have been nearly wiped out from the western market. This has enabled the breakthrough of another type of light source, namely light-emitting diodes (LEDs). Industry and science all over the world agree that LEDs will be the lighting technology of the future. LEDs are unbeaten in efficiency and environmental acceptability throughout their whole production and life cycle.

LEDs generate light by electron-transfer processes in semiconducting materials, whereby each emitter can only produce monochromic emission. Illumination-grade white light, however, requires covering the entire visible spectrum, ranging from blue to deep red. To achieve this, different approaches have been conceived. The easiest way is to combine three semiconducting LEDs with blue, green and red emission. This approach, however, yields only very low quality white light. Instead, LEDs emitting high-energetic blue radiation are nowadays coated with different downconversion (or red-shifting) luminescent materials (so-called phosphors). To obtain a white-light phosphor-converted (pc-)LED, either a broadband yellow emitting (1pc-LED) or a mixture of red and green phosphor materials (2pc-LED) are used in addition to a blue LED die. The additive mixing of the initial blue light with the emission of different luminescent materials produces white light.

Most commercially available 1pc-LEDs use garnet materials doped with Ce^{3+} like YAG:Ce ($Y_{3-x}Gd_xAl_{5-y}Ga_yO_{12}$:Ce) as the yellow broadband emitter. This material has excellent thermal and chemical stability. However, because of its lack of emission in the red spectral range, its application is limited to cool-white light (correlated color temperatures or CCT of 4000-8000 K) with low CRIs of typically <75. To achieve illumination-grade light, CCT values ranging from 2700-4000 K and CRIs typically >80 are required, which only become accessible by using 2pc-LEDs.

For this approach a huge number of materials, especially red-emitters, have been investigated by the lighting industry but without fulfilling their demanding requirements, like chemical and thermal stability, quantum efficiencies close to 100%, and excellent thermal quenching behavior. However, through these investigations, (oxo)nitridosilicates have emerged as intriguing host lattices for doping with rare-earth ions and, therefore, as luminescent materials covering the whole spectral range from blue to red.[1] Novel nitride-based pc-LEDs enable access to acceptable CRI values at CCTs in the desired range. With the state of the art phosphor materials, brilliant CRIs >90 can also easily be obtained, but only by accepting heavy losses in luminous efficacy (efficiency of light conversion relative to the human eye sensitivity in lm/W).

A current challenge for LED industry, therefore, is to further improve the color rendition of illumination-grade light sources without comprising energy efficiency or rather better adapting the pc-LED emission to the sensitivity of human vision to produce a high luminous efficacy. One promising approach is optimizing the spectral peak position and width of the red-emitting component.

The number of adequate red-emitting materials is rather small at present because of the challenging requirements like temperature stability up to 150° C on the LED chip surface. Eu^{2+} doped materials like $(Ca,Sr)SiAlN_3:Eu^{2+}$ (λ_{em} ~610-660 nm, fwhm ~2100-2500 cm^{-1})[2,3] or $(Ba,Sr)_2Si_5N_8:Eu^{2+}$ (λ_{em} ~590-625 nm, fwhm ~2050-2600 cm^{-1})[4-6] have found many applications in commercial white pc-LEDs as a result of the intense emission caused by the 5*d*-4*f* transition. Thanks to rather broad emission bands of both materials, significant parts of the emitted light are above 700 nm and therefore outside the human eye's sensitivity. The width of the Eu^{2+} emission bands in these materials is strongly influenced by several factors. $(Ca,Sr)SiAlN_3:Eu^{2+}$ is affected by the statistical distribution of Si and Al in the host lattice, leading to a broad variety of activator (Eu^{2+}) coordination spheres and, therefore, a rather broad emission band. $(Ba,Sr)_2Si_5N_8:Eu^{2+}$ shows two crystallographic sites accessible for Eu^{2+}. The chemical difference between both sites leads to distinct emission maxima, which also resulting in a relatively broad composite emission.

The recently discovered group of narrow band red-emitting nitride materials like $Sr[Mg_3SiN_4]:Eu^{2+}$ (λ_{em} = 615 nm, fwhm ~1170 cm^{-1})[7] or $Sr[LiAl_3N_4]:Eu^{2+}$ (λ_{em} = 650 nm, fwhm ~1180 cm^{-1})[8] could be the basis for the next generation of illumination-grade pc-LEDs. In these materials the activator ion is situated in cuboid-like polyhedra with N as a counter ion, surrounded by a highly-condensed ordered network of edge- and corner-sharing tetrahedra. Phonons affecting the emission broadness and the thermal quenching are successfully reduced to a minimum thanks to the rigidity of the host lattice. The compound $Sr[LiAl_3N_4]:Eu^{2+}$ already demonstrates the high potential of such materials for industrial applications. The use of this material as a red-emitting component in a pc-LED helps to increase the luminous efficacy of a prototype device

by 14% (R_a8 = 91, R9 = 57) compared to a commercially available high-CRI LED, still keeping a brilliant CRI >90.

To further optimize the luminous efficacy of solid-state light sources for a variety of correlated color temperatures and color rendition requirements, tuning of the red emission spectrum towards shorter wavelengths (~600-630 nm) will be the next challenge for solid-state lighting industry to meet.

2.4.2 References

(1) Zeuner, M., Pagano, S., Schnick, W. *Angew. Chem. Int. Ed.* **2011,** *50*, 7754.

(2) Uheda, K., Hirosaki, N., Yamamoto, H. *Phys. Stat. Sol. A* **2006,** *11*, 2712.

(3) Uheda, K., Hirosaki, N., Yamamoto, H., Naita, A., Nakajima, T., Yamamoto, H. *Electrochem. Solid State Lett.* **2006,** *9*, H22.

(4) Krames, M. R.; Mueller, G. O.; Mueller-Mach, R. B.; Bechtel, H.-H.; Schmidt, P. J. Wavelength conversion for producing white light from high power blue LED. PCT Int. Appl.WO 2010131133 A1, November 18th, 2010.

(5) Höppe, H. A., Lutz, H., Morys, P., Schnick, W., Seilmeier, A. *J. Phys. Chem. Solids* **2000**, *61*, 2001.

(6) Mueller-Mach, R., Mueller, G., Krames, M. R., Höppe, H. A., Stadler, F., Schnick, W., Juestel, T., Schmidt, P. *Phys. Status Solidi A* **2005,** *202*, 1727.

(7) Schmiechen, S., Schneider, H., Wagatha, P., Hecht, C., Schmidt, P. J., Schnick, W. *Chem. Mater.* **2014,** *26*, 2712.

(8) Pust, P., Weiler, V., Hecht, C., Tücks, A., Wochnik, A. S., Henß, A.-K., Wiechert, D., Scheu, C., Schmidt, P. J., Schnick, W. *Nat. Mater.* **2014**, *13*, 891.

2.5 Structural Relationship between the Mg-containing Nitridosilicates $Ca_2Mg[Li_4Si_2N_6]$ and $Li_2Ca_2[Mg_2Si_2N_6]$

Sebastian Schmiechen, Frederik Nietschke, and Wolfgang Schnick

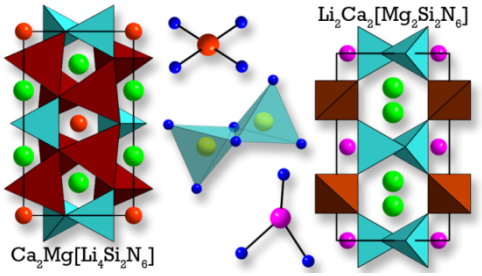

Published in: *Eur.J. Inorg. Chem.* **2015**, 1592; DOI: 10.1002/ejic.201403178
http://onlinelibrary.wiley.com/doi/10.1002/ejic.201403178/abstract

Abstract

$Ca_2Mg[Li_4Si_2N_6]$ and $Li_2Ca_2[Mg_2Si_2N_6]$ were synthesized in sealed tantalum ampules with Li as a fluxing agent. Both compounds crystallize in the monoclinic space group *C*2/*m* (no. 12). The crystal structures were solved and refined on the basis of single-crystal X-ray diffraction data (Z = 2; $Ca_2Mg[Li_4Si_2N_6]$: a = 5.9059(12), b = 9.817(2), c = 5.6109(11) Å, β = 94.90(3)°, R_1 = 0.015, wR_2 = 0.049; $Li_2Ca_2[Mg_2Si_2N_6]$: a = 5.5472(11), b = 9.844(2), c = 5.9978(12) Å, β = 97.13(3)°, R_1 = 0.024, wR_2 = 0.053). $Ca_2Mg[Li_4Si_2N_6]$ is isomorphic to $Ca_3[Li_4Si_2N_6]$ and its crystal structure is homeotypic to that of $Li_2Ca_2[Mg_2Si_2N_6]$. Both structures are built up of edge-sharing $[Si_2N_6]^{10-}$ tetrahedra (bow-tie units). In the nitridolithosilicate $Ca_2Mg[Li_4Si_2N_6]$ the bow-tie units are connected via pairs of LiN_4 tetrahedra, whereas in the nitridomagnesosilicate $Li_2Ca_2[Mg_2Si_2N_6]$ the nitridosilicate substructure is connected by chains of MgN_4 tetrahedra. $Ca_2Mg[Li_4Si_2N_6]$ is only the second example of fourfold planar rectangular coordinated Mg^{2+} in a nitridosilicate. $Li_2Ca_2[Mg_2Si_2N_6]$ is the first nitridosilicate with Li^+

in threefold coordination. The crystal structures were confirmed by lattice-energy calculations (MAPLE), EDX measurements, and powder X-ray diffraction.

2.5.1 Introduction

Numerous multinary nitridosilicates with interesting material properties (e.g., NLO, Li^+-ion conductivity, or luminescence of Eu^{2+}-doped samples) have been synthesized and characterized over the last couple of years.[1-7] This wide-ranging applicability can be ascribed to specific structural features of nitridosilicates. Nitrogen in nitridosilicates can connect up to four neighboring tetrahedral centers and even edge-sharing of SiN_4 tetrahedra is observed frequently. These specific structural features enable a more varied structural diversity as compared to oxosilicates.[1] More complicated variants of nitridosilicates were obtained by partial substitution of Si^{4+} by Al^{3+} or Li^+ and/or N^{3-} by O^{2-} in the anionic substructure, resulting in oxo/nitrido/alumo/litho/silicates (e.g., $La_5[LiSi_4N_{10}O]$ or $(Sr_{0.94}Eu_{0.06})[(Al_{0.3}Si_{0.7})4(N_{0.8}O_{0.2})_6]$).[8,9] Further increase of the variety of nitridosilicates can be achieved by substitution of counterions for the anionic substructure of nitridosilicates. In contrast to Al^{3+}, there are nitridosilicates with Li^+ and Mg^{2+} acting as counterions for the anionic part and thus not participating in the anionic substructure of condensed tetrahedra (e.g., $LiCa_3Si_2N_5$ and $Ba_4Mg[Si_2N_6]$).[10,11] Recently, we succeeded in substituting Mg^{2+} for Si^{4+} within the tetrahedral network structure of nitridosilicates with the isotypic compounds $M[Mg_3SiN_4]$ (M = Ca,Sr,Eu).[4] Hence, Mg^{2+} is the third example, besides Al^{3+} and Li^+, that can replace tetrahedrally coordinated Si^{4+} within the nitridosilicate substructure. Accordingly, the compounds $M[Mg_3SiN_4]$ should be classified as nitridomagnesosilicates.[4]

In this contribution we report on the synthesis and structural characterization of two novel Mg-containing nitridosilicates. $Li_2Ca_2[Mg_2Si_2N_6]$ is the first example of a nitridosilicate with Li^+ in a threefold coordination. The nitridolithosilicate $Ca_2Mg[Li_4Si_2N_6]$ is only the second example with Mg^{2+} acting as a counterion for the anionic nitridosilicate substructure. Furthermore, it is shown how both crystal structures can be derived from the aristotype $Ca_3[Li_4Si_2N_6]$.[12]

2.5.2 Results and Discussion

2.5.2.1 Synthesis and Chemical Analysis

$Ca_2Mg[Li_4Si_2N_6]$ as well as $Li_2Ca_2[Mg_2Si_2N_6]$ have been synthesized in a modified solid-state metathesis reaction in sealed tantalum ampules. As a consequence, heterogeneous reaction mixtures were obtained with both title compounds as side phases along with numerous impurities (e.g., $Ca[Mg_3SiN_4]$ or $Ca[Li_2Si_2N_4]$).[4,13] Only few single crystals of $Ca_2Mg[Li_4Si_2N_6]$ and $Li_2Ca_2[Mg_2Si_2N_6]$ were suitable for further characterization. In general, crystals of the title compounds show an off-white body color with a cube-like habitus, which undergo rapid hydrolysis by contact with air and moisture. The elemental composition was investigated by energy-dispersive X-ray spectroscopy (EDX). Crystals of $Ca_2Mg[Li_4Si_2N_6]$ revealed an atomic ratio Ca/Mg/Si = 2.0:1.2:2.2 and for $Li_2Ca_2[Mg_2Si_2N_6]$ a ratio of 2.0:2.1:2.1 was detected. Li is not determinable with this method, but the other results from the EDX analyses agree well within the standard deviations with the composition obtained from the single-crystal structure analysis.

2.5.2.2 Single-Crystal Structure Analysis

The novel Mg-containing nitridosilicates crystallize in the monoclinic space group *C*2/*m* (no. 12). Details of the structure determination and further crystallographic data are summarized in Table 2.5-1. Atomic coordinates and isotropic displacement parameters are given in Table 2.5-2. Information on selected bond lengths for both compounds is given in Table 2.5-3. Table 6.4-S1 in the Supporting Information lists the anisotropic displacement parameters with figures of the corresponding ellipsoids.

2.5.2.3 Crystal-Structure Description

$Ca_2Mg[Li_4Si_2N_6]$ and $Li_2Ca_2[Mg_2Si_2N_6]$ have homeotypic crystal structures and exhibit structural features of the nitridolithosilicate $Ca_3[Li_4Si_2N_6]$;[12] a detailed comparison will be given later. $Ca_2Mg[Li_4Si_2N_6]$ is isomorphic to $Ca_3[Li_4Si_2N_6]$ with one Ca^{2+} being formally replaced by Mg^{2+}. The crystal structure of $Ca_2Mg[Li_4Si_2N_6]$ (see Figure 2.5-1) consists of $[Si_2N_6]^{10-}$ bow-tie units.

Table 2.5-1. Crystallographic Data of $Ca_2Mg[Li_4Si_2N_6]$ and $Li_2Ca_2[Mg_2Si_2N_6]$

	$Ca_2Mg[Li_4Si_2N_6]$	$Li_2Ca_2[Mg_2Si_2N_6]$
formula mass/g·mol^{-1}	272.47	282.90
crystal system	monoclinic	
space group	*C*2/*m* (no. 12)	
cell parameters/Å,°	*a* = 5.9059(12)	*a* = 5.5472(11)
	b = 9.817(2)	*b* = 9.844(2)
	c = 5.6109(11)	*c* = 5.9978(12)
	β = 94.90(3)	*β* = 97.13(3)
V/Å^3	324.13(11)	325.00(11)
formula units/cell	2	
X-ray density/g·cm^{-3}	2.792	2.891
abs. coefficient μ/mm^{-1}	2.155	2.247
F(000)	268	280
crystal size/mm	0.15×0.13×0.10	0.05×0.04×0.03
diffractometer, radiation	Nonius Kappa CCD	Stoe IPDS I
	Mo-K*α* (*λ* = 0.71073 Å)	
temperature/K	293(2)	
absorption correction	none	multi-scan[14]
θ range/°	3.64-28.00	3.42-27.48
measured reflections	3529	1674
independent reflections	1552	1341
observed reflections	419	396
refined parameters	41	38
GoF	1.092	1.028
R indices ($F_o^2 \geq 2\sigma(F_o^2)$)	R_1 = 0.0159, wR_2 = 0.0498	R_1 = 0.0240, wR_2 = 0.0534
R indices (all data)	R_1 = 0.0159, wR_2 = 0.0498	R_1 = 0.0317, wR_2 = 0.0549
min / max residual electron density/eÅ^{-3}	-0.45 / 0.30	-0.43 / 0.45

Table 2.5-2. Atomic Coordinates and Isotropic Displacement Parameters of $Ca_2Mg[Li_4Si_2N_6]$ and $Li_2Ca_2[Mg_2Si_2N_6]$; Estimated Standard Deviations (e.s.d.'s) in Parentheses

	Atom	Wyckoff position	x	y	z	U_{eq} [Å^3]
$Ca_2Mg[Li_4Si_2N_6]$	Ca	4*g*	0	0.3218(4)	0	0.0051(2)
	Si	4*i*	0.3215(8)	0	0.3670(9)	0.0050(2)
	Mg	2*a*	0	0	0	0.0195(3)
	Li	8*j*	0.3392(5)	0.3283(3)	0.3765(6)	0.0136(6)
	N1	8*j*	0.1787(2)	0.1440(12)	0.2510(2)	0.0070(2)
	N2	4*i*	0.6219(3)	0	0.3126(3)	0.0068(3)
$Li_2Ca_2[Mg_2Si_2N_6]$	Ca	4*g*	0	0.1840(7)	0	0.0095(2)
	Si	4*i*	0.6308(2)	0	0.1790(2)	0.0083(2)
	Mg	4*h*	0	0.2661(12)	1/2	0.0106(3)
	Li	4*i*	0.1709(2)	0	0.4044(10)	0.0199(2)
	N1	8*j*	0.2478(4)	0.3548(2)	0.3106(3)	0.0130(4)
	N2	4*i*	0.3086(5)	0	0.1097(5)	0.0112(5)

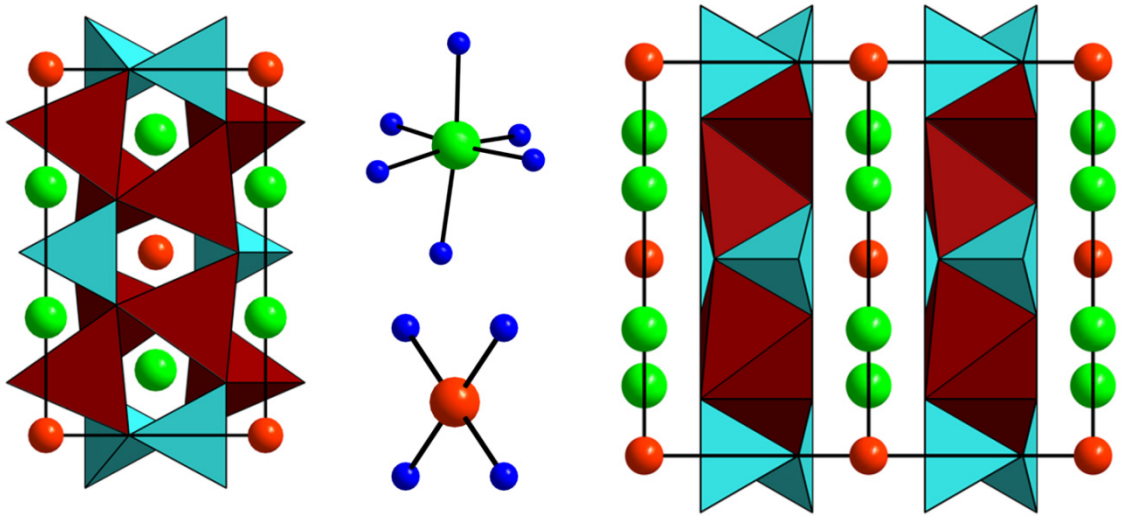

Figure 2.5-1. Crystal structure of $Ca_2Mg[Li_4Si_2N_6]$: viewed along [001] (left) and a double unit cell along [100] (right). Middle: octahedral coordination of Ca^{2+} (top) and fourfold planar rectangular coordination of Mg^{2+} (bottom). SiN_4 tetrahedra aquamarine, LiN_4 tetrahedra brown, Ca^{2+} green, Mg^{2+} red and N^{3-} blue.

Table 2.5-3. Selected Bond Lengths [Å] and Angles [°] of $Ca_2Mg[Li_4Si_2N_6]$ and $Li_2Ca_2[Mg_2Si_2N_6]$; e.s.d.'s in Parentheses

bond/angle name	$Ca_2Mg[Li_4Si_2N_6]$	$Li_2Ca_2[Mg_2Si_2N_6]$
Ca-N1	2.4272(12) (2 x)	2.494(2) (2 x)
Ca-N1	2.4809(2) (2 x)	2.748(2) (2 x)
Ca-N2	2.5377(12) (2 x)	2.523(2) (2 x)
Si-N1	1.7431(12) (2 x)	1.721(2) (2 x)
Si-N2	1.8003(2)	1.784(3)
Si-N2	1.8256(2)	1.805(3)
Mg-N1	2.2003(12) (4 x)	2.066(2) (2 x)
Mg-N1	-	2.081(2) (2 x)
Li-N1	2.119(3)	2.231(5) (2 x)
Li-N1	2.135(3)	-
Li-N1	2.198(3)	-
Li-N2	2.130(3)	2.010(7)
N1-Si-N1	108.36(8)	112.38(15)
N1-Si-N2	112.57(5)	109.60(9)
N1-Si-N2	114.55(5)	114.63(9)
N2-Si-N2	93.81(8)	94.44(2)

This structural motif was first described by DiSalvo et al. in $Ba_5Si_2N_6$.[12,15-17] Caused by edge sharing of the SiN_4 tetrahedra in $Ca_2Mg[Li_4Si_2N_6]$ the corresponding angle N2–Si–N2 is reduced to a value of 93.81(8)° and the involved Si–N2 distances are elongated and range from 1.80–1.83 Å. This results in a rather short Si–Si distance of 2.4772(12) Å. All of these features can be observed for other bow-tie type nitridosilicates as well.[12,15-17] Especially the structurally related $Ca_3[Li_4Si_2N_6]$ shows good accordance with a reduced angle N–Si–N of 95.9°, a Si–N bond length of 1.83 Å, and a Si–Si distance of 2.45 Å.[12] The terminal N atoms are at a distance of 1.7431(12) Å to Si, which is a typical Si–N bond length found in nitridosilicates.[1] The $[Si_2N_6]^{10-}$ bow-tie units are connected along [010] by pairs of edge-sharing $[Li_2N_6]^{16-}$ tetrahedra, forming layers of *dreier* rings along [001].[18,19] Since the layers are built up of SiN_4 and LiN_4 tetrahedra, the compound can be more appropriately classified as a nitridolithosilicate.[20] As a result, the compound has a very high degree of condensation

(i.e., atomic ratio (Li,Si)/N) κ = 1, which is rather uncommon for layered nitridosilicates. Li–N distances vary from 2.12 to 2.20 Å and are in good accordance with those of tetrahedrally coordinated Li and the sum of the ionic radii (2.12 Å).[3,12,13,21] Ca and Mg ions are located between the layers of *dreier* rings. Mg^{2+} has a fourfold planar rectangular coordination with N^{3-} (see Figure 2.5-1, middle, bottom) and, besides $Ba_4Mg[Si_2N_6]$, this is only the second example of Mg^{2+} exhibiting this coordination in nitridosilicates.[11] The Mg–N distances (2.2003(12) Å) are slightly larger than in $Ba_4Mg[Si_2N_6]$ but in good agreement with other fourfold-coordinated Mg-containing nitrides.[4,22,23] The other counterion, Ca^{2+}, is surrounded by six N atoms forming a distorted octahedron (see Figure 2.5-1, middle, top). The corresponding Ca–N bond lengths vary from 2.43 to 2.54 Å and are in a typical range for nitridosilicates.[1,10,12,13,17] The crystal structure of $Li_2Ca_2[Mg_2Si_2N_6]$ (see Figure 2.5-2) is homeotypic to that of $Ca_2Mg[Li_4Si_2N_6]$ and also consists of $[Si_2N_6]^{10-}$ bow-tie units, but has a lower degree of condensation (atomic ratio (Mg,Si)/N) κ = 0.66.

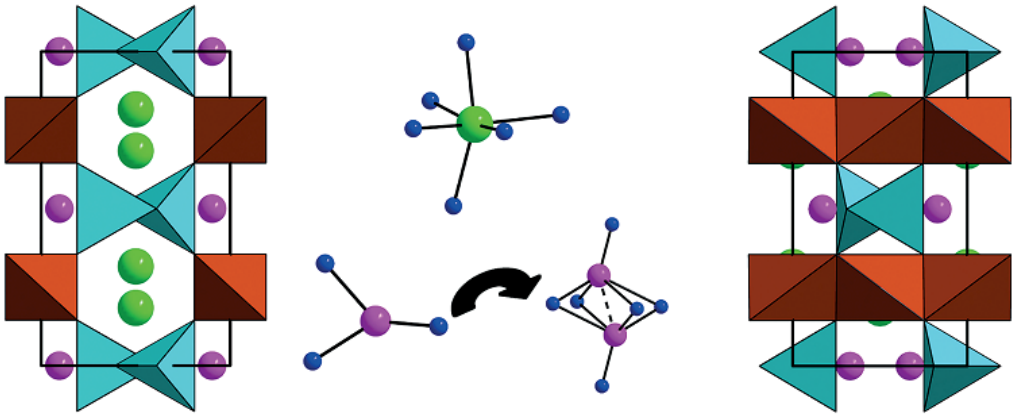

Figure 2.5-2. Crystal structure of $Li_2Ca_2[Mg_2Si_2N_6]$: viewed along [100] (left) and along [001] (right). Middle: octahedral coordination of Ca^{2+} (top), threefold coordination of Li^+ (bottom, left), and octahedral coordination of two Li^+ (bottom, right). SiN_4 tetrahedra aquamarine, MgN_4 tetrahedra orange, Ca^{2+} green, Li^+ purple, and N^{3-} blue.

Edge sharing of SiN_4 tetrahedra in $Li_2Ca_2[Mg_2Si_2N_6]$ induces again a reduced angle N2–Si–N2 of 94.44(2)°. This effects an increased bond length Si–N2 of 1.805(3) Å and therefore a shorter Si–Si distance of 2.4379(2) Å. The bond lengths to terminal N atoms range from 1.72 to 1.78 Å.

These structural features are in good agreement with the results from $Ca_2Mg[Li_4Si_2N_6]$. The nitridosilicate substructure of $Li_2Ca_2[Mg_2Si_2N_6]$ is built up of $[Si_2N_6]^{10-}$ bow-tie units that are connected by MgN_4 tetrahedra. Thus, a classification as a nitridomagnesosilicate is more suitable. MgN_4 tetrahedra are connected via two common edges to each other forming strands running along [100]. Mg–N bond lengths range from 2.07–2.08 Å and are in good accordance with the sum of the ionic radii (2.08 Å) according to Baur and the values found in $MgSiN_2$.[21,22] Ca^{2+} is in sixfold coordination with N (see Figure 2.5-2, middle, top). The distorted octahedron shows Ca–N distances of 2.49 to 2.75 Å; other Ca-containing multinary nitridosilicates, for example $Ca[Li_2Si_2N_4]$ or $LiCa_3SiN_5$,[10,13] have comparable Ca–N distances. CaN_6 octahedra are connected via two common edges to each other forming *sechser* ring layers along [001].[18,19] Li exhibits coordination number three towards N which is very uncommon for nitridosilicates (see Figure 2.5-2, middle, bottom) but has been found in a number of other nitrides (e.g., Li_3N, LiCaN, or $Li_3Sr_2TaN_4$).[24-26] The corresponding distances range from 2.01 to 2.23 Å and correspond well with the sum of the ionic radii and the above-mentioned compounds with Li in threefold coordination. An extended view of the coordination sphere of the Li site leads to a 3+2 coordination, resulting in a short Li–Li distance of 2.336(13) Å that can also be found in $Li_2Sr_4T_4N_8O$ (T = Si^{4+} or Al^{3+}+Ta^{5+}).[27,28] The resulting coordination polyhedron around both Li can be described as a barely distorted octahedron. These isolated octahedra connect the layers of *sechser* rings formed by CaN_6 octahedra.

The nitridolithosilicate $Ca_2Mg[Li_4Si_2N_6]$ as well as the nitridomagnesosilicate $Li_2Ca_2[Mg_2Si_2N_6]$ are structurally related to each other and can be derived from $Ca_3[Li_4Si_2N_6]$, which can be seen as the aristotype for both novel Mg-containing nitridosilicates. How both title compounds can formally be derived from $Ca_3[Li_4Si_2N_6]$ is shown in Figure 2.5-3. The Si/N substructure is not discussed in detail, because it is quite similar in all three compounds.

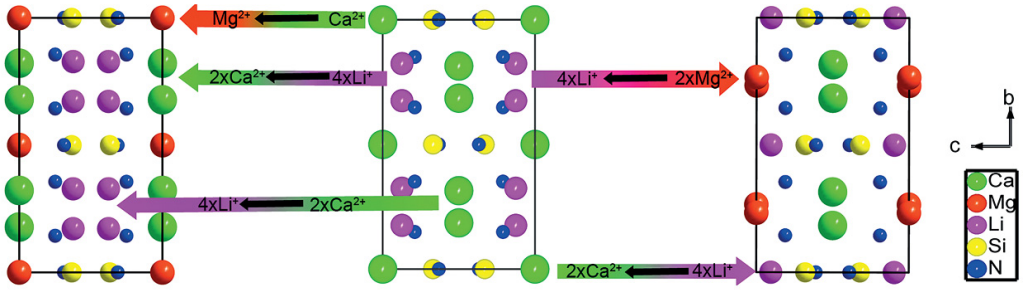

Figure 2.5-3. Graphical derivation of the nitridolithosilicate $Ca_2Mg[Li_4Si_2N_6]$ (left) and the nitridomagnesosilicate $Li_2Ca_2[Mg_2Si_2N_6]$ (right) from the aristotype $Ca_3[Li_4Si_2N_6]$ (middle). Depicted arrows connect correlating atom positions within the crystal structures.

The nitridolithosilicates $Ca_2Mg[Li_4Si_2N_6]$ (Figure 2.5-3, left) and $Ca_3[Li_4Si_2N_6]$ (Figure 2.5-3, middle) are isomorphic to each other with formally one Ca^{2+} (green) substituted by Mg^{2+} (red) as counterion. In contrast to Ca^{2+}, Mg^{2+} is not typically found in sixfold coordination with N^{3-}. As a consequence, in $Ca_2Mg[Li_4Si_2N_6]$ layers of CaN_6 octahedra are present with Mg^{2+} in fourfold rectangular coordination inside the cavities. In contrast, the aristotype $Ca_3[Li_4Si_2N_6]$ shows a *sechser* ring framework of CaN_6 octahedra. Thus, a position change between $4 \times Li^+$ (purple) and $2 \times Ca^{2+}$ (green) is required and LiN_4 tetrahedra are incorporated into the Si/N substructure forming layers of *dreier* rings in $Ca_2Mg[Li_4Si_2N_6]$.

The nitridomagnesosilicate $Li_2Ca_2[Mg_2Si_2N_6]$ (Figure 2.5-3, right) is homeotypic to $Ca_3[Li_4Si_2N_6]$. Hereby, formally $2 \times Li^+$ replace one Ca^{2+} as counterion. As described above, there are short Li–Li distances in the crystal structure of $Li_2Ca_2[Mg_2Si_2N_6]$, which results in a joint octahedral coordination of both Li (Li_2N_6 octahedra). These octahedra are large enough to replace CaN_6 octahedra in the corresponding framework of $Ca_3[Li_4Si_2N_6]$. For the charge balance in $Li_2Ca_2[Mg_2Si_2N_6]$, formally $4 \times Li^+$ are replaced with $2 \times Mg^{2+}$, which are part of the Si/N substructure.

2.5.2.4 Lattice-Energy Calculations

The crystal structures of both title compounds were investigated further using lattice-energy calculations (MAPLE, MAdelung Part of Lattice Energy).[21,29-31]

Table 2.5-4. Results of the MAPLE Calculations [kJ/mol] for $Ca_2Mg[Li_4Si_2N_6]$ and $Li_2Ca_2[Mg_2Si_2N_6]$; Δ = MAPLE sum of Constituting Binary/Ternary Nitrides ÷ MAPLE Sum Compound – 1;[a]

	$Ca_2Mg[Li_4Si_2N_6]$	$Li_2Ca_2[Mg_2Si_2N_6]$
Ca^{2+}	2014	1836
Mg^{2+}	2163	2528
Si^{4+}	9135	9466
Li^{+}	679	655
N^{3-}	5041 – 5519	5067 - 5451
Total	58464	60158
Δ	0.4%	0.3%

Total MAPLE

$Ca_2Mg[Li_4Si_2N_6]$: $Ca_3N_2 + Mg_3N_2 + 2\times Li2SiN_2 – CaMg_2N_2$ = 58684 kJ/mol

$Li_2Ca_2[Mg_2Si_2N_6]$: $2\times CaSiN_2 + 2\times LiMgN$ = 60324 kJ/mol

[a] Typical MAPLE values [kJ/mol], for Ca^{2+}: 1700-2200; Mg^{2+}: 2100-2500; Si^{4+}: 9000-10200; N^{3-}: 4300-6200; Li^{+}: 550-860.[1,3,4,10]

With the aid of this algorithm, the consistency of a structure model can be corroborated by computing electrostatic interactions in dependence on the charge, distance, and coordination spheres of the constituting atoms. The results are summarized in Table 2.5-4. Both title compounds show partial MAPLE values that are in good agreement with reference data. Also, the MAPLE sums of $Ca_2Mg[Li_4Si_2N_6]$ and $Li_2Ca_2[Mg_2Si_2N_6]$ show only a minor deviation in contrast to the total MAPLE values of constituting binary and ternary nitrides. Consequently, the electrostatic consistency of both crystal structures is proven and confirmed.

2.5.3 Conclusion

In this contribution, two novel Mg-containing nitridosilicates, namely $Ca_2Mg[Li_4Si_2N_6]$ and $Li_2Ca_2[Mg_2Si_2N_6]$, were reported. Hitherto, Mg-containing nitridosilicates were rare and the subgroup of nitridomagnesosilicates was only recently described for the first time in the isotypic compounds $M[Mg_3SiN_4]$ (M = Ca,Sr,Eu). $Li_2Ca_2[Mg_2Si_2N_6]$ is a new example of this compound class. In contrast, Mg has a different character in $Ca_2Mg[Li_4Si_2N_6]$. In the latter compound Mg^{2+} is a counterion for the nitridolithosilicate substructure. Consequently, magnesium is a chimera that could greatly increase the

structural variety of nitridosilicates. Our syntheses and characterization of the novel Mg-containing nitridosilicates $Ca_2Mg[Li_4Si_2N_6]$ and $Li_2Ca_2[Mg_2Si_2N_6]$ has showed once more that Mg has to date unjustly received less consideration within the field of synthesis of novel nitridosilicates.

2.5.4 Experimental Section

2.5.4.1 General Experimental Details

Most starting materials and products are sensitive to air and moisture, thus all syntheses are performed under inert-gas conditions. Therefore, either flame-dried Schlenk-type glassware interfaced to a combined Schlenk/vacuum line (10^{-3} mbar) or an argon-filled glove box (Unilab, MBraun, Garching, $O_2 < 1$ ppm, $H_2O < 1$ ppm) were used. The purification of argon (Messer–Griessheim, 5.0) was carried out by passage through columns of silica gel (Merck), molecular sieves (Fluka, 4 Å), KOH (Merck, ≥85 %), P_4O_{10} (Roth, ≥99 %) and titanium sponge (Johnsen Matthey, 99.5 %) at 700 °C. Tantalum ampules (length: 30 mm, inner diameter: 9.5 mm, wall thickness: 0.5 mm) were used as reaction containers. They were arc welded under a pressure of 1 bar of purified argon. During this procedure the crucible holder was cooled with water to avoid chemical reactions. Sealed ampules were heated in evacuated silica tubes with the following temperature program: heating to 950 °C within 5 h, maintaining the temperature for 24 h and cooling down subsequently to 500 °C in 60 h. Finally, the reaction mixture was quenched to room temperature by switching off the furnace.

2.5.4.2 Synthesis of $Ca_2Mg[Li_4Si_2N_6]$

Single crystals of $Ca_2Mg[Li_4Si_2N_6]$ were isolated after the reaction of CaF_2 (0.40 mmol, 31.2 mg, Sigma Aldrich, 99.99 %), Mg_3N_2 (0.13 mmol, 13.5 mg, Sigma Aldrich, 99.5 %), and "$Si(NH)_2$" (0.40 mmol, 23.2 mg, synthesized according to a modified method by Lange et al.).[32,33] The starting materials were ground under argon atmosphere in a glove box and then LiN_3 (0.40 mmol, 19.6 mg, synthesized according to the method by Fair et al.)[34] as a nitrogen source and Li (2.67 mmol, 18.5 mg, Alfa Aesar, 99.9 %) as a

fluxing agent were added. The reaction mixture was placed in a tantalum ampule and handled as described above.

2.5.4.3 Synthesis of $Li_2Ca_2[Mg_2Si_2N_6]$

An analogous synthesis route was used to obtain single crystals of $Li_2Ca_2[Mg_2Si_2N_6]$. Therefore, CaF_2 (0.20 mmol, 15.6 mg), Mg_3N_2 (0.20 mmol, 20.2 mg), "$Si(NH)_2$" (0.40 mmol 23.2 mg), and LiN_3 (0.45 mmol, 22.0 mg) were ground under an argon atmosphere in a glove box. A portion of Li (2.00 mmol, 13.9 mg) was added. The arc-welding and heating procedure is described in the General Experimental Details section.

2.5.4.4 X-ray Spectroscopy

For the determination of the chemical composition of the title compounds crystallites were analyzed by EDX spectroscopy employing a JSM-6500F scanning electron microscope (SEM, Jeol) with a Si/Li EDX detector (Oxford Instruments, model 7418).

2.5.4.5 Single-Crystal X-ray Diffraction

Single crystals of $Ca_2Mg[Li_4Si_2N_6]$ and $Li_2Ca_2[Mg_2Si_2N_6]$ were selected under inert-gas conditions in a glove box with an integrated microscope. Suitable crystals were enclosed in glass capillaries and sealed under argon. X-ray diffraction data of the corresponding single crystals were either collected with a STOE IPDS I diffractometer equipped with a graphite monochromator or with a Nonius Kappa-CCD diffractometer equipped with graded multilayer X-ray optics (both diffractometers use Mo-K_α radiation (λ = 0.71073 Å)). After absorption correction with SADABS[14] for $Li_2Ca_2[Mg_2Si_2N_6]$, the structures were solved by Direct Methods (SHELXS)[35] and refined by full-matrix least-squares methods (SHELXL)[36,37] (see Table 2.5-1 for details).

Further details on the crystal structure investigation may be obtained from the Fachinformationszentrum Karlsruhe, Germany, 76344 Eggenstein-Leopoldshafen, Germany (fax: +49-7247-808-259; e-mail: crysdata@fiz-karlsruhe.de), on quoting the depository numbers CSD-427077 and -427078.

2.5.4.6 Powder X-ray Diffraction

The structural models obtained from single-crystal data were verified with powder X-ray data. Therefore, crystallites of $Ca_2Mg[Li_4Si_2N_6]$ and $Li_2Ca_2[Mg_2Si_2N_6]$ were separated from the heterogeneous reaction products with the aid of a microscope. The ground mixtures were measured in sealed capillaries with a STOE STADI P diffractometer (Cu-$K_{\alpha1}$ or Mo-$K_{\alpha1}$ radiation, Ge(111) monochromator, Mythen1K detector) in Debye–Scherrer geometry. Corresponding powder diffractograms are given in the Supporting Information.

2.5.5 References

(1) Zeuner, M.; Pagano, S.; Schnick, W. *Angew. Chem. Int. Ed.* **2011**, *50*, 7754.

(2) He, X.-H.; Lian, N.; Sun, J.-H.; Guan, M.-Y. *J. Mater. Sci.* **2009**, *44*, 4763.

(3) Lupart, S.; Gregori, G.; Maier, J.; Schnick, W. *J. Am. Chem. Soc.* **2012**, *134*, 10132.

(4) Schmiechen, S.; Schneider, H.; Wagatha, P.; Hecht, C.; Schmidt, P. J.; Schnick, W. *Chem. Mater.* **2014**, *26*, 2712.

(5) Uheda, K.; Hirosaki, N.; Yamamoto, Y.; Naito, A.; Nakajima, T.; Yamamoto, H. *Electrochem. Solid-State Lett.* **2006**, *9*, H22.

(6) Xie, R.-J.; Hirosaki, N.; Li, Y.; Takeda, T. *Materials* **2010**, *3*, 3777.

(7) Zeuner, M.; Schmidt, P. J.; Schnick, W. *Chem. Mater.* **2009**, *21*, 2467.

(8) Lupart, S.; Schnick, W. *Z. Anorg. Allg. Chem.* **2012**, *638*, 94.

(9) Yamane, H.; Shimooka, S.; Uheda, K. *J. Solid State Chem.* **2012**, *190*, 264.

(10) Lupart, S.; Schnick, W. *Z. Anorg. Allg. Chem.* **2012**, *638*, 2015.

(11) Yamane, H.; Morito, H. *J. Alloys Compd.* **2013**, *555*, 320.

(12) Pagano, S.; Lupart, S.; Schmiechen, S.; Schnick, W. *Z. Anorg. Allg. Chem.* **2010**, *636*, 1907.

(13) Zeuner, M.; Pagano, S.; Hug, S.; Pust, P.; Schmiechen, S.; Scheu, C.; Schnick, W. *Eur. J. Inorg. Chem.* **2010**, *2010*, 4945.

(14) Ottinger, F.; Nesper, R. *Z. Anorg. Allg. Chem.* **2005**, *631*, 1597.

(15) Yamane, H.; DiSalvo, F. J. *J. Alloys Compd.* **1996**, *240*, 33.

(16) Yamane, H.; Morito, H. *Inorg. Chem.* **2013**, *52*, 5559.

(17) Sheldrick, G. M. SADABS, v. 2: Multi-Scan Absorption Correction, Bruker-AXS, 2012.

(18) Liebau coined the terms *zweier*, *dreier*, *vierer*, *fünfer*, and *sechser* rings. Thereby, a *dreier* or *sechser* ring can be described as three or six polyhedra connected to each other by common corners, forming a ring. The terms derive from the German numerals *drei* (3), *sechs* (6), etc. by adding the suffixing “er” to the numeral.

(19) Liebau, F. *Structural Chemistry of Silicates*; Springer: Berlin, New York, 1985.

(20) Hofmann, R.; Hoppe, R. *Z. Anorg. Allg. Chem.* **1988**, *560*, 35.

(21) Baur, W. H. *Crystallogr. Rev.* **1987**, *1*, 59.

(22) David, J.; Laurent, Y.; Lang, J. *Bull. Soc. Fr. Mineral. Cristallogr.* **1970**, *93*, 153.

(23) Reckeweg, O.; Molstad, J. C.; DiSalvo, F. J. *J. Alloys Compd.* **2001**, *315*, 134.

(24) Cordier, G.; Gudat, A.; Kniep, R.; Rabenau, A. *Angew. Chem. Int. Ed. Engl.* **1989**, *101*, 1702.

(25) Chen, X. Z.; Eick, H. A. *J. Solid State Chem.* **1997**, *130*, 1.

(26) Rabenau, A.; Schulz, H. *J. Less-Common Met.* **1976**, *50*, 155.

(27) Pagano, S.; Lupart, S.; Zeuner, M.; Schnick, W. *Angew. Chem. Int. Ed. Engl.* ***2009****, 48, 6335*.

(28) Pust, P.; Schnick, W. *Z. Anorg. Allg. Chem.* **2012**, *638*, 352.

(29) Hübenthal, R. MAPLE, v. 4: A program for the calculation of Madelung part of lattice energy, University of Gießen, 1993.

(30) Hoppe, R. *Angew. Chem. Int. Ed.* **1966**, *5*, 95.

(31) Hoppe, R. *Angew. Chem. Int. Ed.* **1970**, *9*, 25.

(32) Lange, H.; Wötting, G.; Winter, G. *Angew. Chem. Int. Ed. Engl.* **1991**, *30*, 1579.

(33) Höppe, H. A. *Doctoral Thesis*, Ludwig Maximilian University Munich, 2003.

(34) Fair, H. D.; Walker, R. F. *Energetic Materials 1, Physics and Chemistry of Inorganic Azides*; 1st ed.; Plenum Press: New York, London, 1977.

(35) Sheldrick, G. M. SHELXS-97: A program for crystal structure solution, University of Göttingen, 1997.

(36) Sheldrick, G. M. *Acta Crystallogr. Sect. A: Found. Crystallogr.* **2008**, *64*, 112.

(37) Sheldrick, G. M. SHELXL-97: A program for crystal structure refinement, University of Göttingen, 1997.

2.6 Nitridolithomagnesoalumosilicate $Ba[(Mg_{2-x}Li_x)(Al_{4-x}Si_x)N_6]$ with x = (0-2) for LED-Backlighting Applications

Sebastian Schmiechen, Philipp Strobel, Markus Siegert, Peter J. Schmidt, and Wolfgang Schnick

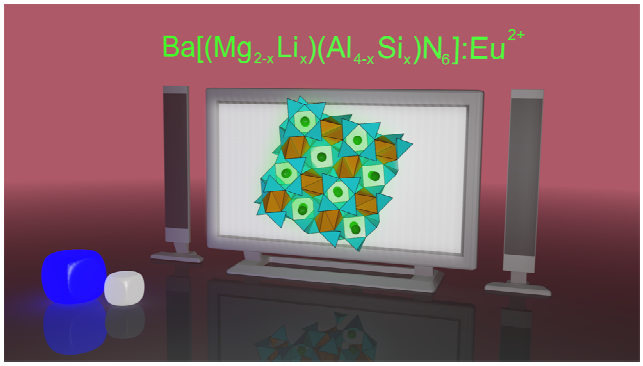

Published in: *To be published.*

Abstract

The Eu^{2+}-doped compounds $Ba[(Mg_{0.4}Li_{1.6})(Al_{2.4}Si_{1.6})N_6]$ and $Ba[(Mg_{0.2}Li_{1.8})(Al_{2.2}Si_{1.8})N_6]$ have been synthesized by a solid-state metathesis reaction in a sealed tantalum ampule. The nitridoalumolithomagnesosilicates crystallize in the tetragonal space group *P*4/*ncc* (no. 130). Crystal structures were solved and refined from single-crystal X-ray diffraction data ($Z = 4$, $Ba[(Mg_{0.4}Li_{1.6})(Al_{2.4}Si_{1.6})N_6]:Eu^{2+}$: $a = 7.892(3)$, $c = 9.995(4)$ Å, $R_1 = 0.017$, $wR_2 = 0.046$; $Ba[(Mg_{0.2}Li_{1.8})(Al_{2.2}Si_{1.8})N_6]:Eu^{2+}$: $a = 7.879(3)$, $c = 9.983(4)$ Å, $R_1 = 0.018$, $wR_2 = 0.049$). The crystal structure of both compounds contains a highly condensed tetrahedra network with a degree of condensation (i.e., atomic ratio (Al,Si,Li,Mg):N) $\kappa = 1$. The Eu^{2+}-doped samples show promising emission in the green to yellow part of the visible spectrum ($\lambda_{max} = 562$ nm, fwhm ~2739 cm^{-1} $Ba[(Mg_{0.4}Li_{1.6})(Al_{2.4}Si_{1.6})N_6]:Eu^{2+}$; $\lambda_{max} = 560$ nm, fwhm ~2654 cm^{-1} $Ba[(Mg_{0.2}Li_{1.8})(Al_{2.2}Si_{1.8})N_6]:Eu^{2+}$). According to this tuneability, an application in white LEDs for backlighting purposes for LCDs is in prospect.

2.6.1 Introduction

Thomas Alva Edison most prominent invention, the incandescent light bulb, was a revolution in the 1880's as general illumination got more and more in the focus and was the start into a new era for the industrialized world.[1] More than 130 years later the incandescent light bulb is a symbol for wasting resources, especially energy.[2,3] The global energy consumption is rising year by year and inefficient products are gradually removed from the global markets. Therefore, it is not surprising that the incandescent light bulb is being replaced by modern alternatives.[4,5] Compact fluorescent lamps (CFLs) were seen for a long time as a qualified replacement. However, the emission spectrum of a CFL shows a lot of gaps which result in a bad color rendition. Moreover, CFLs contain small amounts of mercury which give raise to doubts against ecological suitability. In the mean time, light-emitting diodes (LEDs) have been enhanced and today LEDs are superior candidates for the replacement of other light sources.[3,6,7] For general illumination two phosphor-converted (2pc-)LEDs, which means that the blue light of a primary (In,Ga)N LED is partially converted by red and green phosphors to white light, are the most advanced technique.[8] Correlated color temperatures (CCT) and color rendition (CRI) are by now in the magnitude of incandescent light bulbs. Another important area of application for LEDs is the use in backlighting applications for modern liquid crystal displays (LCDs). These displays influence the direction of polarization of a light source behind the layer of the liquid crystals. Hereby, it is most important that the light source covers the whole visible spectrum and that the emission peaks in the blue, green and red region match the color filters of the LCD.[9] Therefore, a white LED for backlighting applications has to have narrow-band emission in the corresponding regions that no or less energy is wasted. Commonly used 1pc-LEDs with $Y_{3-x}Gd_xAl_{5-y}Ga_yO_{12}:Ce^{3+}$ (YAG:Ce) as green to yellow component cannot fulfill these requirements and the use of three primary blue, green and red LEDs is reserved to high-end LCDs.[10,11] As the blue light of a primary (In,Ga)N is already sufficient, there is a huge demand on novel narrow-band green- and red-emitting phosphors. Recently, Eu^{2+}-doped nitridosilicates, like $(Ba,Sr)_2Si_5N_8:Eu^{2+}$ or $(Ca,Sr)AlSiN_3:Eu^{2+}$ have merged as good candidates as orange to red phosphors, but

both compounds still show too broad emission bands (i.e., full width at half maximum, fwhm) of 2050-2600 cm^{-1} ($(Ba,Sr)_2Si_5N_8:Eu^{2+}$) and 2100-2500 cm^{-1} ($(Ca,Sr)AlSiN_3:Eu^{2+}$).[8,12-16] Quite recently numerous next-generation red phosphors were reported and noticably the nitridolithoaluminate $Sr[LiAl_3N_4]:Eu^{2+}$ can be seen with an fwhm of ~1180 cm^{-1} as the best candidate.[17] In contrast, there are only few reports on Eu^{2+}-doped nitrides with a sufficient green emission. One prominent example is the oxonitridosilicate $SrSi_2O_2N_2:Eu^{2+}$ exhibiting an emission maximum of 535 nm with an fwhm ~2600 cm^{-1}.[18]

Here, the synthesis and characterization of the nitridolithomagnesoalumosilicates $Ba[(Mg_{0.4}Li_{1.6})(Al_{2.4}Si_{1.6})N_6]:Eu^{2+}$ and $Ba[(Mg_{0.2}Li_{1.8})(Al_{2.2}Si_{1.8})N_6]:Eu^{2+}$ which belong to the solid-solution series $Ba[(Mg_{2-x}Li_x)(Al_{4-x}Si_x)N_6]$ with x = (0-2) are reported. The respective Eu^{2+}-doped compounds show promising luminescence properties in the green to yellow region of the visible spectrum which renders them as good candidates for application in white pc-LEDs for LCD backlighting applications.

2.6.2 Experimental Section

2.6.2.1 Synthesis

All manipulations were performed either in flame-dried Schlenk-type glassware attached to a vacuum line (10^{-3} mbar) or in an argon-filled glove box (Unilab, MBraun, Garching, O_2 <1 ppm, H_2O <1 ppm). Argon (Messer-Griessheim, 5.0) was purified out by passage through columns filled with silica gel (Merck), molecular sieve (Fluka, 4 Å), KOH (Merck, ≥85%), P_4O_{10} (Roth, ≥99%), and titanium sponge (Johnsen Matthey, 99.5%) at 700 °C.

The synthesis of $Ba[(Mg_{0.4}Li_{1.6})(Al_{2.4}Si_{1.6})N_6]$ and $Ba[(Mg_{0.2}Li_{1.8})(Al_{2.2}Si_{1.8})N_6]$ was carried out by a solid-state metathesis reaction in sealed tantalum ampules and yielded single crystals of both compounds. Therefore, the stoichiometric ratio of the starting materials was typically selected to 0.08 mmol of "$Ba_3Mg_3N_2F_6$" (50.0 mg, synthesized by reaction of three equivalents of BaF_2 (Sigma-Aldrich, 99.99%) and one equivalent of Mg_3N_2 (Sigma-Aldrich, 99.5%) at 950 °C for 12 h), 0.16 mmol of "$Si(NH)_2$" (9.6 mg, synthesized according to the method by Lange et al.),[19] 0.08 mmol of AlF_3 (84.0 mg,

Sigma-Aldrich, 99.99%) and 0.16 mmol of LiN_3 (7.8 mg, synthesized according to the method by Fair et al.).[20] For the investigation of luminescence properties 2 mol% EuF_3 (Sigma-Aldrich, 99.99%) in respect to the Ba content were added as dopant. The reaction mixture was ground in a glove box and filled into a tantalum ampule and was covered with 1.60 mmol of Li (11.1 mg, Alfa Aesar, 99.9%) as fluxing agent. The Ta ampule was subsequently weld shut in an arc furnace whereby the ampule was cooled with water to avoid any chemical reaction during this procedure. The ampule was placed in a silica tube, which was evacuated afterwards and then heated in a tube furnace. The temperature program consisted of heating to 950 °C within 3 h, dwelling this temperature for 24 h, and subsequently cooling down to 500 °C in 102 h. Finally, the ampule was quenched to room temperature by switching off the furnace.

2.6.2.2 Elemental and Morphological Analysis

Several crystallites of both new nitridolithomagnesoalumosilicates were investigated with respect to their morphology and their elemental composition with a JSM-6500F scanning electron microscope (SEM, Jeol) with a Si/Li EDX detector (Oxford Instruments, model 7418). The given results of the EDX-analysis are an average of five measurements of different crystallites of each compound.

2.6.2.3 Single-Crystal X-ray Diffraction

Single crystals of both compounds, $Ba[(Mg_{0.4}Li_{1.6})(Al_{2.4}Si_{1.6})N_6]$ and $Ba[(Mg_{0.2}Li_{1.8})(Al_{2.2}Si_{1.8})N_6]$, were separated from the inhomogeneous reaction mixture under Ar atmosphere inside a glove box with the aid of a microscope. Afterwards, the crystallites were enclosed in glass capillaries and sealed under argon. A Buerger precession camera was used to check the quality of the extracted crystals. X-ray diffraction data were collected on a Bruker D8 Quest diffractometer (microfocus, graphite monochromator, Mo-K_α radiation (λ = 0.71073 Å)). An absorption correction was executed with SADABS[21] and the crystal structures were solved by Direct Methods (SHELXS)[22] and refined by full-matrix least-squares methods (SHELXL).[23,24] Table 2.6-1 lists the crystallographic data for both compounds. The dopant Eu^{2+} was neglected for

structure determination because the contribution to scattering density is insignificant with only 2 mol%.

Table 2.6-1. Crystallographic Data of $Ba[(Mg_{0.4}Li_{1.6})(Al_{2.4}Si_{1.6})N_6]$ and $Ba[(Mg_{0.2}Li_{1.8})(Al_{2.2}Si_{1.8})N_6]$

formula	$Ba[(Mg_{0.4}Li_{1.6})(Al_{2.4}Si_{1.6})N_6]$	$Ba[(Mg_{0.2}Li_{1.8})(Al_{2.2}Si_{1.8})N_6]$
formula mass/g·mol^{-1}	351.93	348.67
crystal system	tetragonal	
space group	*P*4/*ncc* (no. 130)	
cell parameters/Å	a = 7.8921(3)	a = 7.8785(3)
	c = 9.9948(4)	c = 9.9833(4)
V/Å^3	622.53(4)	619.67(4)
formula units/cell	4	
X-ray density/g·cm^{-3}	3.755	3.737
abs. coefficient μ/mm^{-1}	6.988	7.014
F(000)	645	638
diffractometer, radiation	Bruker D8 Quest	
	Mo-K_α (λ = 0.71073 Å)	
temperature/K	293(2)	
absorption correction	multi-scan[21]	
θ range/°	3.63-40.64	5.44-40.61
measured reflections	11776	11696
independent reflections	384 [R(int) = 0.0259]	382 [R(int) = 0.0262]
observed reflections	381	366
refined parameters	33	32
GoF	1.070	1.057
R indices ($F_o^2 \geq 2\sigma(F_o^2)$)	R_1 = 0.0169, wR_2 = 0.0456	R_1 = 0.0181, wR_2 = 0.0488
R indices (all data)	R_1 = 0.0170, wR_2 = 0.0456	R_1 = 0.0186, wR_2 = 0.0494
min / max residual electron density/eÅ^{-3}	-0.49 / 0.71	-1.20 / 0.55

2.6.2.4 Powder X-ray Diffraction

The powder X-ray diffraction (PXRD) data were collected on a STOE STADI P diffractometer (Cu-$K_{\alpha1}$ radiation, Ge(111) monochromator, position sensitive detector) in Debye–Scherrer geometry. Rietveld refinement was done with TOPAS Academic 4.1

package.[25] The corresponding powder diffractograms are depicted in the Supporting Information.

2.6.2.5 Luminescence

Eu^{2+}-doped $Ba[(Mg_{0.4}Li_{1.6})(Al_{2.4}Si_{1.6})N_6]$ and $Ba[(Mg_{0.2}Li_{1.8})(Al_{2.2}Si_{1.8})N_6]$ show emission in the green to yellow region of the visible spectrum which was investigated with a HORIBA Fluoromax4 spectrofluorimeter system. An Olympus BX51 microscope is attached via fiber optical bundles to the spectrofluorimeter to enable centering of the crystallites, which were sealed inside quartz capillaries. The excitation wavelength was chosen to 400 nm with a spectral width of 10 nm. Excitation spectra were measured between 380 and 530 nm. Emission spectra were collected in the wavelength range between 420 and 780 nm with 2 nm step size.

2.6.3 Results and Discussion

2.6.3.1 Synthesis and Chemical Analysis

Crystallites of the nitridolithomagnesoalumosilicates $Ba[(Mg_{2-x}Li_x)(Al_{4-x}Si_x)N_6]$ with x = 1.6 and 1.8 were both identified in the same reaction product besides some impurities. $Ba[(Mg_{0.4}Li_{1.6})(Al_{2.4}Si_{1.6})N_6]:Eu^{2+}$ forms yellow crystals with intense yellow luminescence under blue light, whereas $Ba[(Mg_{0.2}Li_{1.8})(Al_{2.2}Si_{1.8})N_6]:Eu^{2+}$ forms green crystals with intense green emission under blue excitation. Crystals of both compounds show an octahedral habitus and are stable against air and moisture. Non-doped samples have not been synthesized up to now. Furthermore, colorless crystals of Li_2SiN_2,[26] LiF and $LiBaF_3$ could be identified as side phases. The composition of both title compounds was investigated by EDX spectroscopy on several crystallites and normalized to the Ba content. Within the standard deviations atomic ratios Ba:Mg:Al:Si:N of 1:0.3:2.4:1.7:6.6 for $Ba[(Mg_{0.4}Li_{1.6})(Al_{2.4}Si_{1.6})N_6]:Eu^{2+}$ and 1:0.2:2.3:1.8:6.8 for $Ba[(Mg_{0.2}Li_{1.8})(Al_{2.2}Si_{1.8})N_6]:Eu^{2+}$ were measured. No other elements were detected, Li is not determinable with this method and also Eu was not detected due to its low content in the samples. Nevertheless, both compositions

obtained from EDX-spectroscopy agree well with the compositions obtained from the single-crystal structure analysis.

2.6.3.2 Crystal-Structure Determination

$Ba[(Mg_{0.4}Li_{1.6})(Al_{2.4}Si_{1.6})N_6]$ as well as $Ba[(Mg_{0.2}Li_{1.8})(Al_{2.2}Si_{1.8})N_6]$ crystallize in the tetragonal space group *P*4/*ncc* (no. 130), details of the structure solution and refinment are summarized in Table 2.6-1. Atomic coordinates and isotropic displacement parameters are given in Table 2.6-2. Anisotropic displacement parameters and selected bond lengths for both compounds are listed in the Supporting Information.

Table 2.6-2. Atomic Coordinates and Isotropic Displacement Parameters of $Ba[(Mg_{0.4}Li_{1.6})(Al_{2.4}Si_{1.6})N_6]$ and $Ba[(Mg_{0.2}Li_{1.8})(Al_{2.2}Si_{1.8})N_6]$[a]

	Atom (Wyck.)	x	y	z	U_{eq}/Å^3	*sof*
$Ba[(Mg_{0.4}Li_{1.6})(Al_{2.4}Si_{1.6})N_6]$	Ba (4*c*)	1/4	1/4	0.3424(3)	0.0146(16)	1
	Mg (8*f*)	0.3731(3)	0.6269(3)	1/4	0.0200(7)	0.2
	Li (8*f*)	0.3731(3)	0.6269(3)	1/4	0.0200(7)	0.8
	Al (16*g*)	0.1225(8)	0.5331(8)	0.0817(6)	0.0078(2)	0.6
	Si (16*g*)	0.1225(8)	0.5331(8)	0.0817(6)	0.0078(2)	0.4
	N1 (8*f*)	0.5070(3)	0.1558(3)	0.0446(2)	0.0172(4)	1
	N2 (16*g*)	0.5979(3)	0.4021(3)	1/4	0.0184(6)	1
$Ba[(Mg_{0.2}Li_{1.8})(Al_{2.2}Si_{1.8})N_6]$	Ba (4*c*)	1/4	1/4	0.3419(2)	0.0138(14)	1
	Mg (8*f*)	0.3722(3)	0.6278(3)	1/4	0.0091(6)	0.1
	Li (8*f*)	0.3722(3)	0.6278(3)	1/4	0.0091(6)	0.9
	Al (16*g*)	0.1225(7)	0.5332(7)	0.0819(5)	0.0074(17)	0.55
	Si (16*g*)	0.1225(7)	0.5332(7)	0.0819(5)	0.0074(17)	0.45
	N1 (8*f*)	0.5064(2)	0.1566(2)	0.0445(19)	0.0169(4)	1
	N2 (16*g*)	0.5968(2)	0.4032(2)	1/4	0.0183(5)	1

[a] e.s.d.'s in parentheses

2.6.3.3 Crystal-Structure Description

Both novel nitridolithomagnesoalumosilicates are members of the solid-solution series $Ba[(Mg_{2-x}Li_x)(Al_{4-x}Si_x)N_6]$ with x = (0-2). Therefore, there is only a minor deviation in the lattice parameters of both compounds and consequently only the bond lengths and angles of the phase with the higher Mg-content, namely $Ba[(Mg_{0.4}Li_{1.6})(Al_{2.4}Si_{1.6})N_6]$, will be discussed in the following. Bond lengths for $Ba[(Mg_{0.2}Li_{1.8})(Al_{2.2}Si_{1.8})N_6]$ are given in the Supporting Information.

The crystal structure of $Ba[(Mg_{0.4}Li_{1.6})(Al_{2.4}Si_{1.6})N_6]$ is built up by two *vierer* ring layers of corner- and edge-sharing tetrahedra of $(Al,Si)N_4$ with a statistical distribution of Al^{3+} and Si^{4+}.[27,28] The layers are opposed to each other in [100] direction and connected by common corners. This results in two types of different *vierer* ring channels running along [001]. There are smaller *vierer* ring channels that are made up by $(Al,Si)N_4$ tetrahedra connected to each other by common corners in an up-down sequence and larger *vierer* ring channels where $(Al,Si)N_4$ tetrahedra's corners are all directed in the same way (see Fig. 2.6-1).

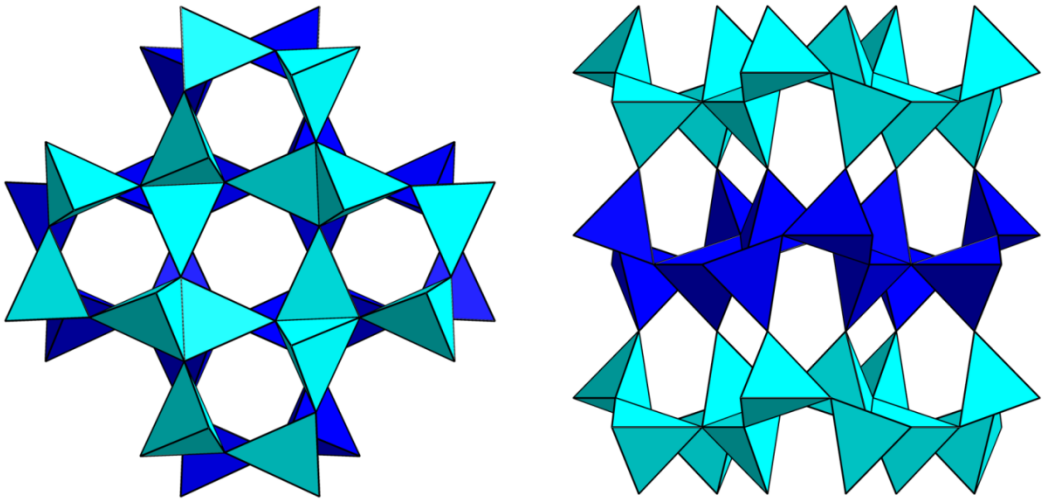

Figure 2.6-1. $(Al,Si)N_4$ tetrahedra layers forming two different types of *vierer* ring channels running along [001] (left). The layers are opposed to each other along [010] (right). $(Al,Si)N_4$ tetrahedra depicted in light and dark blue in the different layers.

(Al,Si)-N bond lengths range from 1.77(1) to 1.85(2) Å giving an average of 1.81 Å. The averaged sum of the ionic radii according to Baur is found to be 1.82 Å,[29] which suits pretty well. Also other nitridoalumosilicates with a mixed occupation of TN_4 tetrahedra

(T = Al,Si) show comparable bond lengths T-N of 1.81 Å ($CaAlSiN_3$)[13,14] and for $Ba_2AlSi_5N_9$ a value of 1.80 Å is found.[30] The smaller *vierer* ring channels are centered by tetrahedra of $(Li,Mg)N_4$. These tetrahedra also show crystallographic disorder of Li^+ and Mg^{2+}. With respect to the fact that both ions are tetrahedrally coordinated and therefore are part of the network (see Fig. 2.6-2, left), $Ba[(Mg_{0.4}Li_{1.6})(Al_{2.4}Si_{1.6})N_6]$ is more appropriately classified as a nitridolithomagnesoalumosilicate.[31] The $(Li,Mg)N_4$ tetrahedra are connected to each other by common edges forming bow-tie units of $(Li,Mg)_2N_6$ which have not been observed in nitridosilicates as yet. This unit is connected to another one forming a tetragonal bisphenoid of $(Li,Mg)_4N_{12}$ inside the smaller *vierer* ring channels and is depicted in Fig. 2.6-2 right, top. The bond lengths of (Li,Mg)-N are in a range of 2.18-2.27 Å and slightly elongated compared to the averaged sum of the ionic radii of 2.08 Å.[29] Yet, there are no reports on nitridosilicates with a mixed occupation of tetrahedrally coordinated Li^+ and Mg^{2+}. Therefore, bond lengths are compared with $(Li_{0.51}Mg_{2.49})N_{1.83}$. The latter compound has (Li,Mg)-N bond lengths ranging from 2.04 to 2.27 Å,[32] that fit well with the observed distances found in $Ba[(Mg_{0.4}Li_{1.6})(Al_{2.4}Si_{1.6})N_6]$.

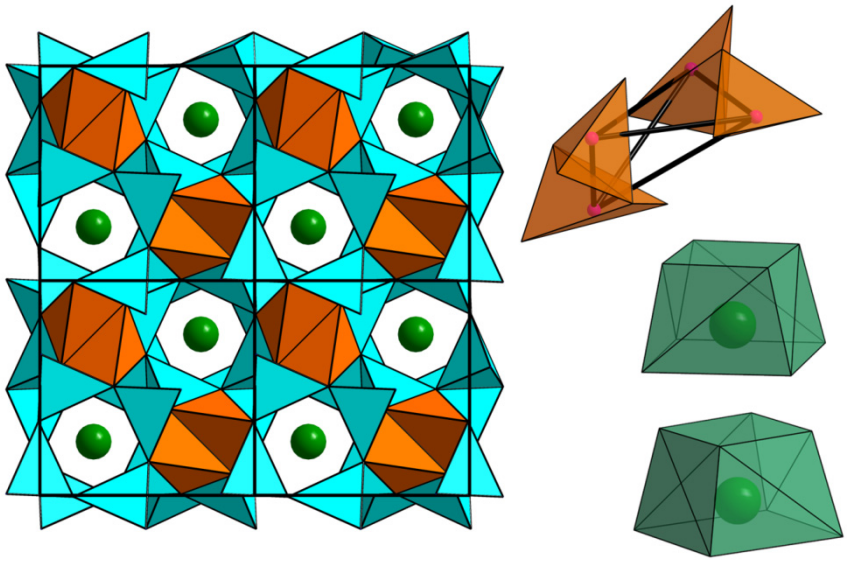

Figure 2.6-2. Left: Crystal structure of $Ba[(Mg_{2-x}Li_x)(Al_{4-x}Si_x)N_6]$ with x = (0-2), viewing direction [001]. Right, top: Bisphenoid of $(Li,Mg)_4N_{12}$. Right, bottom: Truncated square-pyramid coordination of Ba^{2+} by N^{3-}. $(Al,Si)N_4$ tetrahedra light blue, $(Li,Mg)N_4$ tetrahedra orange, Ba^{2+} green, (Li^+,Mg^{2+}) pink. Black lines drawn in the bisphenoid are no chemical bonds.

In general, the (Li,Mg) bond lengths are in the same magnitude as found for other Li- and/or Mg-containing nitridosilicates.[31,33-38] Due to the edge-sharing of the bow-tie units the corresponding (Li,Mg)-(Li,Mg) distances are quite short (2.75 Å), the same tendency can be observed for Si_2N_6 bow-tie units.[34,35,37,39] The larger *vierer* ring channels are exclusively centered by Ba^{2+}. Latter is in eightfold coordination by N^{3-} with a truncated square pyramid as resulting coordination polyhedron. These are connected to each other by common corners in [100] direction and are staggered along [001]. Every second truncated square pyramid has to be shifted by 40° towards the previous one that it fits between the layers of opposed $(Al,Si)N_4$ tetrahedra (see Fig. 2.6-2 right, bottom). The Ba-N bond lengths are in an order of 2.96-3.14 Å. This range in the average corresponds well with the sum of the ionic radii of 3.05 Å.[29] $Ba[Mg_3SiN_4]$ and $Ba_2AlSi_5N_9$, two other compounds with Ba^{2+} in eightfold coordination by N^{3-} show Ba-N bond length comparable to the nitridoalumolithomagnesosilicate.[30,33]

2.6.3.4 Luminescence

Although, $Ba[(Mg_{0.4}Li_{1.6})(Al_{2.4}Si_{1.6})N_6]$ and $Ba[(Mg_{0.2}Li_{1.8})(Al_{2.2}Si_{1.8})N_6]$ have a very similar chemical formula, the luminescence properties of the respective Eu^{2+}-doped compounds are quite different. Under blue irradiation $Ba[(Mg_{0.4}Li_{1.6})(Al_{2.4}Si_{1.6})N_6]:Eu^{2+}$ exhibits luminescence in the yellow spectral region, by contrast $Ba[(Mg_{0.2}Li_{1.8})(Al_{2.2}Si_{1.8})N_6]:Eu^{2+}$ shows emission in the green region of the visible spectrum under the same irradiation. Figure 2.6-3 depicts excitation and emission spectra of both Eu^{2+}-doped compounds. The excitation spectra ($\lambda_{monitor}$ = 550 nm) of both compounds show broad bands in the blue region of the visible spectrum with maxima at 415 nm ($Ba[(Mg_{0.4}Li_{1.6})(Al_{2.4}Si_{1.6})N_6]:Eu^{2+}$), and for $Ba[(Mg_{0.2}Li_{1.8})(Al_{2.2}Si_{1.8})N_6]:Eu^{2+}$ at 470 nm. Therefore, both nitridolitho-magnesoalumosilicates can be effectively excited with blue light as provided for example by (In,Ga)N-LEDs.

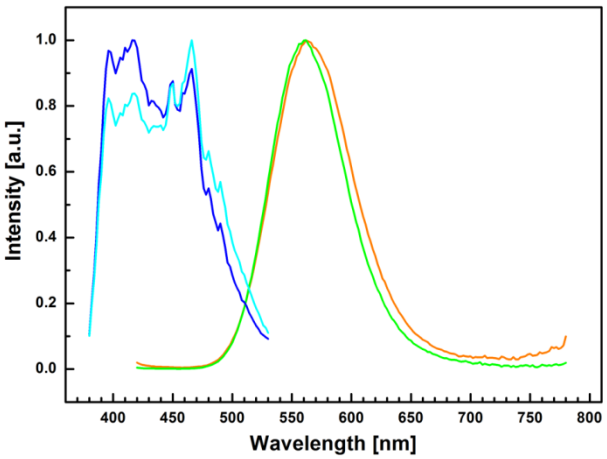

Figure 2.6-3. Typical excitation ($\lambda_{monitor}$ = 550 nm) and emission spectra of Eu^{2+}-doped $Ba[(Mg_{0.4}Li_{1.6})(Al_{2.4}Si_{1.6})N_6]$ (blue and orange curve) and $Ba[(Mg_{0.2}Li_{1.8})(Al_{2.2}Si_{1.8})N_6]$ (cyan and green curve). Emission spectra were recorded at 400 nm excitation. Both compounds were doped with 2 mol% Eu^{2+} (nominal composition).

The emission spectrum at 400 nm excitation of the compound with x = 1.6 exhibits the typical Eu^{2+} broad-band emission centered at 562 nm with an fwhm of ~2739 cm^{-1}. The maximum in the emission spectrum (λ_{exc} = 400 nm) of the other compound is only shifted by 2 nm towards smaller wavelengths and centered at 560 nm (fwhm ~2654 cm^{-1}). Although, the visible luminescence of both compounds differs, green (x = 1.8) vs. yellow (x = 1.6) (see Fig. 2.6-4), the emission spectra of both compounds are quite similar with only a small difference of the maxima.

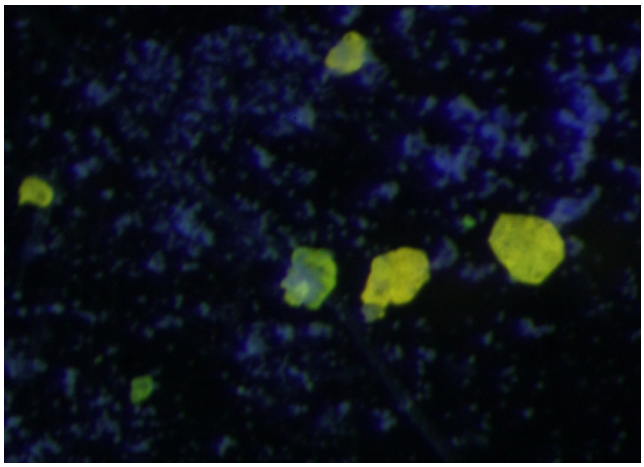

Figure 2.6-4. Microscope image of both nitridoalumolithomagnesosilicates under UV irradiation. Green emitting crystals are $Ba[(Mg_{0.2}Li_{1.8})(Al_{2.2}Si_{1.8})N_6]:Eu^{2+}$ and the yellow ones are $Ba[(Mg_{0.4}Li_{1.6})(Al_{2.4}Si_{1.6})N_6]:Eu^{2+}$.

However, $Ba[(Mg_{0.2}Li_{1.8})(Al_{2.2}Si_{1.8})N_6]:Eu^{2+}$ exhibits a larger portion of emission in the green spectral region and the human eye is in this region notably more sensitive that the green color dominates. In general, there is a tendency that with decreasing Mg and Al content the emission is shifted towards smaller wavelengths.

$SrSi_2O_2N_2:Eu^{2+}$ is another green-emitting nitride phosphor and shows a very similar fwhm of ~2600 cm^{-1} compared to $Ba[(Mg_{0.2}Li_{1.8})(Al_{2.2}Si_{1.8})N_6]:Eu^{2+}$.[18] Nevertheless, the green emission of $SrSi_2O_2N_2:Eu^{2+}$ is centered at 535 nm. Another green phosphor is $Ba_3Si_6N_{12}O_2:Eu^{2+}$, which emission centers at 523 nm with an fwhm of ~2143 cm^{-1}.[40]

There are numerous reports on green-emitting Eu^{2+}-doped (oxo)nitride phosphors, whereas in contrast there are only few reports on (oxo)nitridosilicate phosphors with yellow emission of the respective Eu^{2+}-doped compounds. One example is $Sr_{0.5}Ba_{0.5}Si_2O_2N_2:Eu^{2+}$ that shows an emission band centered at 565 nm with an fwhm of ~2744 cm^{-1}.[18] $CaSi_9Al_3ON_{15}:Eu^{2+}$ (Ca-α-SiAlON) is another prominent yellow-emitting compound with the following luminescence properties. The typical broad emission band for the Eu^{2+}-doped compounds has an fwhm of ~2890 cm^{-1} and is centered at 581 nm.[7]

2.6.4 Conclusion

The nitridolithomagnesoalumosilicates $Ba[(Mg_{0.4}Li_{1.6})(Al_{2.4}Si_{1.6})N_6]:Eu^{2+}$ and $Ba[(Mg_{0.2}Li_{1.8})(Al_{2.2}Si_{1.8})N_6]:Eu^{2+}$ were reported which belong to the solid-solution series $Ba[(Mg_{2-x}Li_x)(Al_{4-x}Si_x)N_6]$ with x = (0-2). In the mean time, Strobel succeeded in synthesis of $Ba[Li_2(Al_2Si_2)N_6]:Eu^{2+}$, but the compound with x = 0 still needs to be synthesized.[41] Nevertheless, the observed tendency of the emission properties described above, was proven by Strobel, as the emission maximum of $Ba[Li_2(Al_2Si_2)N_6]:Eu^{2+}$ is shifted towards smaller wavelengths and centered at 550 nm with a smaller fwhm of ~2414 cm^{-1}. However, the green emission of $Ba[Li_2(Al_2Si_2)N_6]:Eu^{2+}$ is not understood, as yet. In general, green emission is more likely exhibited by oxonitridosilicates as the nephelauxetic effect and crystal-field splitting are smaller for O^{2-} vs. N^{3-} and emission at shorter wavelengths is expected.[7,18,40] Furthermore, the fwhm of $Ba[Li_2(Al_2Si_2)N_6]:Eu^{2+}$ is still too broad (~2414 cm^{-1}) for a

technical application, but optimization, for example of the crystal morphology or the doping level, are major goals to achieve. Also, thermal quenching data are missing for the compounds, especially at elevated temperatures. Nevertheless, luminescence properties not only have showed a high tuneability with varying compositions, also the host lattice seems to be pretty much suitable for various substitutional variants. The crystal structure of $Ba[Li_2(Al_2Si_2)N_6]:Eu^{2+}$ and its mixed crystals is built up by a highly condensed network of $(Al,Si)N_4$ tetrahedra. There are two different types of *vierer* ring channels in size centered by Ba^{2+} (larger ones) and the smaller ones by a bisphenoid of Li_4N_{12}. Therefore, it should be possible to enlarge the smaller *vierer* ring channels by the incorporation of larger ions like Na^+ or Ca^{2+} and thus smaller ions then Ba^{2+}, for example Sr^{2+}, should fit in the other kind of channels. In contrast to the UCr_4C_4 structure type,[42,43] which also has two different *vierer* ring channels, but only one kind is centered by a heavy atom and the other one is empty, the structure type of $Ba[Li_2(Al_2Si_2)N_6]$ has one more degree of freedom for the substitution of elements. Consequently, the latter structure type will be the next to provide numerous novel nitride phosphors with tailor-made luminescence properties for various applications ranging from the use in pc-LEDs to backlighting in modern LCDs.

2.6.5 References

(1) Vögtle, F. *Thomas Alva Edison*; Rowohlt: Reinbek near Hamburg, 1982.

(2) Born, M.; Jüstel, T. *Chem. Unserer Zeit* **2006**, *40*, 294.

(3) Feldmann, C. *Z. Anorg. Allg. Chem.* **2012**, *638*, 2169.

(4) *International Energy Outlook 2013*; U.S. Energy Information Administration, Office of Energy Analysis, U.S. Department of Energy: Washington, D.C., 2013.

(5) U.S. Energy Information Administration (EIA) - FAQ. http://www.eia.gov/tools/faqs/faq.cfm?id=99&t=3 (accessed Nov 14th, 2013)

(6) Setlur, A. *Electrochem. Soc. Interface* **2009**, *18*, 32.

(7) Xie, R.-J.; Hirosaki, N.; Takeda, T.; Suehiro, T. *ECS J. Solid State Sci. Technol.* **2013**, *2*, R3031.

(8) Krames, M. R.; Mueller, G. O.; Mueller-Mach, R. B.; Bechtel, H.-H.; Schmidt, P. J. Wavelength conversion for producing white light from high power blue LED. PCT Int. Appl.WO 2010131133 A1, November 18th, 2010.

(9) Mosier, D. E. LCD backlight with UV light-emitting diodes and planar reactive element. US7036946 B1, May 02nd, 2006.

(10) Blasse, G.; Bril, A. *Appl. Phys. Lett.* **1967**, *11*, 53.

(11) Moriguchi, T.; Noguchi, Y.; Sakano, K.; Shimizu, Y. Light emitting device having a nitride compound semiconductor and a phosphor containing a garnet fluorescent material. US 5998925 A, July 29th, 1997.

(12) ten Kate, O. M.; Zhang, Z.; Dorenbos, P.; Hintzen, H. T.; van der Kolk, E. *J. Solid State Chem.* **2013**, *197*, 209.

(13) Uheda, K.; Hirosaki, N.; Yamamoto, H. *Phys. Status Solidi A* **2006**, *203*, 2712.

(14) Uheda, K.; Hirosaki, N.; Yamamoto, Y.; Naito, A.; Nakajima, T.; Yamamoto, H. *Electrochem. Solid-State Lett.* **2006**, *9*, H22.

(15) Zeuner, M.; Hintze, F.; Schnick, W. *Chem. Mater.* **2008**, *21*, 336.

(16) Zeuner, M.; Pagano, S.; Schnick, W. *Angew. Chem. Int. Ed.* **2011**, *50*, 7754.

(17) Pust, P.; Weiler, V.; Hecht, C.; Tücks, A.; Wochnik, A. S.; Henß, A.-K.; Wiechert, D.; Scheu, C.; Schmidt, P. J.; Schnick, W. *Nat. Mater.* **2014**, *13*, 891.

(18) Seibald, M.; Rosenthal, T.; Oeckler, O.; Schnick, W. *Crit. Rev. Solid State Mater. Sci.* **2014**, *39*, 215.

(19) Lange, H.; Wötting, G.; Winter, G. *Angew. Chem. Int. Ed. Engl.* **1991**, *30*, 1579.

(20) Fair, H. D.; Walker, R. F. *Energetic Materials 1, Physics and Chemistry of Inorganic Azides*; 1st ed.; Plenum Press: New York, London, 1977.

(21) Sheldrick, G. M. SADABS, v. 2: Multi-Scan Absorption Correction, Bruker-AXS, 2012.

(22) Sheldrick, G. M. SHELXS-97: A program for crystal structure solution, University of Göttingen, 1997.

(23) Sheldrick, G. M. *Acta Crystallogr. Sect. A: Found. Crystallogr.* **2008**, *64*, 112.

(24) Sheldrick, G. M. SHELXL-97: A program for crystal structure refinement, University of Göttingen, 1997.

(25) Coelho, A. TOPAS, v. 4.1: A program for Rietveld refinement, Coelho Software, 2007.

(26) Pagano, S.; Zeuner, M.; Hug, S.; Schnick, W. *Eur. J. Inorg. Chem.* **2009**, *2009*, 1579.

(27) Liebau, F. *Structural Chemistry of Silicates*; Springer: Berlin, New York, 1985.

(28) The term *vierer* ring was coined by Liebau and is derived from the german word "vier"; however, for example a *vierer* ring is not a four-membered ring, but an eight-membered ring comprising four tetrahedra centres.

(29) Baur, W. H. *Crystallogr. Rev.* **1987**, *1*, 59.

(30) Kechele, J. A.; Hecht, C.; Oeckler, O.; Schmedt auf der Günne, J.; Schmidt, P. J.; Schnick, W. *Chem. Mater.* **2009**, *21*, 1288.

(31) Schmiechen, S.; Schneider, H.; Wagatha, P.; Hecht, C.; Schmidt, P. J.; Schnick, W. *Chem. Mater.* **2014**, *26*, 2712.

(32) Yamane, H.; Okabe, T. H.; Ishiyama, O.; Waseda, Y.; Shimada, M. *J. Alloys Compd.* **2001**, *319*, 124.

(33) Schmiechen, S.; Strobel, P.; Hecht, C.; Reith, T.; Siegert, M.; Schmidt, P. J.; Huppertz, P.; Wiechert, D.; Schnick, W. *Chem. Mater.* ***2015****, 27*, 1780.

(34) Yamane, H.; Morito, H. *J. Alloys Compd.* **2013**, *555*, 320.

(35) Schmiechen, S.; Nietschke, F.; Schnick, W. *Eur.J. Inorg. Chem.* **2015**, 1592.

(36) Lupart, S.; Schnick, W. *Z. Anorg. Allg. Chem.* **2012**, *638*, 2015.

(37) Pagano, S.; Lupart, S.; Schmiechen, S.; Schnick, W. *Z. Anorg. Allg. Chem.* **2010**, *636*, 1907.

(38) Zeuner, M.; Pagano, S.; Hug, S.; Pust, P.; Schmiechen, S.; Scheu, C.; Schnick, W. *Eur. J. Inorg. Chem.* **2010**, *2010*, 4945.

(39) Ottinger, F.; Nesper, R. *Z. Anorg. Allg. Chem.* **2005**, *631*, 1597.

(40) Braun, C.; Seibald, M.; Börger, S. L.; Oeckler, O.; Boyko, T. D.; Moewes, A.; Miehe, G.; Tücks, A.; Schnick, W. *Chem. Eur. J.* **2010**, *16*, 9646.

(41) Strobel, P. *Master Thesis*, Ludwig Maximilian University Munich, 2014.

(42) Behrens, R. K.; Jeitschko, W. *Monatsh. Chem.* **1987**, *118*, 43.

(43) Pust, P.; Hintze, F.; Hecht, C.; Weiler, V.; Locher, A.; Zitnanska, D.; Harm, S.; Wiechert, D.; Schmidt, P. J.; Schnick, W. *Chem. Mater.* **2014**, *26*, 6113.

3 Ammonothermal Reactions

3.1 Silicon Nitrides in Ammonothermal Reactions

3.1.1 Introduction

In the last two decades nitrides increasingly moved into the focus as the most important non-oxidic ceramics and found various industrial applications. Especially, binary nitrides of group XIII (Al, Ga, In)[1] and XIV (Si, Ge)[2] elements show outstanding material properties with applications ranging from components in modern combustion engines (Si_3N_4) to heat sinks (AlN) and optoelectronic devices (GaN). Commonly, these compounds are synthesized and processed by high-temperature methods like solid-state reactions, pyrolysis of molecular precursors, carbothermal reduction and nitridation or spark-plasma sintering.[3] Hereby, single crystals are only obtained in μm scale which is far too small for some industrial applications. For example, large defect free single crystals of (In,Ga)N, which are used as blue-emitting semiconductor in modern phosphor-converted light-emitting diodes (pc-LEDs) due to its large direct band gap, are needed. Currently, large single crystals of (In,Ga)N are obtained by deposition through heteroepitaxy yielding large defect concentrations depending on the selected substrate material.[4] For homoepitaxial layers and therefore defect-free crystals, large single crystals of GaN are urgently required, but common crystal growth processes, for example Czochralski-process, cannot be used as nitrides would decompose during this process.[5] Similar to the hydrothermal crystal growth of oxides in supercritical water, nitrides can be obtained in ammonothermal conditions with supercritical ammonia.[6,7] Syntheses carried out in *sc*NH_3 have high demands on the technical equipment. The pressure vessel must withstand high pressures and temperatures, be inert to the reaction mixture and supercritical ammonia and additionally the synthesis conditions have to be reproducible. Ammonothermal syntheses are already known since the 1960s with the pioneering work of Juza and

Jacobs in Germany. Since that time, a number of novel binary and multinary metal nitrides, amides and imides were synthesized.[8-10] Many electropositive metals like alkaline (-earth) metals and lanthanides dissolve quite well in liquid ammonia,[11-13] whereas the solubility of other elements is poor and therefore additional reagents are necessary.[14,15] These are called mineralizers and are well known from hydrothermal syntheses forming complexes with the solute and therefore increasing the solubility. Mineralizers are divided in three categories, ammono basic, neutral and acidic. Under ammonobasic conditions amide ions NH_2^- are formed, for example with alkaline (-earth) metals. NH_4^+ species are formed in ammonoacidic conditions with for example NH_4Cl or NH_4F. Especially, latter conditions increase the demands on the autoclaves once more as often contaminations from the autoclave material occur. Therefore, liners are required for the separation of the autoclave wall and the reaction chamber.[16] With the retirement of Jacobs explorative syntheses under ammonothermal conditions vanished more or less. Today, ammonothermal methods are mainly used for the syntheses of AlN and GaN.[17] Although, Si_3N_4 is a widely used ceramic with various applications, there are only few reports about attempts to synthesize it under ammonothermal conditions. Jacobs et al. carried out numerous syntheses, but obtained only amides and imides containing Si at reaction conditions of 600 °C and 6000 bar.[9,18] Kaskel et al. performed ammonothermal syntheses starting from "$Si(NH)_2$" (SDI).[19-21] The latter compound is a well known but up to date poorly characterized molecular precursor for the solid-state synthesis of Si_3N_4 and numerous multinary nitridosilicates.[22,23] With the addition of various ammonobasic mineralizers Kaskel et al. never obtained silicon nitride, but succeeded in the ammonothermal syntheses of the ternary nitridosilicates ASi_2N_3 (A = Li,Na).[20] Both compounds were completely characterized in the 1990s and are crystallizing in a wurtzite-type structure. Quite recently, Watanabe et al. were able to synthesize the nitridoalumosilicates $AEAlSiN_3:Eu^{2+}$ (AE = Ca,Sr) under ammonothermal conditions starting from the respective intermetallic compounds AEAlSi.[24,25] Again, these compounds crystallize in a wurtzite-type structure and remarkably, $SrAlSiN_3:Eu^{2+}$ was hitherto only accessibe by hot-isostatic pressing (HIP) at 1900 °C and 1900 bar N_2.[26]

For the reestablishment of ammonothermal reactions in explorative syntheses the interdisciplinary *Deutsche Forschungsgemeinschaft* (DFG) research group FOR-1600 was found in 2011. Specially designed autoclaves allow ammonothermal reactions up to 600 °C and 3000 bar. The Schnick group is part of the research group with the focus on synthesis and characterization of amides, imides and nitrides of main group metals. Here, the ammonothermal syntheses of nitridosilicates is presented. Therefore, first investigations were carried out with SDI under *sc*NH_3 referring to the work of Kaskel et al.[19-21] Afterwards, the acquired insights were used for the ammonothermal syntheses of novel and known nitridosilicates. Besides SDI also other Si-containing precursors, like intermetallic compounds, were tested and different mineralizers mixtures were evaluated.

3.1.2 Experimental

3.1.2.1 Autoclaves

Ammonothermal syntheses were performed in non-commercial autoclaves that were designed and constructed at the group of Prof. Schlücker in Erlangen (see Fig. 3.1-1). The autoclaves are designed for a maximum temperature of 600 °C and a maximum pressure of 3000 bar. The inner volume was chosen to 97 ml (337 mm long, outer diameter 50 mm). Inconel 718 (material number 2.4668)[27] was selected as material for the pressure vessel, cover and screw flanges, and the screws. C-ring sealings of silver-coated Inconel 718 with a spring inside (GFD Dichtungen, type MCI-(F7)-732-0026, 20-1s1) are used as sealings. The autoclave is connected to the valve (Dieckers, type 720.1523) with an Inconel pipe. The valve can be attached via a DN 16 flange (Fig. 3.1-1, a) to the ammonia filling device. Also, a distribution rack for the bursting disc holder (Fig. 3.1-1, b) and the pressure transmitter (Fig. 3.1-1, c) is connected to the valve. The bursting disc holder (Dieckers, type 720.5022-2) contains a bursting disc (Dieckers, type 7282500-4500) with a bursting pressure of 3300 (±10%) bar.

Figure 3.1-1. Autoclave used for ammonothermal reactions, constructed by engineers at university of Erlangen. Insets are described in the text.[28]

3.1.2.2 Ammonia-Filling Station

Autoclaves were loaded with ammonia at a specially designed filling station. The whole apparatus is made up of glass with PTFE stopcocks in order that no vacuum grease is needed which could react with gaseous ammonia (see Fig. 3.1-2).

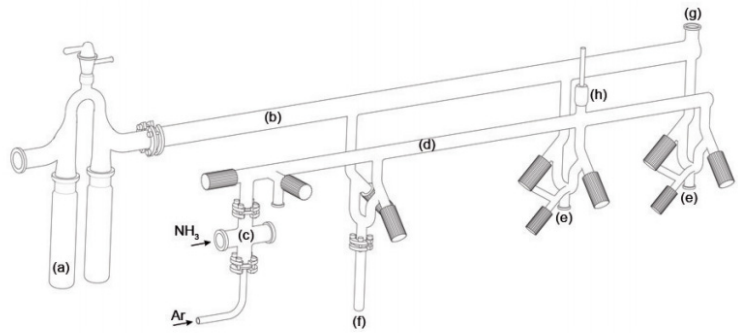

Figure 6: Ammonia filling device.

(a) double cooling trap	(d) gas line	(g) vacuum sensor
(b) vacuum line	(e) taps	(h) thermometer
(c) allocator	(f) glass cylinder with volume scale	

Figure 3.1-2. Specially designed ammonia filling station.[28]

The filling station is constructed like a typical Schlenk line with separated vacuum and gas strands. Vacuum is generated by a rotary vane pump which is connected via a metal bellow hose (flange DN 16) to a double cooling trap (a) in front of the vacuum line (DN 25 flange, (b)) protecting the pump of corrosive gases and contamination with fine dust. Ar or NH_3 are flushed via an allocator (c) to the gas line (d). Both gases are purified *a priori* by special gas purification cartridges (Ar: model FT400-902; NH_3: model MC400-702FV; both from SAES Pure Gas Inc., San Luis Obispo, USA). There

are two connections with flanges (DN 16) for the autoclaves via metal bellow hoses (e). For condensation of ammonia a glass cylinder with a volume scale (f) is connected to a third tap of the filling station. The apparatus is protected by several mercury control valves against overpressure. In addition, a mechanical relief pressure valve is attached to the allocator (DN 25 flange, opposite to NH_3 inlet). A vacuum sensor (g) is furthermore installed at the vacuum line. Finally, a thermometer (h) is connected to the gas strand.

3.1.2.3 General Experimental Procedure

With respect to the air and moisture sensitivity of some starting materials, reaction mixtures were transferred into the autoclave under inert gas conditions in a glove box. Afterwards, the autoclave was closed with the valve, and then screws, which were coated with a BN-suspension lubricant (Henze, HeBoCoat 20E), were tightened up outside the glovebox with 150 Nm in three 50 Nm steps. Subsequently, the loading of the autoclaves with ammonia was carried out at the ammonia-filling station by evacuating the autoclave and the scaled glass cylinder three times with in between flushing with Ar. After the last step the autoclave and the glass cylinder remained evacuated and were cooled down below the boiling point of ammonia (-33 °C) with a dry ice/ethanol mixture. The desired amount of NH_3 was then condensed into the glass cylinder under continuous cooling. Subsequently, the connection between the allocator and the gas line was closed and the glass cylinder and the autoclave were connected to each other via the gas line. Under moderate heating the liquid ammonia was evaporated and recondensed into the autoclave. As soon as all liquid ammonia was removed from the glass cylinder the autoclave was closed with the valve and was brought to room temperature. The autoclave was finally heated in a commercially available tubular furnace. During the heating procedure the cover flange of the autoclave was isolated with quartz wool to minimize the temperature gradient. After the reaction, ammonia was removed from the autoclave by opening the valve and then the autoclave was evacuated and flushed with Ar. After loosening the screws, the autoclave was finally opened in a glovebox.

3.1.2.4 Elemental Analysis

The chemical composition of the ammonothermal products was investigated by energy dispersive X-ray (EDX) spectroscopy. For this purposes a JSM-6500F scanning electron microscope (SEM, Jeol) containing a Si/Li EDX detector (Oxford Instruments, model 7418) was used.

3.1.2.5 Single-Crystal X-ray Diffraction

Some reaction products contained crystals which were further investigated. Therefore, these were separated with the aid of a microscope integrated into a glove box and sealed under argon atmosphere in glass capillaries. The isolated crystallites were checked on a Buerger precession camera. X-ray diffraction data were collected on a STOE IPDS I diffractometer (Mo-K_α radiation, λ = 0.71073 Å) with a graphite monochromator. An absorption correction was carried out with XPREP (semi-empirical), the structures were solved by Direct Methods (SHELXS)[29] and refined by full-matrix least-squares methods (SHELXL)[30,31].

3.1.2.6 Powder X-ray Diffraction

Most reaction products of the ammonothermal syntheses were obtained as bulk samples and investigated by powder X-ray diffraction (PXRD). Therefore, a STOE STADI P diffractometer (Cu-$K_{\alpha1}$ or Mo-$K_{\alpha1}$ radiation, Ge(111) monochromator, Mythen1K detector) in Debye-Scherrer geometry or a Huber G670 diffractometer (Cu-$K_{\alpha1}$, Guinier geometry) were used. Rietveld refinements were carried out with the TOPAS Academic 4.1 package.

3.1.3 Results and Discussion

In a first series of ammonothermal experiments "$Si(NH)_2$" (SDI) was investigated as an appropriate Si source for the synthesis of nitridosilicates under ammonothermal conditions. Especially, the results from Kaskel et al. should be verified and transferred to the special designed autoclaves of the Schnick group which have a larger inner volume and could reach higher temperatures and higher pressures. The obtained insights were used for further syntheses of novel nitridosilicates under

ammonothermal conditions. In addition, other Si sources, mainly silicides, were used in other ammonothermal experiments. Starting from intermetallic compounds in ammonothermal reactions could take advantage of a better use of the available temperature and pressure ranges as an energy consuming intermetallic bond formation has not to be done during the ammonothermal reaction. In a last series of ammonothermal reactions it was tried to synthesize "$SrAlGeN_3:Eu^{2+}$" based on the ammonothermal synthesis of $SrAlSiN_3:Eu^{2+}$ reported by Watanabe et al.[24]

3.1.3.1 "$Si(NH)_2$" in Ammonothermal Reactions

SDI was investigated in ammono-neutral, -acidic and -basic milieu. For comparable conditions for all syntheses 1.72 mmol (100.0 mg) SDI and 45 ml liquid ammonia were used. "$Si(NH)_2$" was prior synthesized by the method reported from Lange et al.[22] The filled autoclave was heated within 3 h to 580 °C, maintained at this temperature for 36 h and finally quenched to room temperature by switching off the furnace.

Both, ammono-neutral and -acidic (mineralizers: NH_4Cl and LiCl) conditions yielded amorphous products. No decomposition of SDI to Si_3N_4, which normally occurs at ~900 °C in high-temperature reactions,[22] or the formation of a multinary nitridosilicate were identified. The reaction product of the ammono-acidic synthesis contained few deep red crystals that were identified by EDX spectroscopy and single-crystal X-ray diffraction as $[CrCl(NH_3)_5]Cl_2$.[32] No Cr compound was used as starting material, accordingly the formation of the deep red crystals could be ascribed to the reaction of supercritical ammonia with the autoclave material under ammono-acidic conditions.[33] This emphasizes the importance to use a suitable liner material for ammonothermal reactions under acidic conditions.[16]

For the synthesis under ammono-basic conditions 0.86 mmol (42.12 mg) of LiN_3 (synthesized by the method of Fair et al.)[34] were mixed with SDI. The azide forms the ammono-basic mineralizer $LiNH_2$ *in situ* under ammonothermal conditions.[35] The autoclave reached a maximum pressure of ~2000 bar. An off-white powder was obtained after the ammonothermal reaction. In contrast to the other two reactions described before, the powder diffractogram (see Fig. 3.1-3) shows sharp reflections giving a hint on crystalline phases.

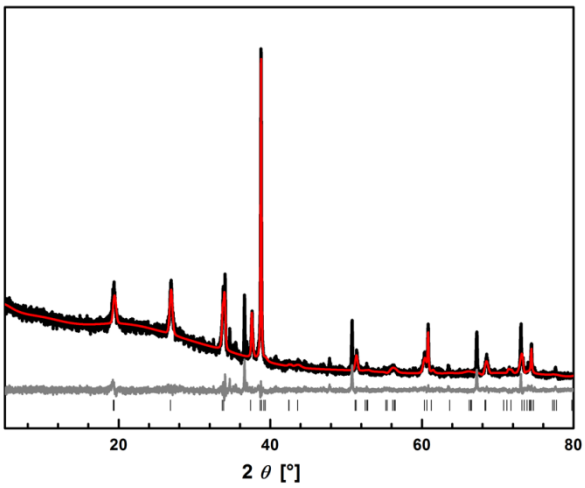

Figure 3.1-3. Rietveld refinement (Cu-$K_{\alpha 1}$ radiation) of the ammonothermal reaction of SDI in ammono-basic conditions. Experimental data (black line), calculated pattern of $LiSi_2N_3$ (red line) and difference curve (gray line). Black tickmarks: $LiSi_2N_3$. Non-described reflections belong to non-identified phases.

Some reflections can be ascribed to $LiSi_2N_3$,[36] whereas the other ones belong to yet non-identified phases. The Li nitridosilicate was also obtained by Kaskel et al. in their autoclaves.[20] The successful synthesis of a nitridosilicate in ammono-basic conditions was a hint for further syntheses and was equipped for the following attempts to synthesize novel nitridosilicates in ammonothermal reactions.

For further experiments, the alkaline-earth (AE) elements Mg-Ba were chosen instead of alkaline metals as reactants and mineralizers, as there are only very few reports on AE nitridosilicates synthesized in ammonothermal reactions.[24,25] Exemplarily, an attempt to synthesize $Ba[Mg_3SiN_4]$ in an ammonothermal reaction starting from SDI is described.[37] Therefore 0.80 mmol of "$Si(NH)_2$" (46.5 mg) and Ba (109.9 mg, Sigma-Aldrich, 99.99%) were mixed together with 2.40 mmol of Mg (58.3 mg, Alfa Aesar, 99.99%) and filled into the autoclave. 50 ml liquid ammonia were added and the reaction mixture was heated to 580 °C within 3 h, kept at this temperature for 30 h (p_{max} ~1700 bar) and finally cooled down to room temperature within 32 h. A white powder was obtained without any metallic residues, but the experimental PXRD (Fig. 3.1-4) data only showed one identifiable crystalline phase, namely $Mg(NH_2)_2$.[10,38]

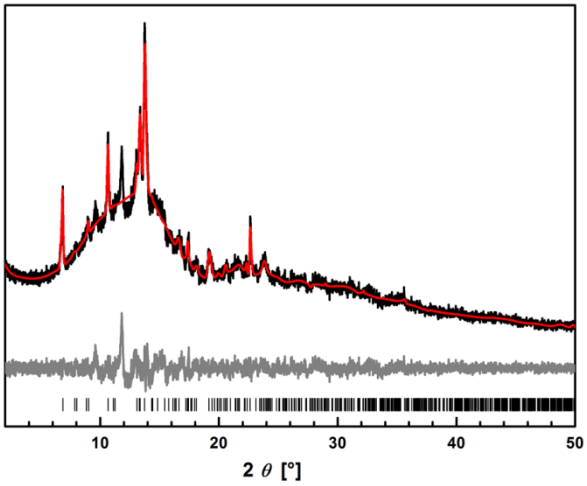

Figure 3.1-4. Rietveld refinement (Mo-$K_{\alpha 1}$ radiation) of the ammonothermal reaction of SDI, Ba and Mg. Experimental data (black line), calculated pattern of $Mg(NH_2)_2$ (red line) and difference curve (gray line). Black tickmarks: $Mg(NH_2)_2$. Non-described reflections belong to non-identified phases.

Ammonothermal syntheses starting from SDI and Ca or Sr without the addition of Mg resulted in amorphous reaction products.

3.1.3.2 Intermetallic Compounds in Ammonothermal Reactions

The prior results showed that up to now no alkaline-earth nitridosilicate, in contrast to alkaline nitridosilicates, can be synthesized in ammonothermal conditions starting from SDI. Watanabe et al. reported on the successful ammonothermal syntheses of $AEAlSiN_3:Eu^{2+}$ (AE = Ca,Sr) starting from the ternary silicides AEAlSi.[24,25]

Consequently, ternary intermetallic compounds were investigated as starting materials. Especially, Mg-containing silicides were used, as the ammonothermal reactions starting from SDI, AE metals and Mg were the most promising ones. Exemplarily, an ammonothermal synthesis starting from 0.80 mmol of CaMgSi (74 mg, synthesized according to Eisenmann et al.)[39] and LiN_3 (39 mg) in 50 ml ammonia is shown. The temperature was increased to 580 °C within 5 h, maintained at this temperature for 48 h and finally cooled down to room temperature in 60 h, during the heating the pressure inside the vessel reached ~1400 bar. The reaction product was a white powder with no residues of the silicide. From the experimental powder diffractogram the amides of Ca and Li as well as the alkaline-earth nitridosilicate $MgSiN_2$ were identified (Fig. 3.1-5).[40,41]

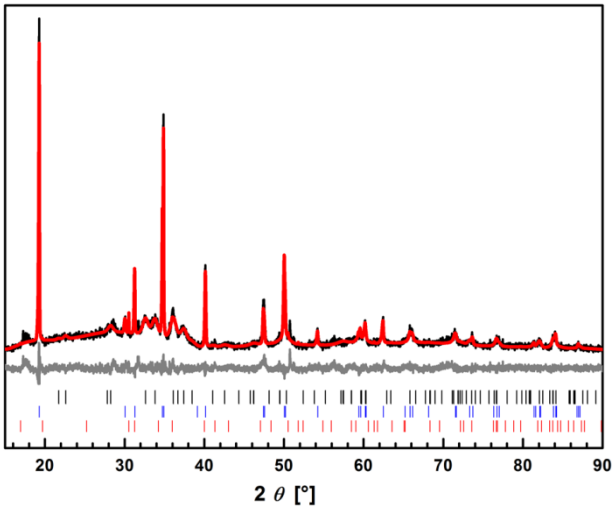

Figure 3.1-5. Rietveld refinement (Cu-$K_{\alpha 1}$ radiation) of the ammonothermal reaction of CaMgSi and LiN_3 in ammono-basic conditions. Experimental data (black line), calculated pattern (red line) and difference curve (gray line). Tickmarks: Black: $MgSiN_2$; blue: $Ca(NH_2)_2$; red: $LiNH_2$. Non-described reflections belong to non-identified phases.

3.1.3.3 Synthesis of "$SrAlGeN_3:Eu^{2+}$" under Ammonothermal Conditions

The successful ammonothermal synthesis of $LiSi_2N_3$ and $MgSiN_2$ as well as the syntheses of $AEAlSiN_3:Eu^{2+}$ (AE = Ca,Sr) by Watanabe et al. indicated that the formation of compounds crystallizing in wurtzite-type structures is favored under ammonothermal-reaction conditions. This suggests that a synthesis of isotypic "$SrAlGeN_3:Eu^{2+}$" in supercritical ammonia should succeed. Above described ammonothermal reactions often showed contamination of the reaction products with the mineralizers, therefore it is necessary to separate the reaction product from the mineralizer inside the pressure vessel. For this purpose an open tantalum ampule was used. The starting materials, consisting of 0.53 mmol $SrAlGe:Eu^{2+}$ (100 mg, 1 mol% Eu^{2+} (nominal composition), synthesized by arc-melting of an equimolar ratio of Sr, Eu, Al and Ge)[42] and 1.07 mmol NaN_3 (69.5 mg, Alfa Aesar, 99%) were mixed together and filled into the Ta ampule, which was put into the autoclave. The pressure vessel was loaded with 49 ml liquid ammonia and then heated to 400 °C in 2 h, maintained at this temperature for 24 h (p_{max} ~1200 bar), further heated to 500 °C in 2 h, kept at this temperature for 600 h (p_{max} ~1600 bar) and finally quenched to room temperature by switching off the furnace. The first heating step should lead to a complete conversion of $SrAlGe:Eu^{2+}$ to a soluble amide and/or imide species, which can be converted to a

nitride at elevated temperatures. After the reaction, the autoclave was opened inside a glovebox whereby the wall of the pressure vessel was covered with a white powder that was identified as $NaNH_2$ (PXRD).[43] The reaction product inside the Ta ampule was an orange powder without any white residues of the mineralizer. The orange powder does not exhibit visible luminescence under UV to blue irradiation, and was further characterized by PXRD (Fig. 3.1-6).

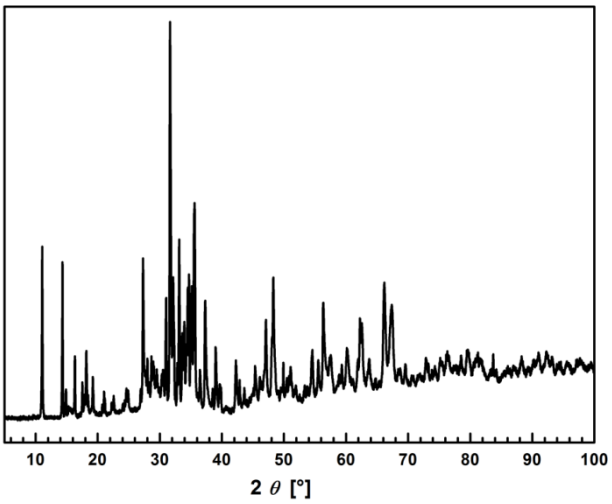

Figure 3.1-6. Experimental PXRD data (Cu-$K_{\alpha 1}$ radiation) of the ammonothermal synthesis of "$SrAlGeN_3:Eu^{2+}$". No reflections could be assigned to known phases.

There are no hints from the powder data that isotypic "$SrAlGeN_3:Eu^{2+}$" was obtained. Screening of numerous databases yielded no match with any known phase(s). The experimental powder diffractogram exhibits sharp reflections as well as broad ones, this is can be hint on the formation of more than one phase. Therefore, indexing of the reflections gave non-distinct results. For further characterization of the reaction product the quality of the PXRD is too poor and attempts to grow larger single crystals have to be carried out.

3.1.4 Conclusion

The challenge to obtain novel nitridosilicates by common high-temperature syntheses routes is more and more increasing. The hydrothermal syntheses of novel oxides showed the potential of solvothermal processes as a powerful tool in modern inorganic syntheses.[44] Therefore, it can be expected that the ammonothermal method

will be in the focus for the synthesis of novel nitrides in the future. Here the basic principles of the ammonothermal synthesis of nitridosilicates are reported. The investigation of the commonly for high-temperature syntheses of nitridosilicates used molecular precursor "$Si(NH)_2$" under ammonothermal conditions revealed that only ammono-basic conditions can be used for a successful synthesis of alkaline nitridosilicates. Until now no alkaline-earth nitridosilicate has been obtained in an ammonothermal reaction with SDI. However, it is imaginable that already a transformation of the starting materials to an amorphous amide and/or imide species was successful and that the reaction temperature is too low for the formation of a nitridosilicate. Novel autoclaves allowing higher reaction temperatures are urgently required. Also the characterization of potential intermediates during ammonothermal syntheses is very important for understanding the reaction mechanism of a nitridosilicate formation in supercritical ammonia. Particularly, progress at in-situ sampling and in-situ spectroscopy will be useful. Furthermore, it was shown that starting from an intermetallic phase can help to better deal with the available temperature and pressure ranges as an energy consuming metal to metal bonding has not to be carried out during the ammonothermal syntheses. Above all, it was shown that nitridosilicates crystallizing in an upmost stable structure type, for example a wurtzite type of structure, seem to be best suitable for ammonothermal syntheses. A huge challenge for the future is to optimize the crystallinity of the nitride samples. Most products were obtained as sparsely crystalline products and up to now no single crystals, for example of "$SrAlGeN_3:Eu^{2+}$", have been obtained. Nevertheless, the interdisciplinary DFG research group FOR-1600 acquired a lot of knowledge within the last three years and will make sure that ammonothermal syntheses will be reestablished as a powerful and advanced tool in modern inorganic syntheses.

3.1.5 References

(1) Grzegory, I.; Jun, J.; Boćkowski, M.; Krukowski, S. T.; Wróblewski, M.; Łucznik, B.; Porowski, S. *J. Phys. Chem. Solids* **1995**, *56*, 639.

(2) Boyko, T. D.; Hunt, A.; Zerr, A.; Moewes, A. *Phys. Rev. Lett.* **2013**, *111*, 097402.

(3) Chung, S.-L.; Huang, S.-C.; Chou, W.-C.; Tangguh, W. W. *Curr. Opin. Chem. Eng.* **2014**, *3*, 62.

(4) Denis, A.; Goglio, G.; Demazeau, G. *Mater. Sci. Eng.* **2006**, *R 50*, 167.

(5) Ehrentraut, D.; Fukuda, T. *J. Cryst. Growth* **2010**, *312*, 2514.

(6) Dwilinski, R.; Doradzinski, R.; Zajac, M. *Compd. Semicond.* **2010**, 12.

(7) Chen, Q.-S.; Prasad, V.; Hu, W. R. *J. Cryst. Growth* **2003**, *258*, 181.

(8) Juza, R.; Jacobs, H.; Gerke, H. *Ber. Bunsenges. physik. Chem.* **1966**, *70*, 1103.

(9) Peters, D.; Jacobs, H. *J. Less-Common Met.* **1989**, *146*, 241.

(10) Juza, R.; Jacobs, H. *Angew. Chem. Int. Ed. Engl.* **1966**, *5*, 247.

(11) Weyl, W. *Ann. Physik* **1864**, *197*, 601.

(12) Juza, R.; Hadenfeldt, C. *Naturwissenschaften* **1968**, *55*, 229.

(13) Hadenfeldt, C.; Juza, R. *Naturwissenschaften* **1969**, *56*, 282.

(14) Ehrentraut, D.; Kagamitani, Y.; Fukuda, T.; Orito, F.; Kawabata, S.; Katano, K.; Tereda, S. *J. Cryst. Growth* **2008**, *310*, 3902.

(15) Bockowski, M. *Cryst. Res. Technol.* **2007**, *42*, 1162.

(16) Hertweck, B.; Zhang, S.; Steigerwald, T. G.; Alt, N. S. A.; Niewa, R.; Schluecker, E. *Chem. Eng. Technol.* **2014**, *37*, 1835.

(17) Wang, B.; Callahan, M. J. *Cryst. Growth Des.* **2006**, *6*, 1227.

(18) Peters, D.; Paulus, E. F.; Jacobs, H. *Z. Anorg. Allg. Chem.* **1990**, *584*, 129.

(19) Kaskel, S.; Farrusseng, D.; Schlichte, K. *Chem. Commun.* **2000**, 2481.

(20) Kaskel, S.; Khanna, M.; Zibrowius, B.; Schmidt, H.-W.; Ullner, D. *J. Cryst. Growth* **2004**, *261*, 99.

(21) Kaskel, S.; Schlichte, K.; Zibrowius, B. *Phys. Chem. Chem. Phys.* **2002**, *4*, 1675.

(22) Lange, H.; Wötting, G.; Winter, G. *Angew. Chem. Int. Ed. Engl.* **1991**, *30*, 1579.

(23) Zeuner, M.; Pagano, S.; Schnick, W. *Angew. Chem. Int. Ed.* **2011**, *50*, 7754.

(24) Watanabe, T.; Nonaka, K.; Li, J.; Kishida, K.; Yoshimura, M. *J. Ceram. Soc. Jpn.* **2012**, *120*, 500.

(25) Li, J.; Watanabe, T.; Wada, H.; Setoyama, T.; Yoshimura, M. *Chem. Mater.* **2007**, *19*, 3592.

(26) Watanabe, H.; Yamane, H.; Kijima, N. *J. Solid State Chem.* **2008**, *181*, 1848.

(27) Metalcor - 2.4668 (Alloy 718), N07718 | Datenblatt | METALCOR. http://www.metalcor.de/datenblatt/105/ (accessed Oct 30, 2014)

(28) Hintze, F. *Doctoral Thesis*, Ludwig Maximilian University Munich, 2013.

(29) Sheldrick, G. M. SHELXS-97: A program for crystal structure solution, University of Göttingen, 1997.

(30) Sheldrick, G. M. *Acta Crystallogr. Sect. A: Found. Crystallogr.* **2008**, *64*, 112.

(31) Sheldrick, G. M. SHELXL-97: A program for crystal structure refinement, University of Göttingen, 1997.

(32) Hambley, T. W.; Lay, P. A. *Inorg. Chem.* **1986**, *25*, 4553.

(33) Hertweck, B.; Steigerwald, T. G.; Alt, N. S. A.; Schluecker, E. *Chem. Eng. Technol.* **2014**, *37*, 1903.

(34) Fair, H. D.; Walker, R. F. *Energetic Materials 1, Physics and Chemistry of Inorganic Azides*; 1st ed.; Plenum Press: New York, London, 1977.

(35) Jacobs, H.; Juza, R. *Z. Anorg. Allg. Chem.* **1972**, *391*, 271.

(36) Orth, M.; Schnick, W. *Z. Anorg. Allg. Chem.* **1999**, *625*, 1426.

(37) Schmiechen, S.; Strobel, P.; Hecht, C.; Reith, T.; Siegert, M.; Schmidt, P. J.; Huppertz, P.; Wiechert, D.; Schnick, W. *Chem. Mater.* **2015**, *27*, 1780.

(38) Jacobs, H.; Juza, R. *Z. Anorg. Allg. Chem.* **1969**, *370*, 254.

(39) Eisenmann, B.; Schäfer, H.; Weiss, A. *Z. Anorg. Allg. Chem.* **1972**, *391*, 241.

(40) David, J.; Laurent, Y.; Lang, J. *Bull. Soc. Fr. Mineral. Cristallogr.* **1970**, *93*, 153.

(41) Petukhov, A. G.; Lambrecht, W. R. L.; Segall, B. *Phys. Rev. B: Condens. Matter* **1994**, *49*, 4549.

(42) Youn, S. J.; Freeman, A. J. *Physica C: Superconductivity* **2012**, *476*, 54.

(43) Juza, R.; Weber, H. H.; Opp, K. *Z. Anorg. Allg. Chem.* **1956**, *284*, 73.

(44) Dhanaraj, G.; Byrappa, K.; Prasad, V.; Dudley, M. *Springer Handbook of Crystal Growth*; Springer: Berlin, Heidelberg, 2010.

3.2 Ammonothermal Synthesis and Crystal Structure of $BaAl_2(NH_2)_8 \cdot 2NH_3$

Philipp Pust, Sebastian Schmiechen, Frauke Hintze and Wolfgang Schnick

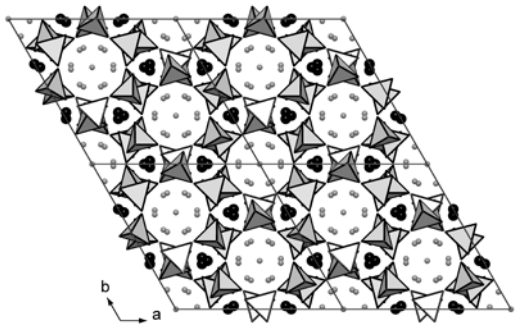

Published in: *Z. Anorg. Allg. Chem.* **2013**, *639*, 1185; DOI: 10.1002/zaac.201300088
http://onlinelibrary.wiley.com/doi/10.1002/zaac.201300088/abstract

Abstract

$BaAl_2(NH_2)_8 \cdot 2NH_3$ was synthesized starting from an intermetallic phase with nominal composition Al_2Ba under ammonothermal conditions in a stainless-steel autoclave at 823 K and 245 MPa. Single crystals were grown on aluminum substrates and prepared under low-temperature conditions. The crystal structure ($R\bar{3}c$ (no. 167), a = 15.7370(17), c = 28.804(6) Å, Z = 1, 1829 reflections, 65 parameters, wR_2 = 0.07) was solved on the basis of single-crystal X-ray diffraction data. $BaAl_2(NH_2)_8 \cdot 2NH_3$ contains isolated $Al(NH_2)_4$ tetrahedra forming two different types of channels along [001].

3.2.1 Introduction

Synthesis of ternary or multinary nitride materials can be carried out with a broad range of synthetic approaches. Due to the high kinetic stability of nitrogen (N_2) regular

high-temperature routes starting from metals and nitrogen require typically rather high temperatures above 1000 °C. Unfortunately, such reactions lead frequently to non phase-pure products.[1,2] We have recently reported on another approach for nitrides starting from binary amides and imides as precursor compounds to form nitridosilicates.[3,4] In such amides or imides the proximity of nitrogen and the corresponding metal ions on an atomic level facilitates a significant reduction of synthesis temperature. Employment of thermally less stable ternary amides could lead to further reduction of temperatures and may enable access to kinetically controlled nitridic products. This method could be of interest, especially in the nitridoaluminate system with respect to the thermodynamically very stable binary compound AlN.

Rouxel et al. were the first to report on ternary alkaline-earth aluminum amides.[5–7] The syntheses were performed in liquid ammonia in sealed glass tubes starting from an alkaline-earth electride solution and an excess of metallic aluminum. A stoichiometric formula $M^{II}Al_2(NH_2)_8$ (M^{II} = Sr, Ba) was derived from elemental analysis and IR spectroscopy as well as thermal decomposition measurements have been performed. The compounds showed a rapid decomposition after being extracted from ammonia atmosphere and thus it was not possible to determine the crystal structure.[5–7]

Another method to access ternary aluminum amides has been demonstrated by Peters et al. employing ammonothermal conditions.[8] To increase the solubility of aluminum in super-critical NH_3 ammonobasic mineralizers like K or $K(NH_2)_2$ are useful. Formation of intermediate $KAl(NH_2)_2$ and subsequent thermal decomposition induces the generation of AlN.

We adapted this technique to our needs and performed the ammonothermal synthesis of an alkaline-earth aluminum amide employing stainless-steel autoclaves. Crystal structure determination was achieved by low-temperature single-crystal preparation and measurement.

3.2.2 Results and Discussion

$BaAl_2(NH_2)_8{\cdot}2NH_3$ was synthesized starting from an intermetallic phase with nominal composition Al_2Ba and dry ammonia in a stainless-steel autoclave at 823 K and 245 MPa under supercritical conditions.

Table 3.2-1. Crystallographic Data of $BaAl_2(NH_2)_8{\cdot}2NH_3$

formula	$BaAl_2(NH_2)_8{\cdot}2NH_3$
crystal system	trigonal
space group	$R\bar{3}c$ (no. 167)
lattice parameters /Å	$a = b$ = 15.7370(17) c = 28.804(6)
cell volume /Å^3	6177.7(16)
formula units /cell	1
$\rho_{calcd.}$ /g·cm^{-3}	1.673
μ /mm^{-1}	3.004
T /K	200(2)
F(000)	3036
diffractometer	Kappa CCD
radiation, monochromator	Mo-K_α (λ = 0.71073 Å), graphite
absorption correction	multi-scan[12]
max. / min. transmission	0.4322 / 0.2100
θ range /°	3.2 - 29.6
index ranges	$-21 \le h \le 21$
	$-21 \le k \le 21$
	$-37 \le l \le 39$
independent reflections	1829 (R_{int} = 0.0685)
refined parameters	65
goodness of fit	1.021
R_1 (all data); R_1 ($F^2 > 2\sigma(F^2)$)	0.0280, 0.0246
wR_2 (all data); wR_2 ($F^2 > 2\sigma(F^2)$)	0.0700, 0.0674
max. / min. residual electron density /e·Å^{-3}	0.84 / -1.51

Colorless crystals, which exhibited a high sensitivity towards hydrolysis and thermal decomposition under ambient conditions, were grown on an aluminum substrate and isolated under low-temperature conditions (213 K).

The crystal structure of $BaAl_2(NH_2)_8{\cdot}2NH_3$ was solved from single-crystal diffraction data and refined in trigonal space group $R\bar{3}c$ (no. 167) with a = 15.7370(17) and c = 28.804(6) Å. The crystallographic data of $BaAl_2(NH_2)_8{\cdot}2NH_3$ are summarized in Table 3.2-1, atomic coordinates and isotropic displacement parameters are listed in Table 3.2-2.

Table 3.2-2. Atomic Coordinates and Isotropic Displacement Parameters / Å^2 of $BaAl_2(NH_2)_8{\cdot}2\ NH_3$, Standard Deviations in Parentheses

Atom	*x*	*y*	*z*	U_{eq}
Ba1	0.35543(1)	⅓	0.8333	0.02367(9)
Al1	0.35806(6)	0.15825(5)	0.00234(2)	0.02902(17)
N1	0.24822(18)	0.07955(19)	-0.03310(9)	0.0404(5)
N2	0.3991(2)	0.28800(17)	-0.01122(8)	0.0407(6)
N3	0.3232(2)	0.13391(17)	0.06434(7)	0.0377(5)
N4	0.45903(18)	0.13427(18)	-0.01033(8)	0.0368(5)
N5	0.5474(6)	0.3481(10)	0.0731(4)	0.070(3)
N6	0	0	-0.0832(4)	0.143(5)

The crystal structure of $BaAl_2(NH_2)_8{\cdot}2NH_3$ is built up of isolated $Al(NH_2)_4$ tetrahedra forming two different types of channels along [001] (see Figure 3.2-1). Ba^{2+}-ions are located in the smaller voids, whereas the bigger channels are occupied by ammonia molecules. Volume calculations with PLATON[9] delivered a pore volume of 1242.5 Å^3 in the larger tubes, leading to sufficient space to enclose two NH_3 molecules per unit cell.

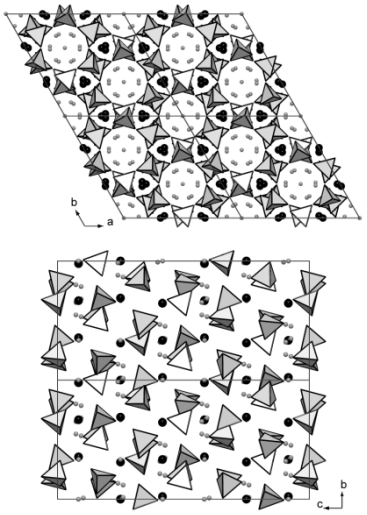

Figure 3.2-1. Crystal structure of $BaAl_2(NH_2)_8{\cdot}2NH_3$. $Al(NH_2)_4$ tetrahedra gray, Ba^{2+} black, ammonia nitrogen atoms bright gray. Hydrogen atoms of the amide groups and of the ammonia molecules are not displayed. Top: Viewing direction along [001], bottom: Viewing direction along [100].

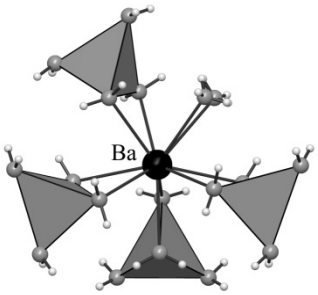

Figure 3.2-2. Coordination of Ba^{2+} in $BaAl_2(NH_2)_8{\cdot}2NH_3$. $Al(NH_2)_4$ tetrahedra gray, Ba^{2+} black, N bright gray, H white.

The shortest distance between ammonia molecules and surrounding amide groups (2.885(13) Å) is too large to form stabilizing hydrogen bonds, resulting in high mobility of the enclosed molecules and large isotropic displacement parameters. Therefore hydrogen atoms bound to ammonia nitrogen N6 were disregarded in the crystal structure refinement assuming severe rotational disorder in the NH_3 molecules.

$Al(NH_2)_4$ tetrahedra show interatomic distances (Al–N) of 1.85 Å, which correspond with Al–N distances in nitridoaluminates like $LiCaAlN_2$ (Al–N: 1.92–1.96 Å)[10] or $Ba_3Al_2N_4$ (Al–N: 1.91–1.98 Å).[2]

Ba^{2+}-ions are aligned in the smaller tubes along [001] (see Figure 3.2-1). The Ba^{2+}-site is coordinated by eight amide groups and one ammonia molecule with Ba–N distances

ranging from 2.93 to 2.98 Å (see Figure 3.2-2). Similar values can also be observed in $Ba(NH_2)_2$ (Ba–N: 2.79–3.17 Å).[11]

3.2.3 Conclusions

In this contribution it was possible to elucidate the crystal structure of $BaAl_2(NH_2)_8{\cdot}2NH_3$ and to confirm the assumed stoichiometric formula given by Rouxel et al.[6] The structure shows tube like pores with a calculated volume of 1242.5 $Å^3$ leaving space for incorporation of two NH_3 molecules per unit cell. $BaAl_2(NH_2)_8{\cdot}2NH_3$ may be a suitable precursor material for nitridoaluminate synthesis since constituting atoms are already arranged on an atomic level and a ternary compound in the system Ba-Al-N may be formed by thermal treatment and evolution of NH_3.

3.2.4 Experimental Section

3.2.4.1 Synthesis

All manipulations were performed with rigorous exclusion of oxygen and moisture in flame-dried Schlenk-type glassware on a Schlenk line interfaced to a vacuum (10^{-4} mbar) line or in an argon-filled glove box (Unilab, MBraun, Garching, O_2 <1 ppm, H_2O <1 ppm). Ammonia was purified using a cleaning cartridge (Micro Torr MC400-702FV, SAES Pure Gas Inc., San Luis Obispo, CA, USA).

The synthesis of $BaAl_2(NH_2)_8{\cdot}2NH_3$ was performed in specially designed autoclaves made from Inconel stainless steel (No. 2.4668), sustaining a maximum pressure of 300 MPa and a maximum temperature of 873 K (development and design of the autoclaves was performed by the workgroup of Prof. Dr.-Ing. E. Schlücker and Dr.-Ing. Dipl.-Wirt.-Ing. N. Alt within the DFG-Forschergruppe FOR-1600 “Chemie und Technologie der Ammonothermal-Synthese von Nitriden”). 191.3 mg (1.00 mmol) of an intermetallic phase with nominal composition Al_2Ba, synthesized from the elements at 1423 K, were placed into the autoclave together with aluminum substrates. Substrates were cut from an aluminum foil and surface-ground with a rasp. A volume of ammonia (44 mL) was condensed onto the compounds at 200 K, reaching a filling degree of 45 Vol.-% inside the autoclave. The autoclave was positioned vertically in a

tube furnace. The autoclave lid protruded from the furnace resulting in a measured temperature gradient of 100 K from bottom to top. Within 3 h temperature was raised to 823 K, maintained for 700 h, gaining a measured pressure of 245 MPa, and quenched down to room temperature by switching of the furnace.

3.2.4.2 Single-Crystal Preparation

For the crystal preparation, we adapted the technique described by Stalke et al.[13] to our needs. After reaction the ammonia within the autoclave was recondensed at 200 K, the aluminum substrate was extracted and directly put into perfluoroether (Galden), which was cooled by an ethanol/dry-ice freezing mixture and a stream of cooled nitrogen to 213 K. Colorless, block-shaped single crystals grown on the aluminum substrate were isolated under a microscope, collected on the tip of a glass fiber, immediately submerged in liquid nitrogen and transferred to the diffractometer.

3.2.4.3 Single-Crystal X-ray Diffraction

Single-crystal diffraction data were collected with a Nonius Kappa CCD diffractometer (Mo-K_α radiation, graphite monochromator) at 200 K. A spherical absorption correction using the program SADABS[12] was applied. The crystal structure was solved by using direct methods with SHELXS.[14] The refinement of the structure was carried out by the method of least-squares using SHELXL.[14] The atomic ratio Ba:Al was confirmed by energy-dispersive X-ray spectroscopy (EDX) using a JSM-6500F scanning microscope (Jeol) equipped with an EDX detector 7418 (Oxford Instruments). An atomic ratio Ba:Al = 1:1.9 was measured by EDX analysis and agrees with the composition of $BaAl_2(NH_2)_8{\cdot}2NH_3$. As a result of the high sensitivity at ambient temperature of the compound the nitrogen ratio was not determinable. Hydrogen positions of the $Al(NH_2)_4$ tetrahedra could be determined by difference Fourier syntheses and were refined isotropically using restraints for nitrogen-hydrogen distances, all other atoms were refined anisotropically.

Further details of the crystal structure investigations can be obtained from the Fachinformationszentrum Karlsruhe, 76344 Eggenstein-Leopoldshafen, Germany

(fax: +49-7247-808-666; E-Mail: crysdata@fiz-karlsruhe.de) on quoting the depository number CSD-425323.

3.2.5 References

(1) Ludwig, M.; Jaeger, J.; Niewa, R.; Kniep, R. *Inorg. Chem.* **2000**, *39*, 5909.

(2) Ludwig, M.; Niewa, R.; Kniep, R. *Z. Naturforsch. B: Chem. Sci.* **1999**, *54*, 461.

(3) Zeuner, M.; Hintze, F.; Schnick, W. *Chem. Mater.* **2009**, *21*, 336.

(4) Zeuner, M.; Pagano, S.; Schnick, W.*Angew. Chem. Int. Ed.* **2011**, *50*, 7754.

(5) Palvadeau, P.; Trélohan, A.-M.; Rouxel, J. *Compt. Rend.* **1969**, *269C*, 126.

(6) Rouxel, J.; Palvadeau, P. *Compt. Rend.* **1971**, *272C*, 63.

(7) Palvadeau, P.; Drew, M.; Charlesworth, G.; Rouxel, J.; *Seances, C. Acad. Sci. (Ser. C)* **1972**, 275.

(8) Peters, D. *J. Cryst. Growth* **1990**, *104*, 411.

(9) Spek, A. L. *PLATON - A Multipurpose Crystallographic Tool, v1.07,* Utrecht University, Utrecht, Netherlands, 2003.

(10) Pust, P.; Pagano, S.; Schnick, W. *Eur. J. Inorg. Chem.* **2013**, 1157.

(11) Jacobs, H.; Hadenfeldt, C. *Z. Anorg. Allg. Chem.* **1975**, *418*, 132.

(12) Sheldrick, G. M. *SADABS, v2, Multi-Scan Absorption Correction*, University of Göttingen, Germany, 2001.

(13) Kottke, T.; Stalke, D. *J. Appl. Crystallogr.* **1993**, *26*, 615.

(14) Sheldrick, G. M. *Acta Crystallogr., Sect. A: Found. Crystallogr.* **2008**, *64*, 112.

4 Conclusion and Outlook

Eu^{2+}-doped alkaline-earth nitridosilicates have proven their applicability as orange to red components in modern pc-LEDs. However, currently applied phosphors like $(Ba,Sr)_2Si_5N_8:Eu^{2+}$ (λ_{em} ~590-625 nm, fwhm ~2050-2600 cm^{-1})[1-3] or $(Ca,Sr)SiAlN_3:Eu^{2+}$ (λ_{em} ~610-660 nm, fwhm ~2100-2500 cm^{-1})[4,5] show a large portion of emitted light outside the human-eye sensitivity in the infrared region wasting energy and therefore reducing the efficacy of a pc-LED. For a further enhancement of illumination grade white pc-LEDs novel narrow-band red emitting materials are required.[6] For years, the search for suitable materials bothered scientific researchers in the solid-state lighting industry as well as in the university environment. Numerous novel multinary alkaline-earth nitridosilicates were synthesized and investigated in detail, but none could fulfill the requirments (λ_{em} ~610-650 nm with an fwhm ~50 nm) on narrow-band red-emitting phosphors. Conspicuously, Mg-containing nitridosilicates have not been investigated as suitable host lattices and $MgSiN_2$ was the only Mg-containing nitridosilicate mentioned in the literature.[7,8] Only when the group of Yamane reported on $Ba_4Mg[Si_2N_6]$ new hope for the Mg-containing nitridosilicates arose.[9] Within this thesis novel Mg-containing nitridosilicates were synthesized and their luminescence properties were investigated. Especially, $Sr[Mg_3SiN_4]:Eu^{2+}$ is not only the first nitridosilicate with a partial substituion of Mg^{2+} for Si^{4+} on the tetrahedrally-coordinated sites, but also set the world record for Eu^{2+}-doped phosphors in the red spectral region with λ_{em} ~615 nm and an fwhm ~43 nm.[10] Due to a small band gap and therefore severe thermal quenching already at room temperature an application in next-generation illumination grade white pc-LEDs is aggravated. Nevertheless, the compound gave a lot of hints, which structural requirements narrow-band red-emitting materials have to fulfill. The crystallographically ordered and highly condensed network proved to be unavoidable. Also, only one heavy atom site in a highly symmetric coordination (here: cuboidal) is beneficial. Based on this, numerous other nitridosilicates and -aluminates were

synthesized that fulfilled a majority of the requirements.[11-14] All of these compounds can be derived from the UCr_4C_4 structure type,[15] however, only ordered variants crystallizing in the $Na[Li_3SiO_4]$ or $Cs[Na_3PbO_4]$ structure types show intriguing luminescence properties.[10,13,14,16,17] Yet, structure determining factors are not understood for the different compounds and thus no structure prediction could be carried out. Within this thesis several further Mg-containing alkaline-earth nitridosilicates were synthesized. All of these compounds have a similar sum formula $Sr[T_4N_4]$ with T = Mg,Li,Al,Si (e.g., $Sr[Mg_{2.1}Li_{0.6}Si_{1.3}N_4]$,[18] $Sr[Mg_2Li_{0.5}Al_{0.5}SiN_4]$ or $Sr[Mg_{2.4}Li_{0.3}Al_{0.3}SiN_4]$)[19] to $Sr[Mg_3SiN_4]$. Nevertheless, all of these compounds crystallize in the UCr_4C_4 structure type exhibiting crystallographic disorder of the network-forming cations. Consequently, the respective Eu^{2+}-doped compounds show less narrow-emission properties (e.g., $Sr[Mg_2Li_{0.5}Al_{0.5}SiN_4]:Eu^{2+}$: $\lambda_{em} = 646$ nm and an fwhm ~100 nm).[19] However, for the syntheses of further novel narrow-band emitting materials it is absolutely necessary to understand these relations.

Furthermore, besides these described "N_4-phosphors" the first next-generation "N_6-phosphors" were reported. First of all, two compounds of the solid-solution series $Ba[(Mg_{2-x}Li_x)(Al_{4-x}Si_x)N_6]$ with x = (0-2) were synthesized. The crystal structure of the host lattice is a further promising one. It exhibits analogies to the UCr_4C_4 structure type, but in contrast to this structure type both *vierer* ring channels are centered by cations. Therefore, there is one more degree of freedom for substitutional variants and more nitridosilicates and/or –aluminates crystallizing in this structure type can be expected. In addition, Eu^{2+}-doped $Ba[(Mg_{0.4}Li_{1.6})(Al_{2.4}Si_{1.6})N_6]$ and $Ba[(Mg_{0.2}Li_{1.8})(Al_{2.2}Si_{1.8})N_6]$ show promising emission properties in the green to yellow range of the visible spectrum. It was shown that a decreasing Mg content shifts the emission maximum into the green region λ_{em} = 550 nm with an fwhm ~73 nm.[20] Therefore, $Ba[Li_2(Al_2Si_2)N_6]:Eu^{2+}$ can be seen as a good candidate as a narrow-band green-emitting phosphor with the potential for an application in pc-LEDs for backlighting applications in modern LCDs. Nevertheless, the green emission of $Ba[Li_2(Al_2Si_2)N_6]:Eu^{2+}$ is up to now not understood. Typically, green emission is expected from oxonitrides, as the nephelauxetic effect and the crystal-field splitting

are reduced due to the larger difference in electronegativity of O^{2-} vs. Si^{4+} and therefore the emission is shifted towards smaller wavelengths (i.e., higher energy).[21-23] $Li_2Ca_2[Mg_2Si_2N_6]:Eu^{2+}$ can also be attributed to the group of next-generation "N_6-phosphors". In the mean time, Strobel succeeded in the optimization of the doping level and the resulting emission properties of λ_{em} = 639 nm with an fwhm ~1550 cm^{-1} are in the magnitude of further discussed narrow-band red-emitting Eu^{2+}-doped nitridosilicates and –aluminates.[20] Remarkably, this host lattice contradicts the structural assumptions that the other narrow-band red-emitting nitrides had shown. Neither, the $Li_2Ca_2[Mg_2Si_2N_6]$ host lattice is made up of a highly condensed rigid network, nor is the heavy-atom site in a cube-like coordination and anyhow the respective Eu^{2+}-doped compound shows intriguing luminescence properties in the red spectral region of the visible spectrum. Similar observations can be found in the compound $Ca_{18.75}Li_{10.5}Al_{39}N_{55}:Eu^{2+}$ reported by Pust.[24] Therefore, it is obvious that there are still many shades in luminescence that are not yet understood and more knowledge on detailed structure-property relations are urgently required.

All of these reported compounds were synthesized by a modified solid-state metathesis route that uses the formation of LiF as driving force. Traditional solid-state syntheses routes only worked partly, often only few wt% of the compounds were obtained with numerous impurities and also the crystal quality was worse. Therefore, it can be asserted that it is more and more difficult to obtain novel compounds with classic syntheses routes. Especially, ammonothermal syntheses are a very promising tool in modern inorganic syntheses. Compared to the hydrothermal process, with more than 600 novel compounds synthesized in this process, there are only very few reports on novel nitrides synthesized in supercritical ammonia.[25] After some initial difficulties that had to be overcome, the DFG-*Forschergruppe* FOR-1600 proceeded to acquire important knowledge and through applying this, first results were achieved.[26-28] The here described fundamentals for the synthesis of novel nitridosilicates in ammonothermal conditions guided the direction. Particularly, the ammonothermal syntheses of nitridosilicates crystallizing in a wurtzite-type structure gave a first hint. It led to a broad investigation of further nitrides crystallizing in this

structure type and the ammonothermal syntheses of the phases $ZnTN_2$ with T = Si,Ge,Sn.[29-31] These compounds are currently discussed as replacements for the semiconductor material (In,Ga)N. For further investigations on their material properties sufficiently large single crystals are required, whereby the ammonothermal process could help. Besides the already discussed Eu^{2+}-doped nitridosilicates and -aluminates as phosphors for application in pc-LEDs, also nitridogermanates are an interesting material class. It is expected that they show similar crystal chemistry as the nitridosilicates and therefore Eu^{2+}-doped nitridogermanates are expected to show promising luminescence properties. It was attempted to synthesize to $SrAlSiN_3:Eu^{2+}$ isotypic "$SrAlGeN_3:Eu^{2+}$". Conventionally, $SrAlSiN_3:Eu^{2+}$ is synthesized by a hot-isostatic pressing (HIP) process,[32] but Watanabe et al. succeeded in an ammonothermal synthesis of the compound.[33] Therefore, it is suggesting that "$SrAlGeN_3:Eu^{2+}$" can also be synthesized in an ammonothermal reaction. The here described ammonothermal reaction gave an orange powder, which gave a first hint on a successful conversion of the starting materials. Yet, no single crystals suitable for further characterization have been obtained and corresponding PXRD data are non-distinct. Numerous further syntheses yielded only sparsely crystalline products that the crystallization process during an ammonothermal reaction has to be further optimized. Furthermore, novel autoclaves that enable ammonothermal reactions at higher temperatures can lead to more crystalline products and also the conversion from intermediates like amides or imides to nitrides can more easily be achieved.

The results of this doctoral thesis provided the basic knowledge for various further results. The synthesized compounds, especially $Sr[Mg_3SiN_4]:Eu^{2+}$ pointed the way toward the nitridoaluminate $Sr[LiAl_3N_4]:Eu^{2+}$ that will be used as red component in next-generation pc-LEDs.[13] Also, the compound $Ba[(Mg_{2-x}Li_x)(Al_{4-x}Si_x)N_6]:Eu^{2+}$ gave a first hint on the next generation of narrow-band emitting phosphors with a new type of host lattice. Perceptions from ammonothermal reactions, especially the suitability of nitrides crystallizing in a wurtzite-type structure, were a breakthrough. Last but not least, it was shown that Mg was unjustly handled by the syntheses of novel

nitridosilicates before this thesis and that there will be more very interesting Mg-containing nitridosilicates synthesized with outstanding material properties.

References

(1) Zeuner, M.; Hintze, F.; Schnick, W. *Chem. Mater.* **2008**, *21*, 336.

(2) Zeuner, M.; Pagano, S.; Schnick, W. *Angew. Chem. Int. Ed.* **2011**, *50*, 7754.

(3) Zeuner, M.; Schmidt, P. J.; Schnick, W. *Chem. Mater.* **2009**, *21*, 2467.

(4) Uheda, K.; Hirosaki, N.; Yamamoto, H. *Phys. Status Solidi A* **2006**, *203*, 2712.

(5) Uheda, K.; Hirosaki, N.; Yamamoto, Y.; Naito, A.; Nakajima, T.; Yamamoto, H. *Electrochem. Solid-State Lett.* **2006**, *9*, H22.

(6) Krames, M. R.; Mueller, G. O.; Mueller-Mach, R. B.; Bechtel, H.-H.; Schmidt, P. J. Wavelength conversion for producing white light from high power blue LED. PCT Int. Appl.WO 2010131133 A1, November 18th, 2010.

(7) David, J.; Laurent, Y.; Lang, J. *Bull. Soc. Fr. Mineral. Cristallogr.* **1970**, *93*, 153.

(8) Petukhov, A. G.; Lambrecht, W. R. L.; Segall, B. *Phys. Rev. B: Condens. Matter* **1994**, *49*, 4549.

(9) Yamane, H.; Morito, H. *J. Alloys Compd.* **2013**, *555*, 320.

(10) Schmiechen, S.; Schneider, H.; Wagatha, P.; Hecht, C.; Schmidt, P. J.; Schnick, W. *Chem. Mater.* **2014**, *26*, 2712.

(11) Schmiechen, S.; Strobel, P.; Hecht, C.; Reith, T.; Siegert, M.; Schmidt, P. J.; Huppertz, P.; Wiechert, D.; Schnick, W. *Chem. Mater.* **2015**, *27*, 1780.

(12) Pust, P.; Hintze, F.; Hecht, C.; Weiler, V.; Locher, A.; Zitnanska, D.; Harm, S.; Wiechert, D.; Schmidt, P. J.; Schnick, W. *Chem. Mater.* **2014**, *26*, 6113.

(13) Pust, P.; Weiler, V.; Hecht, C.; Tücks, A.; Wochnik, A. S.; Henß, A.-K.; Wiechert, D.; Scheu, C.; Schmidt, P. J.; Schnick, W. *Nat. Mater.* **2014**, *13*, 891.

(14) Pust, P.; Wochnik, A. S.; Baumann, E.; Schmidt, P. J.; Wiechert, D.; Scheu, C.; Schnick, W. *Chem. Mater.* **2014**, *26*, 3544.

(15) Behrens, R. K.; Jeitschko, W. *Monatsh. Chem.* **1987**, *118*, 43.

(16) Nowitzki, B.; Hoppe, R. *Rev. Chim. Miner.* **1986**, *23*, 217.

(17) Weiß, C.; Hoppe, R. *Z. Anorg. Allg. Chem.* **1996**, *622*, 1715.

(18) Reith, T. *Bachelor Thesis*, Ludwig Maximilian University Munich, 2013.

(19) Siegert, M. *Bachelor Thesis*, Ludwig Maximilian University Munich, 2013.

(20) Strobel, P. *Master Thesis*, Ludwig Maximilian University Munich, 2014.

(21) Seibald, M.; Rosenthal, T.; Oeckler, O.; Schnick, W. *Crit. Rev. Solid State Mater. Sci.* **2014**, *39*, 215.

(22) Braun, C.; Seibald, M.; Börger, S. L.; Oeckler, O.; Boyko, T. D.; Moewes, A.; Miehe, G.; Tücks, A.; Schnick, W. *Chem. - Eur. J.* **2010**, *16*, 9646.

(23) Xie, R.-J.; Hirosaki, N.; Takeda, T.; Suehiro, T. *ECS J. Solid State Sci. Technol.* **2013**, *2*, R3031.

(24) Pust, P. *Doctoral Thesis*, Ludwig Maximilian University Munich, 2014.

(25) Dhanaraj, G.; Byrappa, K.; Prasad, V.; Dudley, M. *Springer Handbook of Crystal Growth*; Springer: Berlin, Heidelberg, 2010.

(26) Zhang, S.; Hintze, F.; Schnick, W.; Niewa, R. *Eur. J. Inorg. Chem.* **2013**, *2013*, 5387.

(27) Zhang, S.; Alt, N. S. A.; Schlücker, E.; Niewa, R. *J. Cryst. Growth* **2014**, *403*, 22.

(28) Richter, T.; Niewa, R. *Inorganics* **2014**, *2*, 29.

(29) Punya, A.; Lambrecht, W. R. L. *Phys. Rev. B* **2013**, *88*, 075302.

(30) Narang, P.; Chen, S.; Coronel, N. C.; Gul, S.; Yano, J.; Wang, L.-W.; Lewis, N. S.; Atwater, H. A. *Adv. Mater.* **2014**, *26*, 1235.

(31) Shaposhnikov, V. L.; Krivosheeva, A. V.; Arnaud D'Avitaya, F.; Lazzari, J. L.; Borisenko, V. E. *Phys. Status Solidi B* **2008**, *245*, 142.

(32) Watanabe, H.; Yamane, H.; Kijima, N. *J. Solid State Chem.* **2008**, *181*, 1848.

(33) Watanabe, T.; Nonaka, K.; Li, J.; Kishida, K.; Yoshimura, M. *J. Ceram. Soc. Jpn.* **2012**, *120*, 500.

5 Summary

5.1 Toward New Phosphors for Application in Illumination-Grade White pc-LEDs: The Nitridomagnesosilicates $Ca[Mg_3SiN_4]:Ce^{3+}$, $Sr[Mg_3SiN_4]:Eu^{2+}$, and $Eu[Mg_3SiN_4]$

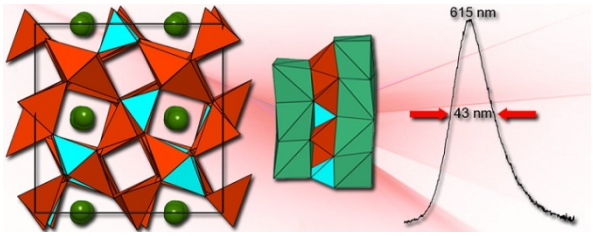

The isotypic compounds $M[Mg_3SiN_4]$ with M = Ca,Sr,Eu crystallize in the $Na[Li_3SiO_4]$ structure type (space group $I4_1/a$, no. 88) and have been synthesized by high-temperature routes. The nitridomagnesosilicates are the first examples for the partial substitution of Mg^{2+} for Si^{4+} in the nitridosilicate substructure. Their crystal structure is made up by a condensed tetrahedra network with a high degree of condensation (i.e., atomic ratio (Mg,Si):N) $\kappa = 1$. The tetrahedral network forms *vierer* ring channels along [001] with half of them centered by M^{2+} in a cuboidal coordination by N^{3-}. The crystal structures, which were solved from single-crystal X-ray diffraction data, were confirmed by Rietveld refinement, lattice energy (MAPLE) calculations, and further investigated by ^{29}Si-MAS NMR. Doping of the Ca and Sr compound with Ce^{3+} or Eu^{2+}, respectively, yielded intriguing luminescence properties in the yellow and red region of the visible spectrum. Especially, $Sr[Mg_3SiN_4]:Eu^{2+}$ exhibits the most narrow red emission of Eu^{2+}-phosphors reported in the literature so far ($\lambda_{max} = 615$ nm, fwhm ~1170 cm^{-1} (~43 nm)). Therefore, $Sr[Mg_3SiN_4]:Eu^{2+}$ is pointing the way to next generation red phosphor materials for application in illumination-grade white pc-LEDs.

5.2 Nitridomagnesosilicate $Sr[Mg_3SiN_4]$: Optical properties of Ce^{3+},Pr^{3+},Sm^{3+}, Eu, Yb Doping and Energy-Level Locations of all Lanthanides in the Host Lattice

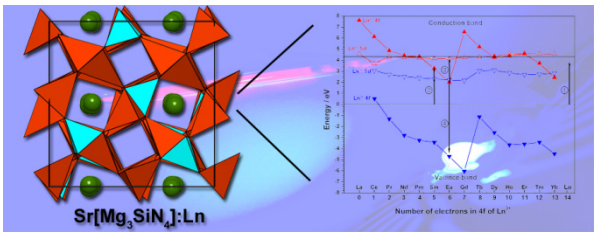

The nitridomagnesosilicate $Sr[Mg_3SiN_4]$ shows outstanding luminescence properties upon doping with Eu^{2+} in the red spectral region of the visible spectrum (λ_{em} = 615 nm, fwhm ~1170 cm^{-1}). Severe thermal quenching already at room temperature hinders an application in illumination-grade white pc-LEDs. It was assumed that the small band gap of the compound (~3.9 eV) leads to photoionization of Eu^{2+} to Eu^{3+}. Therefore, a detailed energy-level diagram of the host lattice containing the energetic levels of the 4*f* ground state and lowest excited 5*d* levels of all divalent and trivalent lanthanides was constructed. Hereto, the spectroscopic data of RE-doped $Sr[Mg_3SiN_4]$ (RE = Ce^{3+},Pr^{3+},Sm^{3+},Eu,Yb) was used. $Sr[Mg_3SiN_4]:Ce^{3+}$ shows typical $5d^1 \rightarrow 4f^1$ emission (λ_{em} = 545 and 605 nm, fwhm ~3840 cm^{-1}). Typical 4*f*-4*f* line emission was identified for the Pr^{3+}- and Sm^{3+}-doped compound. $Sr[Mg_3SiN_4]$ doped with Eu or Yb shows besides typical 5*d*-4*f* emission for the respective 2+-doped compounds, also 4*f*-4*f* line emissions typical for the 3+-doped compounds, which was attributed to photoionization. UV/vis-reflectance data of all doped compounds gave further information for the construction of the energy-level diagram. With the acquired data the diagram was constructed and discussed. Thermal properties of the Eu^{2+}-doped compound were explained with the aid of the energy-level diagram, the lowest excited 5*d* state of Eu^{2+} is ~0.2 eV above the edge of the conduction band and therefore photoionization is more likely the reason for high TQ and also explains the presence of Eu^{3+}. Also, the energy-level diagram was used to predict optical properties of further up to now non-investigated lanthanide-doped $Sr[Mg_3SiN_4]$ compounds.

5.3 Nitridomagnesosilicate $Ba[Mg_3SiN_4]:Eu^{2+}$ and Structure-Property Relations of Similar Narrow-Band Red Nitride Phosphors

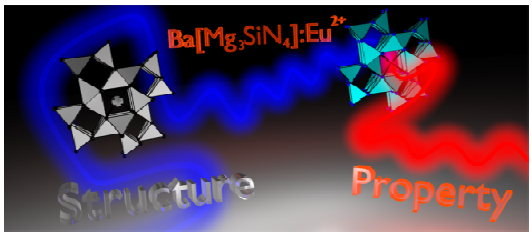

The nitridomagnesosilicate $Ba[Mg_3SiN_4]$ crystallizes, in contrast to the isoelectronic phases $M[Mg_3SiN_4]$ with M = Ca,Sr,Eu, in a distorted triclinic variant of UCr_4C_4 structure type (space group $P\bar{1}$ (no. 2), Z = 1, a = 3.451(1), b = 6.069(5), c = 6.101(4) Å, α = 85.200(7), β = 73.697(5), γ = 73.566(8)°). $Ba[Mg_3SiN_4]$ has been synthesized in an arc welded Ta ampule and its crystal structure was solved and refined from single crystal X-ray data and Rietveld refinement (R_p = 0.0218, R_{wp} = 0.0290). The crystal structure of $Ba[Mg_3SiN_4]$ consists of a highly condensed network of $(Mg,Si)N_4$ tetrahedra with Ba^{2+} centered inside *vierer* ring channels along [100] in a cuboidal coordination by N^{3-}. From UV/vis-reflectance data a band gap of ~4.0 eV was estimated. Doping with Eu^{2+} resulted in promising luminescence properties of λ_{em} = 670 nm with an fwhm ~1970 cm^{-1}. The luminescence properties of $Ba[Mg_3SiN_4]:Eu^{2+}$ differ significantly from the ones of $Sr[Mg_3SiN_4]:Eu^{2+}$. Besides typical emission from Eu^{2+}, in addition trapped-exciton emission was identified. Especially, the unexpected disordering of the tetrahedrally coordinated ions Mg^{2+} and Si^{4+} in $Ba[Mg_3SiN_4]$ give a hint for the different luminescence properties of the respective compounds. Therefore, the structure-property relations of recently reported Eu^{2+}-doped nitrides with narrow-band red-emission are discussed, which is a fundamental step toward the structure prediction and the design on demand of further new phosphors.

5.4 Narrow-Red Emitters for Brighter White Light

This comment gives an overview of the challenges for the LED technology in the presence and the future. Phosphor-converted LEDs are undisputed in efficiency and environmental acceptability, during the whole production period and life cycle. State of the art phosphor materials already give high CRIs >90 (like common incandescent light bulbs), however, by accepting losses in luminous efficacy. The current challenge for the LED industry is to further improve the color rendition without comprising energy efficiency. Especially, novel narrow-band red-emitting materials are most beneficial for this. Optimizing the spectral peak position and width of the red-emitting component will lead to elimination of emission in the infrared region. Narrow-band red-emitting materials like $Sr[Mg_3SiN_4]:Eu^{2+}$ or $AE[LiAl_3N_4]:Eu^{2+}$ (AE = Ca,Sr) convince with outstanding luminescence properties and point the way toward the next generation of white light LEDs.

5.5 Structural Relationship between the Mg-containing Nitridosilicates $Ca_2Mg[Li_4Si_2N_6]$ and $Li_2Ca_2[Mg_2Si_2N_6]$

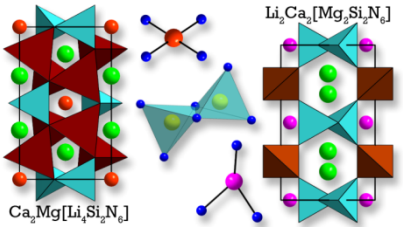

The nitridolithosilicate $Ca_2Mg[Li_4Si_2N_6]$ and the nitridomagnesosilicate $Li_2Ca_2[Mg_2Si_2N_6]$ have been synthesized in sealed Ta ampules. Both compounds exhibit different roles for Mg^{2+}, in $Ca_2Mg[Li_4Si_2N_6]$ it acts as a counterion, whereas in $Li_2Ca_2[Mg_2Si_2N_6]$ Mg^{2+} is part of the anionic nitridosilicate substructure. Both novel compounds crystallize in the monoclinic space group *C*2/*m* (no. 12). The crystal structures were solved and refined on basis of single-crystal X-ray diffraction data ($Z = 2$; $Ca_2Mg[Li_4Si_2N_6]$: $a = 5.9059(12)$, $b = 9.817(2)$, $c = 5.6109(11)$ Å, $\beta = 94.90(3)°$, $R_1 = 0.015$, $wR_2 = 0.049$; $Li_2Ca_2[Mg_2Si_2N_6]$: $a = 5.5472(11)$, $b = 9.844(2)$, $c = 5.9978(12)$ Å, $\beta = 97.13(3)°$, $R_1 = 0.024$, $wR_2 = 0.053$). $Ca_2Mg[Li_4Si_2N_6]$ and $Li_2Ca_2[Mg_2Si_2N_6]$ show homeotypic crystal structures that can both be derived from $Ca_3[Li_4Si_2N_6]$. Both structures are made up by edge sharing $[Si_2N_6]^{10-}$ tetrahedra (bow-tie units). In the nitridolithosilicate $Ca_2Mg[Li_4Si_2N_6]$ bow-tie units are connected via pairs of LiN_4 tetrahedra, whereas in the nitridomagnesosilicate $Li_2Ca_2[Mg_2Si_2N_6]$ the nitridosilicate substructure is connected by chains of MgN_4 tetrahedra. $Ca_2Mg[Li_4Si_2N_6]$ is only the second example for fourfold planar rectangular coordinated Mg^{2+} in a nitridosilicate. $Li_2Ca_2[Mg_2Si_2N_6]$ is the first nitridosilicate with Li^+ in a threefold coordination. The crystal structures were confirmed by lattice energy (MAPLE) calculations, PXRD investigations and EDX measurements.

5.6 Nitridolithomagnesoalumosilicate $Ba[(Mg_{2-x}Li_x)(Al_{4-x}Si_x)N_6]$ with x = (0-2) for LED-Backlighting Applications

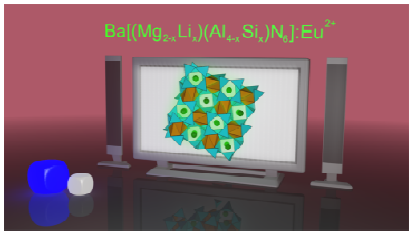

The novel nitridoalumolithomagnesosilicates $Ba[(Mg_{0.4}Li_{1.6})(Al_{2.4}Si_{1.6})N_6]$ and $Ba[(Mg_{0.2}Li_{1.8})(Al_{2.2}Si_{1.8})N_6]$ are the first examples for an Mg-containing SiAlN. The compounds have been synthesized by a solid-state metathesis reaction in a sealed tantalum ampule. The compounds crystallize in the tetragonal space group *P*4/*ncc* (no. 130). Crystal structures were solved and refined from single-crystal X-ray diffraction data ($Z = 4$, $Ba[(Mg_{0.4}Li_{1.6})(Al_{2.4}Si_{1.6})N_6]$: $a = 7.892(3)$, $c = 9.995(4)$ Å, $R_1 = 0.017$, $wR_2 = 0.046$; $Ba[(Mg_{0.2}Li_{1.8})(Al_{2.2}Si_{1.8})N_6]$: $a = 7.879(3)$, $c = 9.983(4)$ Å, $R_1 = 0.018$, $wR_2 = 0.049$). The crystal structure of both compounds is built up by crystallographicaly disordered $(Al,Si)N_4$ tetrahedra forming two types of *vierer* ring channels along [001]. One half of the channels is centered by a bisphenoid of $(Mg,Li)N_4$ tetrahedra giving a highly condensed tetrahedra network with a degree of condensation (i.e., atomic ratio (Al,Si,Li,Mg):N) $\kappa = 1$. The other half of the *vierer* ring channels is centered by Ba^{2+} in eightfold coordination by N^{3-}. The Eu^{2+}-doped samples show promising luminescence properties in the green to yellow part of the visible spectrum ($\lambda_{max} = 562$ nm, fwhm ~2739 cm^{-1} $Ba[(Mg_{0.4}Li_{1.6})(Al_{2.4}Si_{1.6})N_6]:Eu^{2+}$; $\lambda_{max} = 560$ nm, fwhm ~2654 cm^{-1} $Ba[(Mg_{0.2}Li_{1.8})(Al_{2.2}Si_{1.8})N_6]:Eu^{2+}$). According to this tuneability, an application in white LEDs for backlighting purposes for LCDs is in prospect.

5.7 Silicon Nitrides in Ammonothermal Reactions

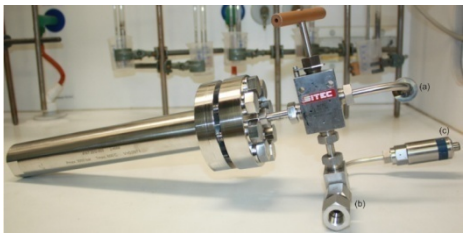

Silicon diimide ("$Si(NH)_2$", SDI) is a common precursor in high-temperature syntheses of nitridosilicates. Up to now, there are only few reports of the usage of SDI in ammonothermal reactions. An experimental series for the investigation of SDI with and without the addition of alkaline-containing mineralizers in ammonothermal reactions was carried out. It was shown that only ammono-basic conditions are suitable for the syntheses of alkaline nitridosilicates. Similar investigations with alkaline-earth mineralizers yielded only the respective amides. Another syntheses approach is to use intermetallic compounds of Si that no energy consuming metal to metal bond formation has to be done during the ammonothermal syntheses with its limited temperature and pressure ranges. Starting from the ternary silicide CaMgSi resulted in the formation of $MgSiN_2$ in ammonothermal conditions for the first time. The wurtzite-type structure of $MgSiN_2$ gave a hint that this structure type is remarkably accessible in ammonothermal conditions. Therefore, it was attempted to synthesize "$SrAlGeN_3:Eu^{2+}$" in an ammonothermal reaction. Due to the low crystallinity of the product, no single-crystal structure elucidation can be carried out, and also indexing of PXRD data was non-distinct.

5.8 Ammonothermal Synthesis and Crystal Structure of $BaAl_2(NH_2)_8{\cdot}2NH_3$

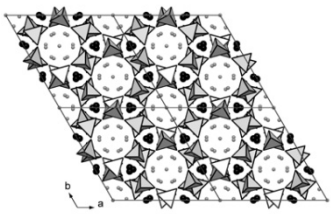

$BaAl_2(NH_2)_8{\cdot}2NH_3$ was synthesized in an ammonothermal reaction in a specially designed autoclave. The compound has already been known since the 1960s, but no structure elucidation has been carried out. Single crystals suitable for further characterization were obtained for the first time of this material by growing them on Al substrates and a subsequent preparation and measurement under low-temperature conditions. The crystal structure ($R\bar{3}c$ (no. 167), a = 15.7370(17), c = 28.804(6) Å, Z = 1, R_1 = 0.03, wR_2 = 0.07) was solved on the basis of single-crystal X-ray diffraction data and the structure shows tube like pores with a calculated volume of 1242.5 $Å^3$. $BaAl_2(NH_2)_8{\cdot}2NH_3$ is a suitable precursor for the synthesis of nitridoaluminates since constituting atoms are already arranged on an atomic level.

6 Appendix

6.1 Supporting Information for Chapter 2.1

Sebastian Schmiechen, Hajnalka Schneider, Peter Wagatha, Cora Hecht, Peter J. Schmidt, and Wolfgang Schnick, *Chem. Mater.* **2014**, *26*, 2712.

Table 6.1-S1. Anisotropic Displacement Parameters (Å²) of $M[Mg_3SiN_4]$ (M = Ca,Sr,Eu)[a]

	Atom	U_{11}	U_{22}	U_{33}	U_{12}	U_{13}	U_{23}
$Ca[Mg_3SiN_4]$	Ca	0.0090(3)	0.0086(4)	0.0139(4)	-0.0029(2)	0.0006(2)	0.0005(2)
	Si	0.0103(4)	0.0094(4)	0.0111(5)	0.0001(3)	-0.0007(3)	-0.0004(3)
	Mg1	0.0159(6)	0.0187(6)	0.0173(7)	0.0002(5)	0.0008(5)	-0.0022(4)
	Mg2	0.0161(6)	0.0166(6)	0.0168(7)	-0.0008(5)	0.0001(5)	-0.0016(4)
	Mg3	0.0191(7)	0.0172(6)	0.0176(8)	0.0001(5)	0.0003(5)	0.0034(5)
	N1	0.0158(15)	0.0175(15)	0.0188(18)	-0.0009(12)	-0.0005(12)	-0.0016(12)
	N2	0.0152(15)	0.0191(15)	0.0181(19)	0.0004(12)	0.0008(11)	-0.0015(12)
	N3	0.0164(14)	0.0165(14)	0.0188(17)	-0.0019(12)	-0.0009(12)	-0.0012(11)
	N4	0.0198(15)	0.0171(14)	0.0176(17)	0.0015(12)	-0.0010(12)	0.0017(12)
$Sr[Mg_3SiN_4]$	Sr	0.0143(4)	0.0158(4)	0.0156(4)	-0.0061(17)	-0.0011(16)	0.0010(19)
	Si	0.0142(8)	0.0141(8)	0.0109(8)	0.0018(5)	-0.0016(5)	-0.0037(6)
	Mg1	0.0131(10)	0.0168(10)	0.0134(10)	0.0013(7)	-0.0004(6)	-0.0030(8)
	Mg2	0.0120(10)	0.0160(10)	0.0099(10)	-0.0008(6)	0.0012(6)	-0.0017(8)
	Mg3	0.0243(11)	0.0169(11)	0.0124(10)	0.0030(6)	0.0037(7)	0.0106(8)
	N1	0.0190(3)	0.0220(3)	0.0170(2)	0.0046(18)	0.0028(18)	0.0030(2)
	N2	0.0160(3)	0.0190(3)	0.0190(2)	-0.0042(18)	-0.0015(17)	-0.0028(19)
	N3	0.0130(2)	0.0180(3)	0.0200(3)	0.0020(17)	-0.0012(17)	-0.0048(18)
	N4	0.0240(3)	0.0190(3)	0.0230(2)	0.0050(19)	0.0082(19)	0.0060(2)
$Eu[Mg_3SiN_4]$	Eu	0.0079(10)	0.0096(10)	0.0106(12)	-0.0051(5)	0.0014(5)	-0.0005(5)
	Si	0.0037(4)	0.0028(3)	0.0030(3)	0.0002(2)	0.0000(3)	0.0003(3)
	Mg1	0.0058(4)	0.0080(5)	0.0051(4)	0.0007(3)	0.0004(3)	-0.0017(4)
	Mg2	0.0051(4)	0.0074(5)	0.0041(4)	0.0003(3)	-0.0002(3)	-0.0019(4)
	Mg3	0.0081(5)	0.0065(5)	0.0035(4)	-0.0003(3)	0.0001(3)	0.0035(4)
	N1	0.0051(11)	0.0033(10)	0.0053(10)	-0.0002(8)	0.0010(8)	0.0008(9)
	N2	0.0067(11)	0.0070(12)	0.0037(10)	-0.0010(8)	-0.0013(8)	-0.0006(9)
	N3	0.0058(11)	0.0073(12)	0.0053(10)	0.0007(8)	0.0001(8)	-0.0009(9)
	N4	0.0072(11)	0.0066(11)	0.0041(11)	-0.0005(8)	-0.0004(8)	0.0021(9)

[a] *e.s.d.'s in parentheses*

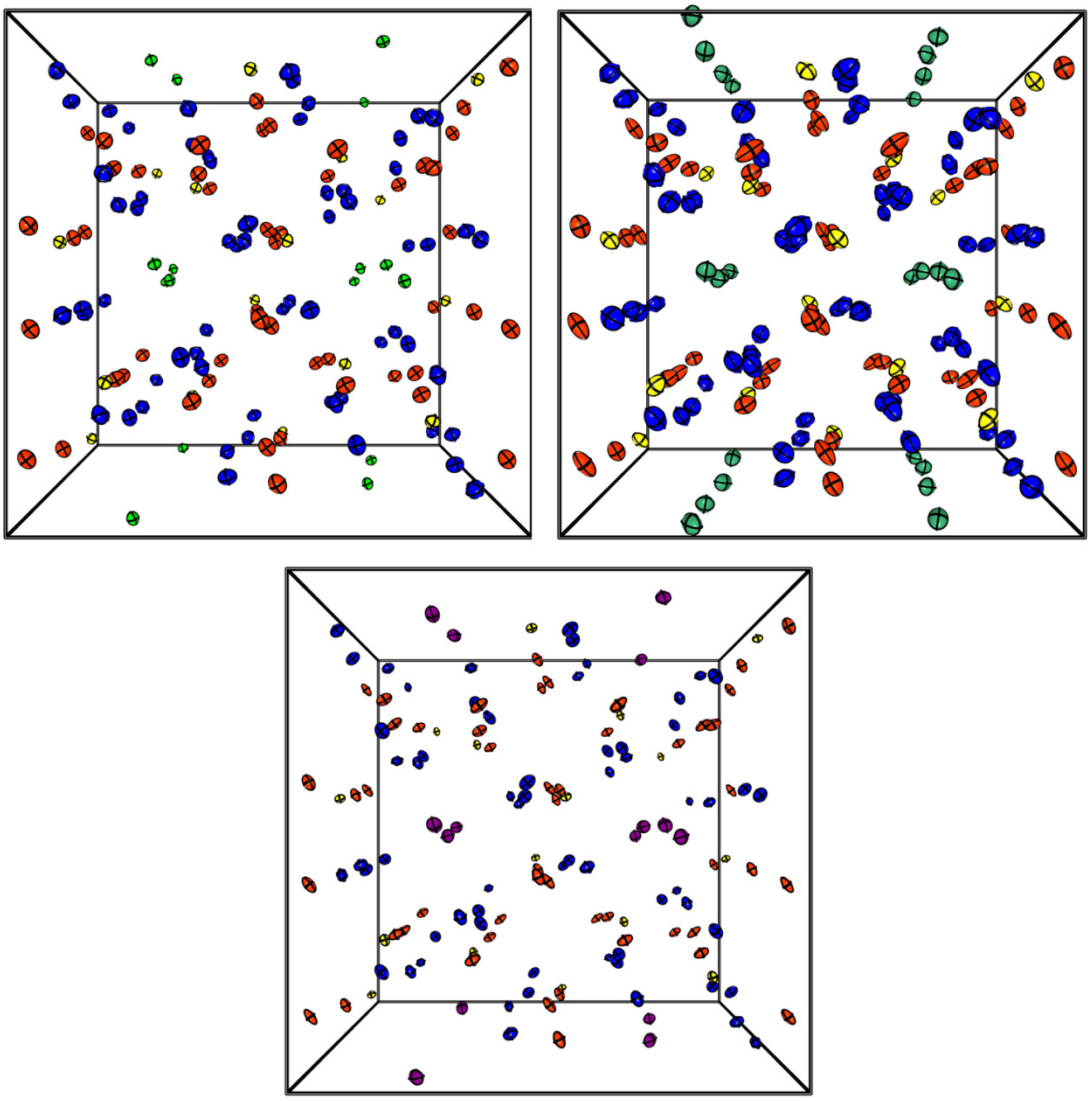

Figure 6.1-S1. Unit cells of $Ca[Mg_3SiN_4]$ (top, left), $Sr[Mg_3SiN_4]$ (top, right) and $Eu[Mg_3SiN_4]$ (bottom); projection along [001]; ellipsoids with 70 % probability; Ca^{2+} green, Sr^{2+} dark green, Eu^{2+} plum, Si^{4+} yellow, Mg^{2+} red, N^{3-} blue.

Table 6.1-S2. Selected Bond Lengths (Å) of M[Mg_3SiN_4] (M = Ca,Sr,Eu)[a]

bond name	Ca[Mg_3SiN_4]	bond name	Sr[Mg_3SiN_4]	bond name	Eu[Mg_3SiN_4]
Ca-N1	2.608(4)	Sr-N1	2.647(5)	Eu-N1	2.644(2)
Ca-N1	2.695(3)	Sr-N1	2.799(5)	Eu-N1	2.772(2)
Ca-N2	2.569(3)	Sr-N2	2.811(5)	Eu-N2	2.845(2)
Ca-N2	3.107(3)	Sr-N2	2.951(5)	Eu-N2	2.868(2)
Ca-N3	2.682(3)	Sr-N3	2.697(5)	Eu-N3	2.665(2)
Ca-N3	2.858(3)	Sr-N3	2.910(5)	Eu-N3	3.014(2)
Ca-N3	3.720(4)	Sr-N4	2.793(5)	Eu-N4	2.732(2)
Ca-N4	2.611(3)	Sr-N4	3.293(4)	Eu-N4	3.498(2)
Si-N1	1.767(3)	Si-N1	1.799(5)	Si-N1	1.757(2)
Si-N2	1.773(3)	Si-N2	1.790(5)	Si-N2	1.763(2)
Si-N3	1.763(4)	Si-N3	1.824(5)	Si-N3	1.778(2)
Si-N4	1.772(4)	Si-N4	1.789(5)	Si-N4	1.775(2)
Mg1-N2	1.980(3)	Mg1-N3	1.986(5)	Mg1-N3	1.996(2)
Mg1-N2	2.050(4)	Mg1-N3	2.054(5)	Mg1-N3	2.070(2)
Mg1-N4	2.070(4)	Mg1-N4	2.064(4)	Mg1-N4	2.082(2)
Mg1-N4	2.194(4)	Mg1-N4	2.157(5)	Mg1-N4	2.191(2)
Mg2-N1	2.067(4)	Mg2-N1	2.049(5)	Mg2-N1	2.071(2)
Mg2-N1	2.162(3)	Mg2-N1	2.200(5)	Mg2-N1	2.238(2)
Mg2-N3	2.065(3)	Mg2-N2	2.049(5)	Mg2-N2	2.059(2)
Mg2-N3	2.094(4)	Mg2-N2	2.068(5)	Mg2-N2	2.099(2)
Mg3-N1	2.097(4)	Mg3-N1	2.067(5)	Mg3-N1	2.080(2)
Mg3-N2	2.113(4)	Mg3-N2	2.215(5)	Mg3-N2	2.267(2)
Mg3-N3	2.253(3)	Mg3-N3	2.076(4)	Mg3-N3	2.103(2)
Mg3-N4	2.074(4)	Mg3-N4	2.042(5)	Mg3-N4	2.066(2)

[a] *e.s.d.'s in parentheses*

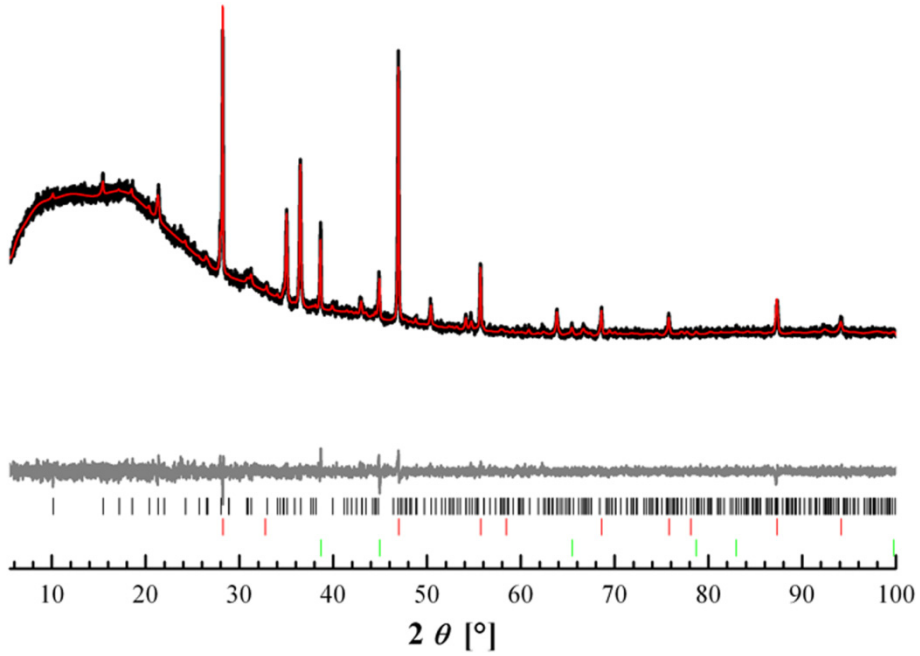

Figure 6.1-S2. Rietveld plot (Cu-$K_{\alpha 1}$) of $Ca[Mg_3SiN_4]$ (black tick marks). Side phases: CaF_2 (red bars), LiF (green).

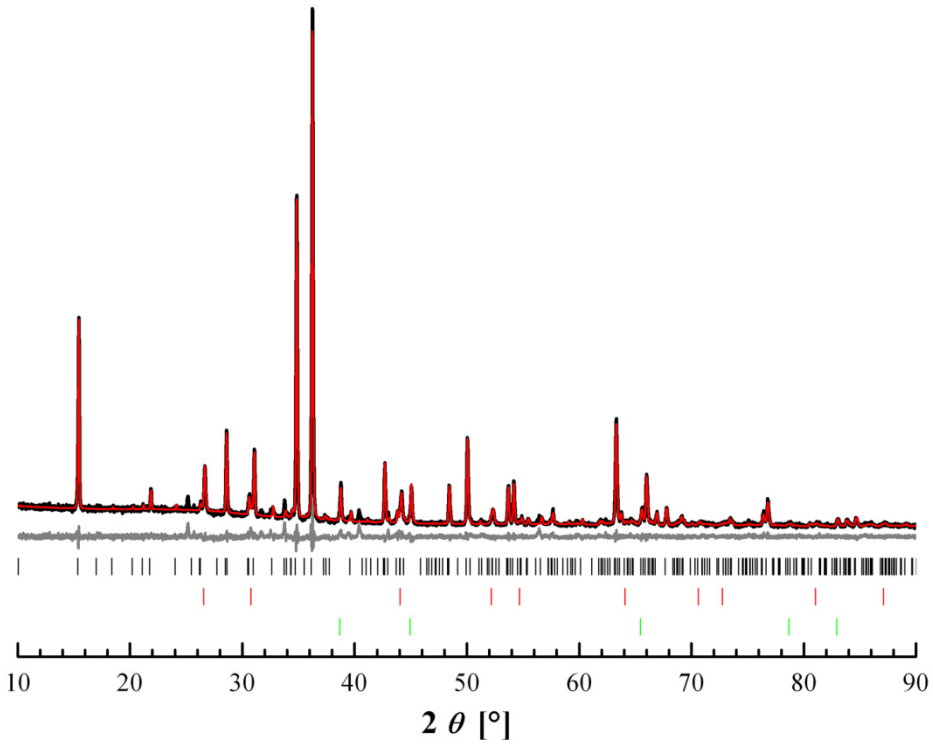

Figure 6.1-S3. Rietveld plot (Cu-$K_{\alpha 1}$) of $Sr[Mg_3SiN_4]$ (black tick marks). Side phases: SrF_2 (red bars), LiF (green), residual non-indexed reflections belong to unknown side phase(s).

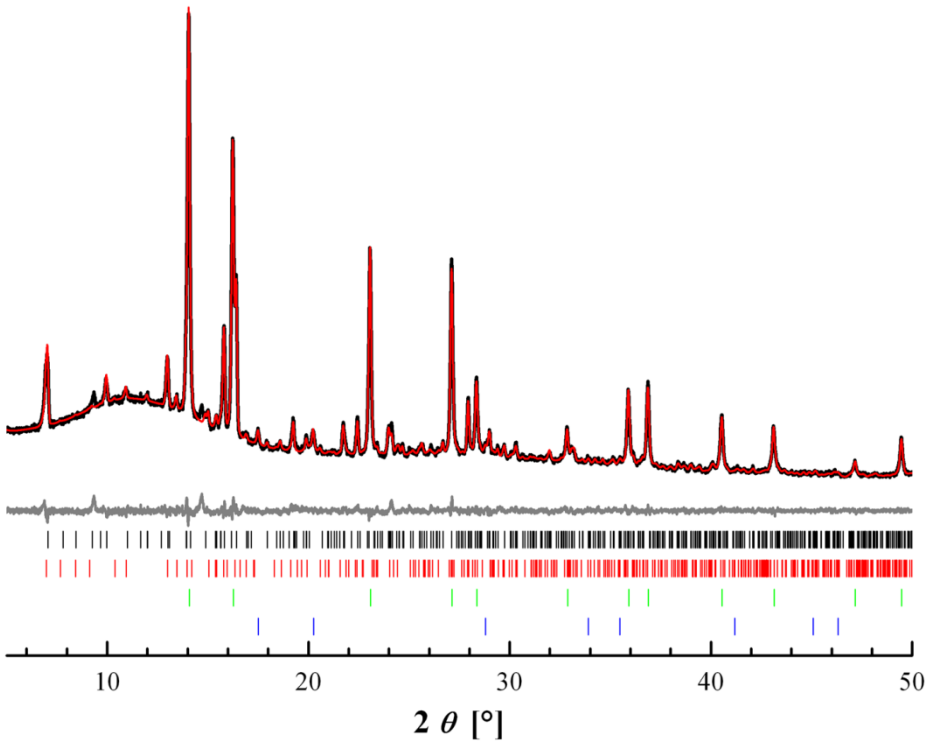

Figure 6.1-S4. Rietveld plot (Mo-$K_{\alpha 1}$) of $Eu[Mg_3SiN_4]$ (black tick marks). Side phases: Eu_2SiN_3[1] (red bars), EuN (green), LiF (blue), residual non-indexed reflections belong to unknown side phase(s).

Table 6.1-S3. Partial MAPLE Values [kJ/mol] for Mg^{2+}

Compound	Mg^{2+}
Mg_3N_2[2]	2246
$MgSiN_2$[3,4]	2260
$Ba_4Mg[Si_2N_6]$[5]	2340
LiMgN[6,7]	2210

(1) Zeuner, M.; Pagano, S.; Matthes, P.; Bichler, D.; Johrendt, D.; Harmening, T.; Pöttgen, R.; Schnick, W. *J. Am. Chem. Soc.* **2009**, *131*, 11242.

(2) Partin, D. E.; Williams, D. J.; O'Keeffe, M. *J. Solid State Chem.* **1997**, *132*, 56.

(3) David, J.; Laurent, Y.; Lang, J. *Bull. Soc. Fr. Mineral. Cristallogr.* **1970**, *93*, 153.

(4) Petukhov, A. G.; Lambrecht, W. R. L.; Segall, B. *Phys. Rev. B: Condens. Matter* **1994**, *49*, 4549.

(5) Yamane, H.; Morito, H. *J. Alloys Compd.* **2013**, *555*, 320.

(6) Kalarasse, F.; Bennecer, B.; Mellouki, A. *J. Phys.: Condens. Matter* **2006**, *18*, 7237.

(7) Yamane, H.; Okabe, T. H.; Ishiyama, O.; Waseda, Y.; Shimada, M. *J. Alloys Compd.* **2001**, *319*, 124.

6.2 Supporting Information for Chapter 2.2

Sebastian Schmiechen, Robin Niklaus, Petra Huppertz, Detlef Wiechert, Peter J. Schmidt, and Wolfgang Schnick, *to be published*.

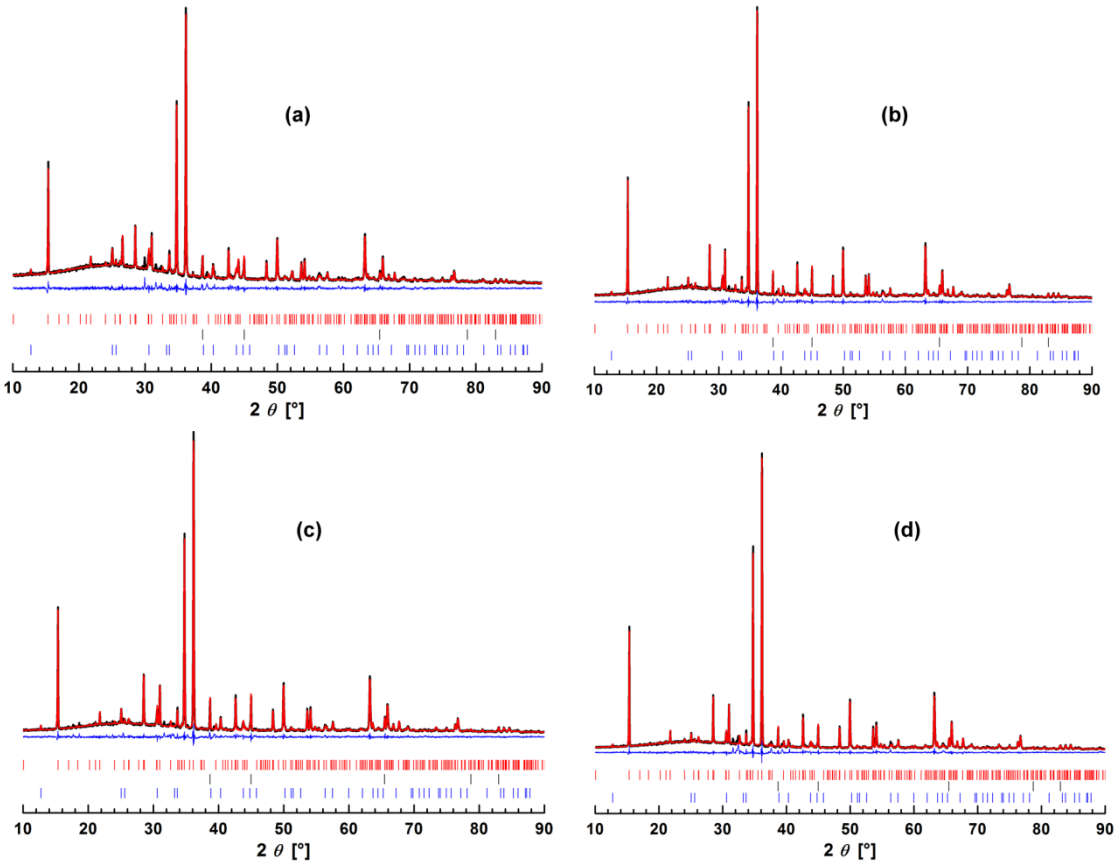

Figure 6.2-S1. Rietveld refinement of $Sr[Mg_3SiN_4]$:RE (RE = Pr^{3+} (a), Sm^{3+} (b), Eu (c), Yb (d)) PXRD data (Cu-$K_{\alpha1}$) with experimental data (black line), calculated pattern (red line) and difference curve (blue line). Tick marks give the positions of the refined phases: Red: $Sr[Mg_3SiN_4]$:RE (RE: a=Pr^{3+} doped, b=Sm^{3+} doped, c=Eu doped, d=Yb doped), black: LiF and blue: SrClF.

6.3 Supporting Information for Chapter 2.3

Sebastian Schmiechen, Philipp Strobel, Cora Hecht, Thomas Reith, Markus Siegert, Peter J. Schmidt, Petra Huppertz, Detlef Wiechert, and Wolfgang Schnick, *Chem. Mater.* **2015**, *27*, 1780; DOI: 10.1021/cm504604d.

Table 6.3-S1. Crystallographic Data of a $Ba[Mg_3SiN_4]$ Single Crystal

formula	$Ba[Mg_3SiN_4]$
formula mass/g·mol^{-1}	294.4
crystal system	triclinic
space group	$P\bar{1}$ (no. 2)
cell parameters/Å,°	a = 3.4567(7) b = 6.0426(12) c = 6.0877(12) α = 85.58(3) β = 73.53(3) γ = 73.93(3)
V/Å^3	117.17(4)
formula units/cell	1
X-ray density/g·cm^{-3}	4.172
abs. coefficient μ/mm^{-1}	4.750
F(000)	134
diffractometer, radiation	Stoe IPDS I Ag-K_α (λ = 0.56087 Å)
temperature/K	293(2)
absorption correction	numerical[1]
θ range/°	1.15-21.0
measured reflections	1109
independent reflections	472 [$R_{(int)}$ = 0.1301]
observed reflections	372
refined parameters	43
GoF	1.039
R indices ($F_o^2 \geq 2\sigma(F_o^2)$)	R_1 = 0.1013, wR_2 = 0.2451
R indices (all data)	R_1 = 0.1187, wR_2 = 0.2572
min / max residual electron density/eÅ^{-3}	-2.69/ 4.66

Table 6.2-S2. Selected Bond Lengths (Å) of $Ba[Mg_3SiN_4]$ from the Rietveld Refinement; e.s.d.'s in Parentheses

bond name	$Ba[Mg_3SiN_4]$
Ba-N1a (2x)	2.946(2)
Ba-N1b (2x)	3.041(3)
Ba-N2a (2x)	2.885(2)
Ba-N2b (2x)	2.933(2)
(Mg1,Si1)-N1	1.983(2)
(Mg1,Si1)-N2a	1.988(3)
(Mg1,Si1)-N2b	2.044(3)
(Mg1,Si1)-N2c	2.076(2)
(Mg2,Si2)-N1a	1.895(3)
(Mg2,Si2)-N1b	2.082(3)
(Mg2,Si2)-N1c	2.139(2)
(Mg1,Si1)-N2a	2.042(2)

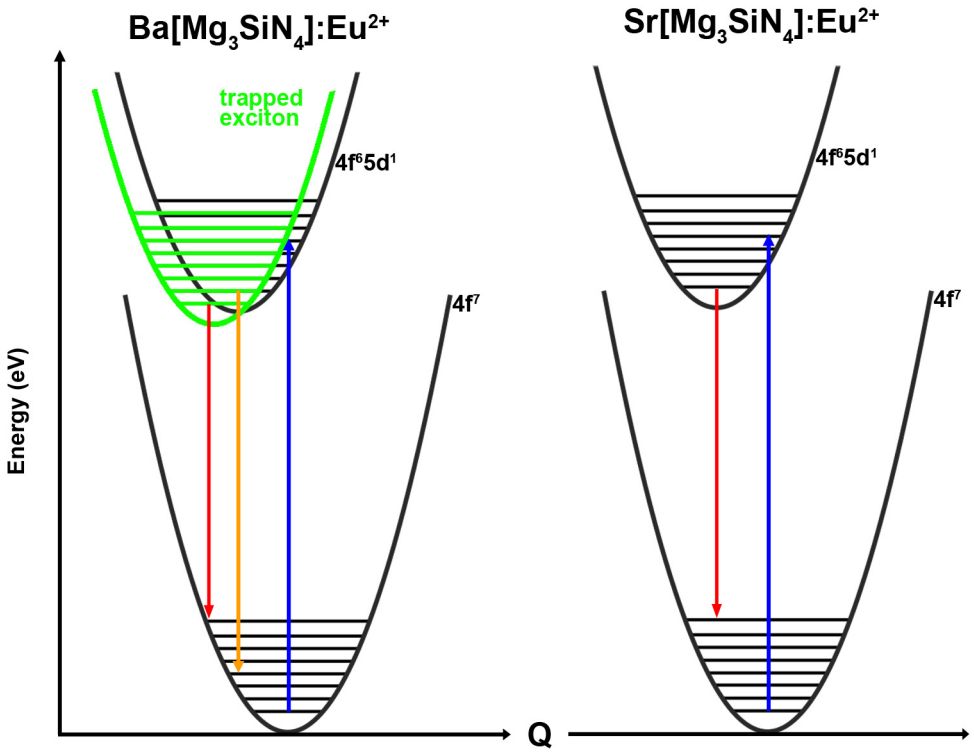

Figure 6.2-S1. Schematic configurational-coordinate diagrams of Eu^{2+} in $Ba[Mg_3SiN_4]$ (left) and $Sr[Mg_3SiN_4]$ (right). The emission process of $Ba[Mg_3SiN_4]:Eu^{2+}$ consists of typical Eu^{2+} $4f^6 5d^1 \rightarrow 4f^7$ emission and ETE over the whole investigated temperature region. In contrast, $Sr[Mg_3SiN_4]:Eu^{2+}$ only shows Eu^{2+} $4f^6 5d^1 \rightarrow 4f^7$ emission.

(1) Sheldrick, G. M. XPREP, v. 2008/2: Data Preparation & Reciprocal Space Exploration, Bruker-AXS, 2008.

6.4 Supporting Information for Chapter 2.5

Sebastian Schmiechen, Frederik Nietschke, and Wolfgang Schnick, *Eur.J. Inorg. Chem.* **2015**, 1592; DOI: 10.1002/ejic.201403178.

Table 6.4-S1. Anisotropic Displacement Parameters [Å²] of $Ca_2Mg[Li_4Si_2N_6]$ and $Li_2Ca_2[Mg_2Si_2N_6]$[a]

	Atom	U_{11}	U_{22}	U_{33}	U_{12}	U_{13}	U_{23}
$Ca_2Mg[Li_4Si_2N_6]$	Ca	0.0053(2)	0.0050(2)	0.0052(2)	0	0.0006(2)	0
	Si	0.0057(3)	0.0045(3)	0.0048(3)	0	-0.0005(2)	0
	Mg	0.0240(6)	0.0081(5)	0.0234(6)	0	-0.0156(5)	0
	Li	0.0125(2)	0.0156(2)	0.0128(2)	-0.0037(8)	-0.0002(10)	0.0017(8)
	N1	0.0075(5)	0.0057(5)	0.0077(5)	0.0002(4)	-0.0003(4)	0.0004(4)
	N2	0.0071(7)	0.0068(7)	0.0064(7)	0	-0.0004(5)	0
$Li_2Ca_2[Mg_2Si_2N_6]$	Ca	0.0094(3)	0.0125(3)	0.0068(3)	0	0.0021(2)	0
	Si	0.0082(4)	0.0089(5)	0.0078(4)	0	0.0006(3)	0
	Mg	0.0095(5)	0.0114(6)	0.0107(5)	0	0.0011(4)	0
	Li	0.0250(3)	0.0220(3)	0.0130(3)	0	0.0030(2)	0
	N1	0.0124(10)	0.0142(11)	0.0128(9)	0.0037(7)	0.0032(7)	0.0030(8)
	N2	0.0086(12)	0.0177(14)	0.0073(11)	0	0.0004(9)	0

[a] *e.s.d.'s in parentheses*

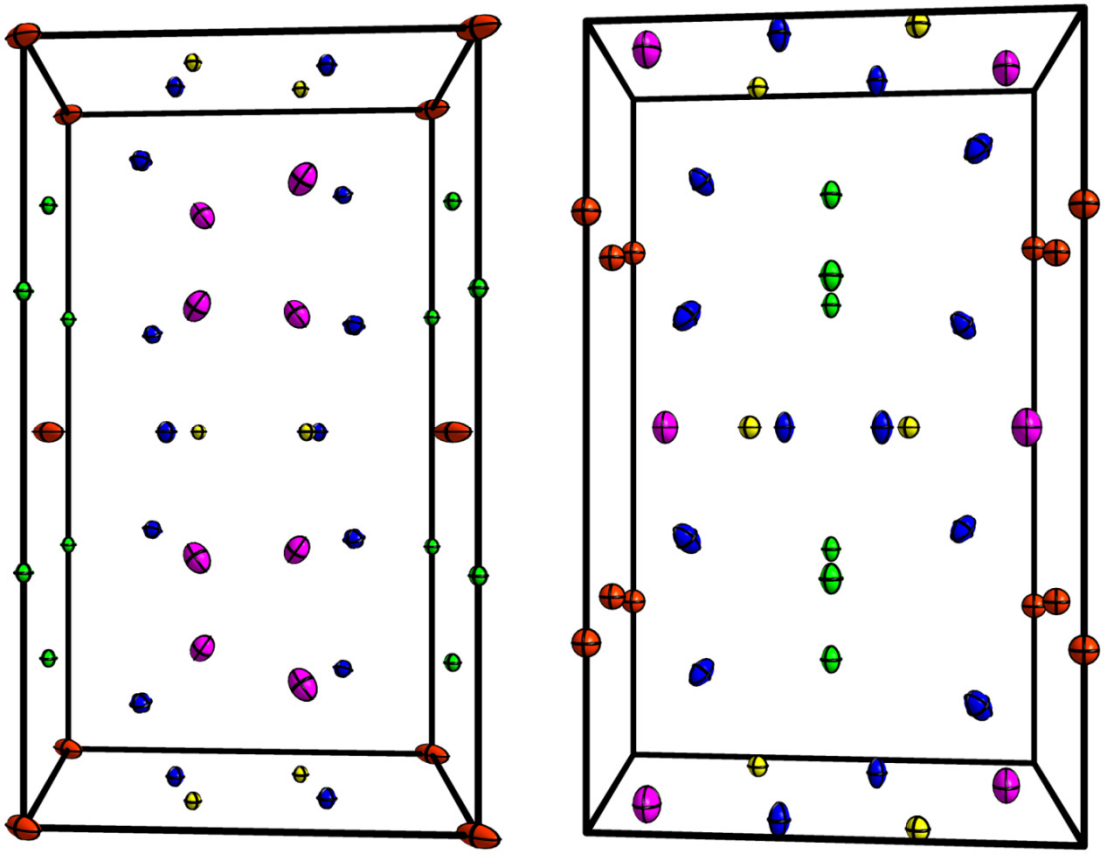

Figure 6.4-S1. Unit cells of $Ca_2Mg[Li_4Si_2N_6]$ (left) and $Li_2Ca_2[Mg_2Si_2N_6]$ (right) with projection along [100]; ellipsoids with 50 % probability; Ca^{2+} green, Si^{4+} yellow, Mg^{2+} red, Li^{+} pink, N^{3-} blue.

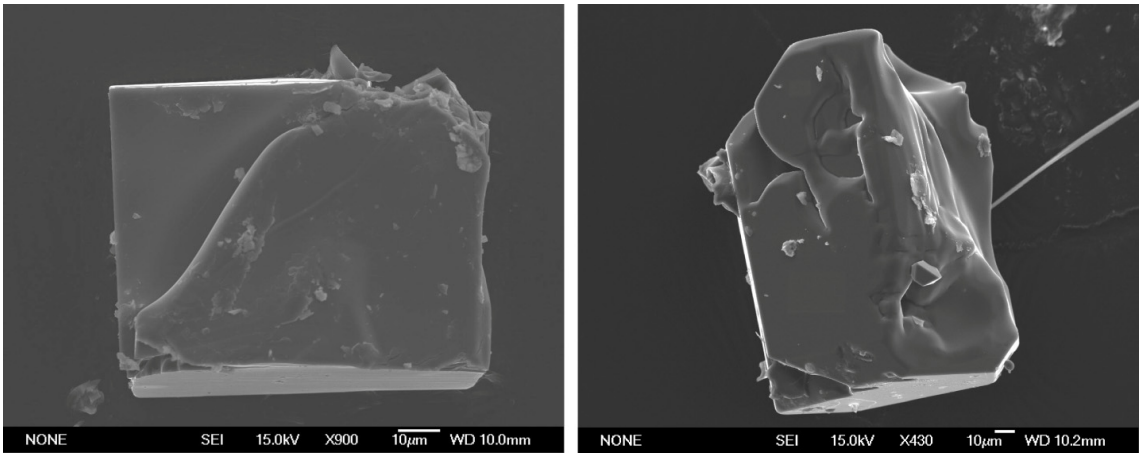

Figure 6.4-S2. SEM images of a cube-like crystallites of $Ca_2Mg[Li_4Si_2N_6]$ (left) and $Li_2Ca_2[Mg_2Si_2N_6]$ (right).

Table 6.4-S2. EDX Spectroscopy Results of $Ca_2Mg[Li_4Si_2N_6]$ and $Li_2Ca_2[Mg_2Si_2N_6]$[a]

	Atom-%	Theoretical	Atom-%	Theoretical
	$Ca_2Mg[Li_4Si_2N_6]$		$Li_2Ca_2[Mg_2Si_2N_6]$	
Ca	13	18	14	17
Si	14	18	15	17
Mg	8	9	15	17
N	58	55	55	50
O	7	-	1	-

[a] *given measured values are the average of five measurements*

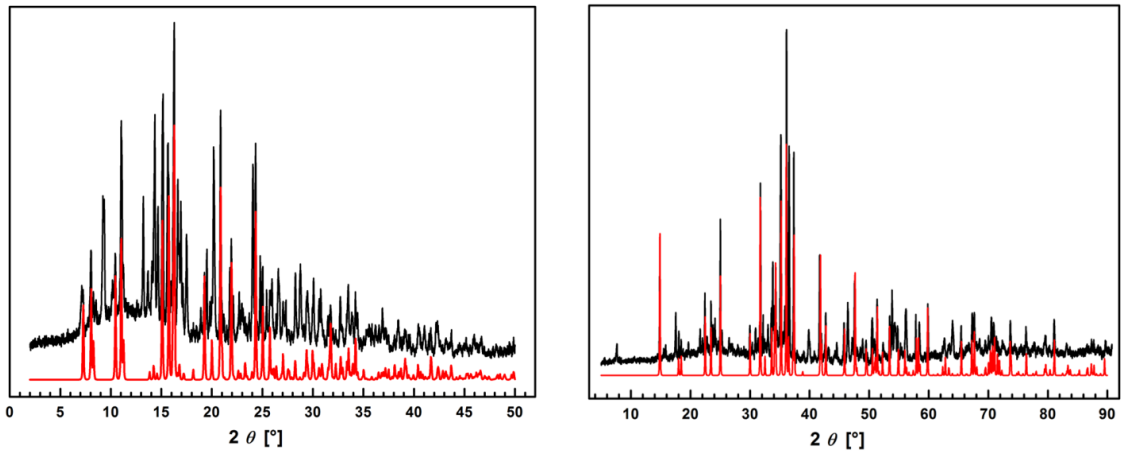

Figure 6.4-S3. Experimental PXRD data (black) of optically separated crystallites of $Ca_2Mg[Li_4Si_2N_6]$ (left, Mo-$K_{\alpha 1}$) and $Li_2Ca_2[Mg_2Si_2N_6]$ (right, Cu-$K_{\alpha 1}$). Red lines are the simulation of the structural models obtained from single-crystal structure elucidation of the respective compound. Non-described reflections belong to common side phases, e.g., $Ca[Mg_3SiN_4]$, $Li_2CaSi_2N_4$, or unknown side phases.

6.5 Supporting Information for Chapter 2.6

Sebastian Schmiechen, Philipp Strobel, Markus Siegert, Peter J. Schmidt, and Wolfgang Schnick, *to be published*.

Table 6.5-S1. Anisotropic Displacement Parameters (Å²) of $Ba[(Mg_{0.4}Li_{1.6})(Al_{2.4}Si_{1.6})N_6]$ and $Ba[(Mg_{0.2}Li_{1.8})(Al_{2.2}Si_{1.8})N_6]$[a]

	Atom	U_{11}	U_{22}	U_{33}	U_{12}	U_{13}	U_{23}
$Ba[(Mg_{0.4}Li_{1.6})(Al_{2.4}Si_{1.6})N_6]$	Ba	0.01439(18)	0.01439(18)	0.0150(2)	0	0	0
	Si	0.0063(3)	0.0094(3)	0.0078(3)	-0.0009(2)	0.00035(19)	-0.0002(2)
	Al	0.0063(3)	0.0094(3)	0.0078(3)	-0.0009(2)	0.00035(19)	-0.0002(2)
	Mg	0.0213(10)	0.0213(10)	0.0176(15)	0.0008(9)	0.0008(9)	-0.0042(12)
	Li	0.0213(10)	0.0213(10)	0.0176(15)	0.0008(9)	0.0008(9)	-0.0042(12)
	N1	0.0208(9)	0.0108(8)	0.0200(10)	-0.0034(7)	-0.0025(8)	-0.0035(7)
	N2	0.0208(9)	0.0208(9)	0.0137(13)	-0.0013(8)	-0.0013(8)	0.0001(11)
$Ba[(Mg_{0.2}Li_{1.8})(Al_{2.2}Si_{1.8})N_6]$	Ba	0.01361(16)	0.01361(16)	0.0141(2)	0	0	0
	Si	0.0058(3)	0.0094(3)	0.0071(3)	-0.00072(18)	0.00050(16)	-0.00008(18)
	Al	0.0058(3)	0.0094(3)	0.0071(3)	-0.00072(18)	0.00050(16)	-0.00008(18)
	Mg	0.0103(9)	0.0103(9)	0.0067(14)	0.0001(8)	0.0001(8)	-0.0043(11)
	Li	0.0103(9)	0.0103(9)	0.0067(14)	0.0001(8)	0.0001(8)	-0.0043(11)
	N1	0.0210(8)	0.0104(7)	0.0194(10)	-0.0024(6)	-0.0036(8)	-0.0027(6)
	N2	0.0209(8)	0.0209(8)	0.0131(11)	-0.0001(7)	-0.0001(7)	-0.0006(10)

[a] *e.s.d.'s in parentheses*

Table 6.5-S2. Selected Bond Lengths (Å) of $Ba[(Mg_{0.4}Li_{1.6})(Al_{2.4}Si_{1.6})N_6]$ and $Ba[(Mg_{0.2}Li_{1.8})(Al_{2.2}Si_{1.8})N_6]$[a]

bond name	$Ba[(Mg_{0.4}Li_{1.6})(Al_{2.4}Si_{1.6})N_6]$	bond name	$Ba[(Mg_{0.2}Li_{1.8})(Al_{2.2}Si_{1.8})N_6]$
Ba-N1	2.959(2) (4x)	Ba-N1	2.951(2) (4x)
Ba-N2	3.136(1) (4x)	Ba-N2	3.125(9) (4x)
(Si,Al)-N1	1.800(2)	(Si,Al)-N1	1.793(19)
(Si,Al)-N1	1.834(2)	(Si,Al)-N1	1.837(2)
(Si,Al)-N1	1.845(2)	(Si,Al)-N1	1.846(2)
(Si,Al)-N2	1.769(7)	(Si,Al)-N2	1.763(6)
(Mg,Li)-N1	2.272(2) (2x)	(Mg,Li)-N1	2.275(2) (2x)
(Mg,Li)-N2	2.184(3) (2x)	(Mg,Li)-N2	2.184(3) (2x)

[a] *e.s.d.'s in parentheses*

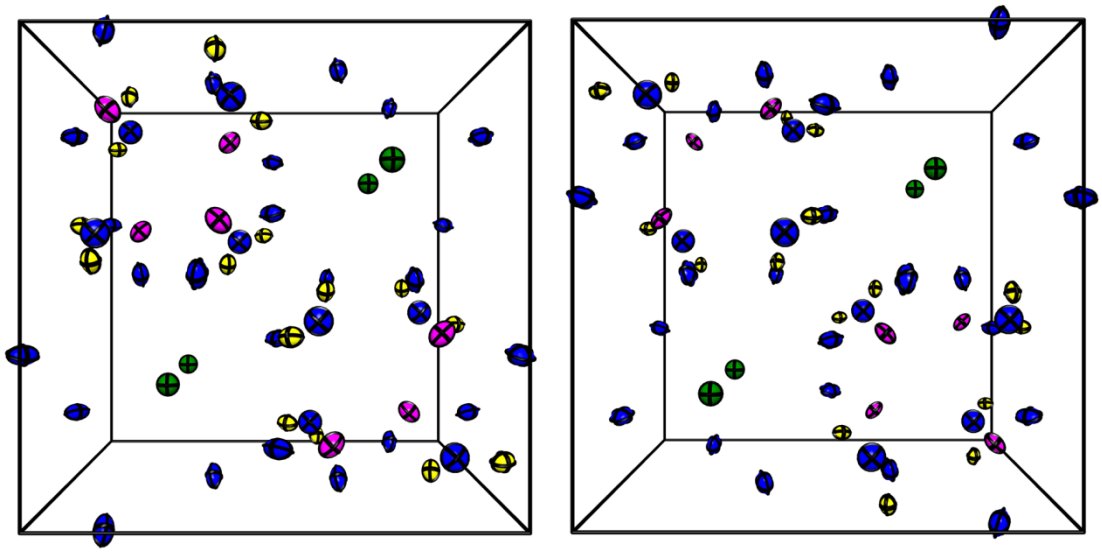

Figure 6.5-S1. Unit cells of $Ba[(Mg_{0.4}Li_{1.6})(Al_{2.4}Si_{1.6})N_6]$ (left) and $Ba[(Mg_{0.2}Li_{1.8})(Al_{2.2}Si_{1.8})N_6]$ (right); projection along [001]; ellipsoids with 70 % probability; Ba^{2+} green, (Al^{3+},Si^{4+}) yellow, (Mg^{2+},Li^{+}) pink, N^{3-} blue.

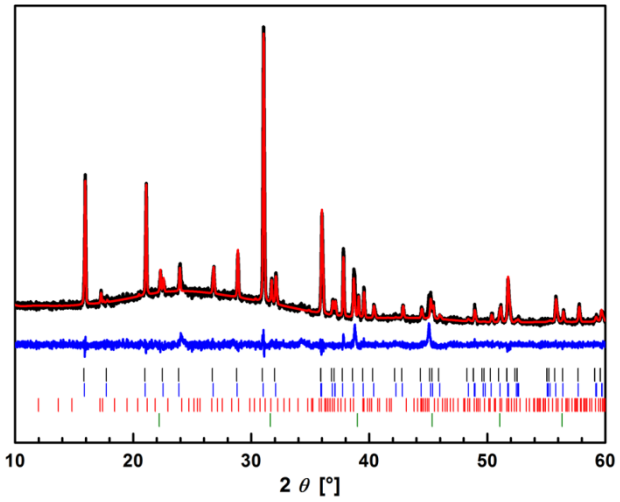

Figure 6.5-S2. Rietveld refinement of raw PXRD data (Cu-$K_{\alpha1}$) with experimental data (black line), calculated pattern (red line) and difference curve (blue line). Tick marks give the positions of the refined phases: $Ba[(Mg_{0.4}Li_{1.6})(Al_{2.4}Si_{1.6})N_6]$ (black, 62 wt%), $Ba[(Mg_{0.2}Li_{1.8})(Al_{2.2}Si_{1.8})N_6]$ (blue, 27 wt%), Li_2SiN_2 (red, 7 wt%) and $LiBaF_3$ (green, 4 wt%).

7 Publications

Major results of this thesis were published in scientific journals by way of the following publications. References of publications, which are not included in this work, as well as patents, oral and poster presentations, are included separately below.

A Published as part of this thesis:

1. **Toward New Phosphors for Application in Illumination-Grade White pc-LEDs: The Nitridomagnesosilicates $Ca[Mg_3SiN_4]:Ce^{3+}$, $Sr[Mg_3SiN_4]:Eu^{2+}$ and $Eu[Mg_3SiN_4]$**
   Sebastian Schmiechen, Hajnalka Schneider, Peter Wagatha, Cora Hecht, Peter J. Schmidt, and Wolfgang Schnick
   Chem. Mater. **2014**, *26*, 2712.

   In this contribution, writing the main part of the manuscript, screening of literature, structure determination based on single-crystal and powder XRD data, interpretation of NMR and UV/vis measurements and image preparation were done by Sebastian Schmiechen. Sample syntheses and synthesis optimization were done by Hajnalka Schneider, Cora Hecht, Peter Wagatha and Sebastian Schmiechen. Luminescence investigations and interpretation of measured values were done by Peter J. Schmidt and Sebastian Schmiechen. Supervision of the research project was carried out by Wolfgang Schnick.

2. **Nitridomagnesosilicate Sr[Mg_3SiN_4]: Optical properties of Ce^{3+},Pr^{3+},Sm^{3+}, Eu, Yb Doping and Energy-Level Locations of all Lanthanides in the Host Lattice**

   Sebastian Schmiechen, Robin Niklaus, Petra Huppertz, Detlef Wiechert, Peter J. Schmidt, and Wolfgang Schnick.

   To be published.

   For this contribution, writing the manuscript, screening of literature, verification of the phase formation based on powder XRD data, and image preparation were done by Sebastian Schmiechen. Sample syntheses were carried out by Robin Niklaus. Optical investigations and interpretation of measured values were done by Petra Huppertz, Sebastian Schmiechen, Detlef Wiechert and Peter J. Schmidt. Supervision of the research project was carried out by Wolfgang Schnick.

3. **Nitridomagnesosilicate Ba[Mg_3SiN_4]:Eu^{2+} and Structure-Property Relations of Narrow-Band Red Nitride Phosphors**

   Sebastian Schmiechen, Philipp Strobel, Cora Hecht, Thomas Reith, Markus Siegert, Peter J. Schmidt, Petra Huppertz, Detlef Wiechert, and Wolfgang Schnick

   Chem. Mater. ***2015****, 27*, 1780.

   This paper, writing the main part of the manuscript, screening of literature, structure determination based on single-crystal and powder XRD data, interpretation of UV/vis measurements and image preparation were done by Sebastian Schmiechen. Sample syntheses and synthesis optimization were done by Philipp Strobel, Cora Hecht, Thomas Reith, Markus Siegert and Sebastian Schmiechen. Luminescence investigations and interpretation of measured data were done by Petra Huppertz, Detlef Wiechert, Sebastian Schmiechen, and Peter J. Schmidt. Supervision of the research project was carried out by Wolfgang Schnick.

4. **Narrow Red Emitters for Brighter White Light**

   Philipp Pust, Sebastian Schmiechen and Wolfgang Schnick

   Mater. Today **2014**, Comment, 29.08.2014.

   For this comment, writing the manuscript was done by Sebastian Schmiechen and Philipp Pust. Literature screening was done by Philipp Pust. Supervision of the research project was carried out by Wolfgang Schnick.

5. **Structural Relationship between the Mg-containing Nitridosilicates $Ca_2Mg[Li_4Si_2N_6]$ and $Li_2Ca_2[Mg_2Si_2N_6]$**

   Sebastian Schmiechen, Frederik Nietschke, and Wolfgang Schnick

   Eur.J. Inorg. Chem. **2015**, 1592.

   Within this article, writing the manuscript, screening of literature, structure determination based on single-crystal and powder XRD data, and image preparation were done by Sebastian Schmiechen. Sample syntheses and synthesis optimization were done by Frederik Nietschke and Sebastian Schmiechen. Supervision of the research project was carried out by Wolfgang Schnick.

6. **Nitridolithomagnesoalumosilicate $Ba[(Mg_{2-x}Li_x)(Al_{4-x}Si_x)N_6]$ with x = (0-2) for LED-Backlighting Applications**

   Sebastian Schmiechen, Philipp Strobel, Markus Siegert, Peter J. Schmidt, and Wolfgang Schnick

   To be published.

   This manuscript, writing the main part of it, screening of literature, structure determination based on single-crystal and powder XRD data, and image preparation were done by Sebastian Schmiechen. Sample syntheses and synthesis optimization were done by Markus Siegert and Philipp Strobel. Luminescence investigations and interpretation of measured values were done by Sebastian Schmiechen, Philipp Strobel, and Peter J. Schmidt. Supervision of the research project was carried out by Wolfgang Schnick.

7. **Ammonothermal Synthesis and Crystal Structure of $BaAl_2(NH_2)_8 \cdot 2NH_3$**
   Philipp Pust, Sebastian Schmiechen, Frauke Hintze, and Wolfgang Schnick
   Z. Anorg. Allg. Chem. **2013**, *639*, 1185.

   In this contribution, Sebastian Schmiechen and Frauke Hintze helped developing and installing the used autoclaves and the filling device. Synthesis of samples, construction of a low-temperature single-crystal preparation device, single-crystal structure refinement, literature screening and writing the main part of the manuscript were done by Philipp Pust. Supervision of the research project was carried out by Wolfgang Schnick.

B Other publications:

1. **$Li_4Ca_3Si_2N_6$ and $Li_4Sr_3Si_2N_6$ – Quaternary Lithium Nitridosilicates with Isolated $[Si_2N_6]^{10-}$ Ions**
   Sandro Pagano, Saskia Lupart, Sebastian Schmiechen, and Wolfgang Schnick
   Z. Anorg. Allg. Chem. **2010**, *636*, 1907.

2. **$Li_2CaSi_2N_4$ and $Li_2SrSi_2N_4$ - A Synthetic Approach to Three-Dimensional Lithium Nitridosilicates**
   Martin Zeuner, Sandro Pagano, Stefan Hug, Philipp Pust, Sebastian Schmiechen, Christina Scheu, and Wolfgang Schnick
   Eur. J. Inorg. Chem. **2010**, 4945.

3. **Luminescence Tuning of MOFs via Ligand to Metal and Metal to Metal Energy Transfer by Co-Doping of $[Gd_2Cl_6(bipy)_3] \cdot 2bipy$ with Europium and Terbium**
   Philipp R. Matthes, Christoph J. Höller, M. Mai, J. Heck, Stefan J. Sedlmaier, Sebastian Schmiechen, Claus Feldmann, Wolfgang Schnick, and Klaus Müller-Buschbaum
   J. Mater. Chem. **2012**, *22*, 10179.

4. **Weißes Licht aus Nitriden**

   Sebastian Schmiechen, Philipp Pust, Peter J. Schmidt, and Wolfgang Schnick

   Nachr. Chem. **2014**, *62*, 847.

C Patent Applications:

1. **New Phosphors, such as New Narrow-Band Red Emitting Phosphors, for Solid State Lighting**

   Peter J. Schmidt, Frauke Hintze, Philipp A.H. Pust, Volker Weiler, Cora Hecht, Sebastian F. Schmiechen, Wolfgang Schnick, and Detlef U. Wiechert

   PCT Int. Appl. **2013**, WO 2013175336, A1

   Koninklijke Philips Electronics NV, Philips Intellectual Property & Standards GmbH, Germany.

2. **New nitridoalumosilicate phosphor for solid-state lighting**

   Andreas Tücks, Baby-Seriyati Schreinemacher, Peter J. Schmidt, Sebastian F. Schmiechen, and Wolfgang Schnick

   PCT Int. Appl. **2015**, WO 2015044106, A1

   Koninklijke Philips Electronics NV, Philips Intellectual Property & Standards GmbH, Germany.

3. **LED phosphors comprising bow tie shaped A_2N_6 building blocks**

   Peter J. Schmidt, Philipp Strobel, Sebastian Schmiechen, Cora Hecht, Volker Weiler, and Wolfgang Schnick

   EPO Appl. **2014**, Filling date: 14.11.2014

   Koninklijke Philips Electronics NV, Philips Intellectual Property & Standards GmbH, Germany.

D Conference contributions:

1. **Nitride Phosphor Materials - Research, Application and Pertinence** (poster)
   S. Schmiechen, F. Hintze, M. Seibald, P. Pust, W. Schnick
   Phosphor Global Summit 2012, Scottsdale, (AZ, USA), 20. – 22. March 2012

2. **Synthesis and Analysis - Strategies for New Phosphor Materials** (poster)
   F. Hintze, M. Seibald, P. Pust, S. Schmiechen, W. Schnick
   Phosphor Global Summit 2012, Scottsdale (AZ, USA), 20. – 22. March 2012

3. **Carbothermal Reduction and Nitridation: From Bolgnian Stone to pc-LEDs** (poster)
   T. Reith, S. Schmiechen, P. Pust and W. Schnick
   Undergraduate Research Conference on Molecular Sciences (URCUP), Wildbad Kreuth (Germany), 29. – 30. September 2013

4. **Mg-containing Nitridosilicates: A Novel Material Class with Interesting Luminescence Properties**
   S. Schmiechen, and W. Schnick
   1. Obergurgl-Seminar Festkörperchemie, Obergurgl (Austria), 28. - 31. January 2014

5. **The First Mg and Li containing Nitridoalumosilicate: $Ba[(Mg_{2-x}Li_x](Al_{4-x}Li_x]N_6]$** (poster)
   M. Siegert, S. Schmiechen, P. Pust and W. Schnick
   Undergraduate Research Conference on Molecular Sciences (URCUP), Wildbad Kreuth (Germany), 27. - 28. July 2014

6. **Narrow-Band Red-Emitting Nitridoaluminates** (poster)
   P. Pust, S. Schmiechen, W. Schnick
   8th International Symposium on Nitrides (ISNT), Wildbad Kreuth (Germany), 31. August - 05. September 2014

7. **Towards Novel Narrow Band Red-Emitting Phosphors: The Nitridomagnesosilicate $Sr[Mg_3SiN_4]:Eu^{2+}$** (poster)
   S. Schmiechen, P. Pust, W. Schnick
   8th International Symposium on Nitrides (ISNT), Wildbad Kreuth (Germany), 31. August - 05. September 2014

E Depository numbers of the single crystal data:

Crystallographic data (cif file) of investigated compounds can be obtained from the Fachinformationszentrum Karlsruhe, 76344 Eggenstein-Leopoldshafen, Germany (fax, (+49)7247-808-666; e-mail, crysdata@fiz-karlsruhe.de) by quoting the corresponding depository numbers.

$Ca[Mg_3SiN_4]$	CSD-427074
$Sr[Mg_3SiN_4]$	CSD-427076
$Eu[Mg_3SiN_4]$	CSD-427075
$Ba[Mg_3SiN_4]$	CSD-428510
$Ca_2Mg[Li_4Si_2N_6]$	CSD-427077
$Li_2Ca_2[Mg_2Si_2N_6]$	CSD-427078
$BaAl_2(NH_2)_8{\cdot}2NH_3$	CSD-42532